BOEING

COMMERCIAL
AIRPLANE DIVISION

REV LTR

THE BOEING COMPANY

AIRPLANE DIVISION
P.O. BOX 707
RENTON, WASHINGTON 98055

CODE IDENT. NO. 81205

NUMBER D6-19559

TITLE: A STUDY OF THE TRANSMISSION OF ELECTROMAGNETIC WAVES THROUGH A PERIODICALLY APERTURED CONDUCTING SCREEN BY VARIATIONAL METHOD

Distribution of this document is unlimited;
it may be released to the general public.

MODEL RESEARCH CONTRACT

ISSUE NO. 1 ISSUED TO: Defense Doc Center

PREPARED BY S. Y. Peng 4/27/68
S. Y. Peng

SUPERVISED BY C. D. Lunden 5-4-68
C. D. Lunden

APPROVED BY O. W. Jansen 5-1-68
O. W. Jansen

APPROVED BY A. F. Norwood 5-17-68
A. F. Norwood (Date)

Approved by R. A. Peterson 5-10-68
R. A. Peterson (Date)

THE BOEING COMPANY

NUMBER 06-19559
REV LTR

ACTIVE SHEET RECORD

SHEET NUMBER	REV LTR	ADDED SHEETS				SHEET NUMBER	REV LTR	ADDED SHEETS			
		SHEET NUMBER	REV LTR	SHEET NUMBER	REV LTR			SHEET NUMBER	REV LTR	SHEET NUMBER	REV LTR
T		43		88							
a		44		89							
b		45		90							
1		46		91							
2		47		92							
3		48		93							
4		49		94							
5		50		95							
6		51		96							
7		52		97							
8		53		98							
9		54		99							
10		55		100							
11		56		101							
12		57		102							
13		58		103							
14		59		104							
15		60		105							
16		61		106							
17		62		107							
18		63		108							
19		64									
20		65									
21		66									
22		67									
23		68									
24		69									
25		70									
26		71									
27		72									
28		73									
29		74									
30		75									
31		76									
32		77									
33		78									
34		79									
35		80									
36		81									
37		82									
38		83									
39		84									
40		85									
41		86									
42		87									

REVISIONS			
LTR	DESCRIPTION	DATE	APPROVAL

TABLE OF CONTENTS

ABSTRACT

This document presents a theoretical and experimental investigation of the transmission coefficient of a periodically apertured plane conducting screen for all angles of incidence. Equations are formulated by variational methods and equivalent circuit concept. Measurements as well as calculations are made to verify the theoretical analysis.

Numerical results of the equivalent susceptance for normal incidence are included and discussed. The results can be important in the further study of the design of a fenestrated metal radome and rain erosion metal cap and other applications.

KEY WORD LIST

Variational Method
Transmission Coefficient
Equivalent Susceptance
Periodically Apertured Conducting Screen
Rectangular Aperture
Radomes

SUMMARY

A. STATEMENT OF THE PROBLEM

Transmission of plane electromagnetic (E-M) waves through a periodically apertured plane conducting screen is of current interest.

Applications have recently been made to the studies of a fenestrated metal radome[1] and rain erosion cap[5]. To establish their electric characteristics, the degree of transparency of a periodically fenestrated plane conducting screen to microwaves for oblique incidence, as well as for normal incidence, should be investigated. The purpose of this report is to present the results of these investigations theoretically and experimentally.

B. RESULTS

From the Poynting theorem and normalized equivalent circuit concept, a set of integral equations in the variational form were formulated to evaluate the impedance of a fenestrated plane conducting screen and were reported by other researchers[2].

Applying the integral equations in the variational form to the screen of rectangular or square apertures, equations to evaluate the impedance and voltage transmission coefficient for oblique incidence were obtained. Numerical values of the impedance and the transmission coefficient were thus calculated for the different aperture spacings and sizes at the different frequencies and incident angles.

The voltage transmission coefficient for normal incidence is a special case of that for oblique incidence, since the angle of incidence is zero. Curves of T vs. $k_n a$, where T is the transmission coefficient, k_n is wave number, and a is the aperture spacing along the x-axis (Fig. 1), were also plotted (Figs. 58-81) for this case to complete the whole analysis.

Experimental measurements were conducted for both normal and oblique incidence. Close agreement was obtained which verified the theoretical investigation.

C. CONCLUSIONS

Equations to evaluate the voltage transmission coefficient of a periodically apertured conducting plane by oblique incident plane E-M waves were formulated by S. W. Chien in 1962[1]. Unfortunately, the results were incorrect.

From an extensive theoretical study and experimental investigation, the correct equations were formulated and were verified by a comparison of calculated and measured values.

Some striking phenomena have been observed. For normal incidence, as has been observed by other researchers[1,3], there is a peak of transmission across a certain frequency band. Surprisingly enough, at a certain frequency the amplitude of the peak will reach its maximum (full power transmitting through the apertured conducting plane). This frequency is different from the resonant frequency of a single aperture, at which the maximum transmission cross section occurs. Wood anomalies[8] were observed. That is, with an exceedingly slight change of the incident frequency, the peak of transmission becomes a dip. However, this phenomenon is not very explicit for the apertures loaded with high dielectric constant material.

For normal polarization, as the angle of incidence increases (from 0° to 5°), the amplitude of the peak of transmission decreases (Fig. 1). However, as the angle increases further ($>5^\circ$), the amplitude increases also (Figs. 5-9). The peak of transmission occurs at a higher frequency as the angle of incidence is increased.

For parallel polarization there are two peaks of transmission across the frequency band of 7-11 Gc/s (Fig. 2). As the angle of incidence increases (from 0° to 5°), frequency separation between the two peaks becomes wider and the amplitudes of the peaks decrease (Figs. 20-30). With a further increase in the angle of incidence ($>5^\circ$), one peak, moving toward the lower

frequency, first increases its amplitude (from 5^{o} to 10^{o}) and then decreases ($>10^{o}$), while the other, moving toward the higher frequency simply increases its amplitude (Figs. 24-27). At the time that the angle of incidence is zero, one peak coincides with the other. A similar phenomenon was also observed by R. W. Wood[8-11] and L. Rayleigh[6] early in the twentieth century.

LIST OF FIGURES

LIST OF FIGURES (Continued)

LIST OF FIGURES (Continued)

LIST OF FIGURES (Continued)

LIST OF FIGURES (Continued)

REFERENCES

1. C. H. Chiou, "Fenestrated Metal Radomes for Microwaves", Boeing Document No. D6-9034, June 15, 1962

2. R. B. Kieburtz, A. Ishimaru and G. Heid, "The Variational Method for Evaluation of Scattering of E-M Waves by Obstacles", Technical Reports Nos. 45 and 47, January 1961, Microwave Lab., E. E. Dept. U. of Washington

3. R. B. Kieburtz and A. Ishimaru, "Scattering by a Periodically Apertured Conducting Screen", IRE Trans. on Ant. and Prop., Nov. 1961, pp. 506-514

4. H. Levine and J. Schwinger, "On the Theory of Diffraction by an Aperture in an Infinite Plane Screen (I) and (II)", Phys. Rev., Vol. 74 & 75: Oct. 1948 and May 1949, pp. 958-974 and 1423-1432

5. L. L. Oh, "A Fenestrated Metal Rain Erosion Cap for Aircraft Nose Radome", Boeing Document No. D6-15373 TN, May 26, 1966

6. L. Rayleigh, "Note on the Remarkable Case of Diffraction Spectra Described by Prof. Wood", Phil. Mag. S. 6. Vol. 14, No. 79, July 1907, pp. 60-65

7. J. Schwinger, Discontinuities in Waveguides, unpublished notes, 1945

8. R. W. Wood, "Anomalous Diffractive Gratings", Phil. Mag., Vol. 4, Sept. 1902, pp. 396-402

9. R. W. Wood, "A Simple Treatment of the Secondary Maxima of Grating Spectra", Phil. Mag., S. 6. Vol. 14, No. 82, Oct. 1907, pp. 477-482

10. R. W. Wood, "Diffractive Gratings and Controlled Groove Form With Abnormal Distribution of Density", Phil. Mag., Vol. 23, Feb. 1912, pp. 310-317

11. R. W. Wood, "On a Remarkable Case of Uneven Distribution of Light in a Diffraction Grating Spectrum", Phys. Rev., Vol. 48, Dec. 1935, pp. 928-936

I. INTRODUCTION

Scattering of plane electromagnetic (E-M) waves by an obstacle is a classical problem and is still of great current interest.

A variational method was first introduced by Schwinger[7] to evaluate the scattering by lossless obstacles in waveguide and then generalized by Levine and Schwinger[4] to certain diffraction problems. Later, the method was shown to follow from the properties of an energy operator by R. B. Kieburtz, A. Ishimaru and G. Held[2], and was applied to evaluate the scattering by an infinite, lossless, periodically apertured, thin conducting plane of square apertures.

Some applications have recently been made to the study of a fenestrated metal radome[1] and rain erosion cap[5] which will increase the strength of the nose radome of a jet aircraft without degrading the performance of a weather radar which resides in the radome.

The purpose of this study is to investigate the transparency of a periodically apertured conducting plane of rectangular and square apertures, theoretically and experimentally, which is incident by plane E-M waves at all angles (from 0 to 90 degrees). Equations are formulated by variational methods for the field both perpendicular and parallel to the plane of incidence (normal and parallel polarizations) in Section II and Section III, respectively. In Section IV, equations for normal incidence are also obtained for the completeness of the analysis. Numerical results are presented in Section V, along with comparisons with measured transmission coefficients and those calculated by this method.

II. FIELD PERPENDICULAR TO THE PLANE OF INCIDENCE (Normal Polarization)

A periodically apertured conducting screen of infinitesimal thickness and rectangular apertures is placed in the xy plane with the large side of the apertures parallel to the x-axis (Fig. 1). The incident plane is the xz plane.

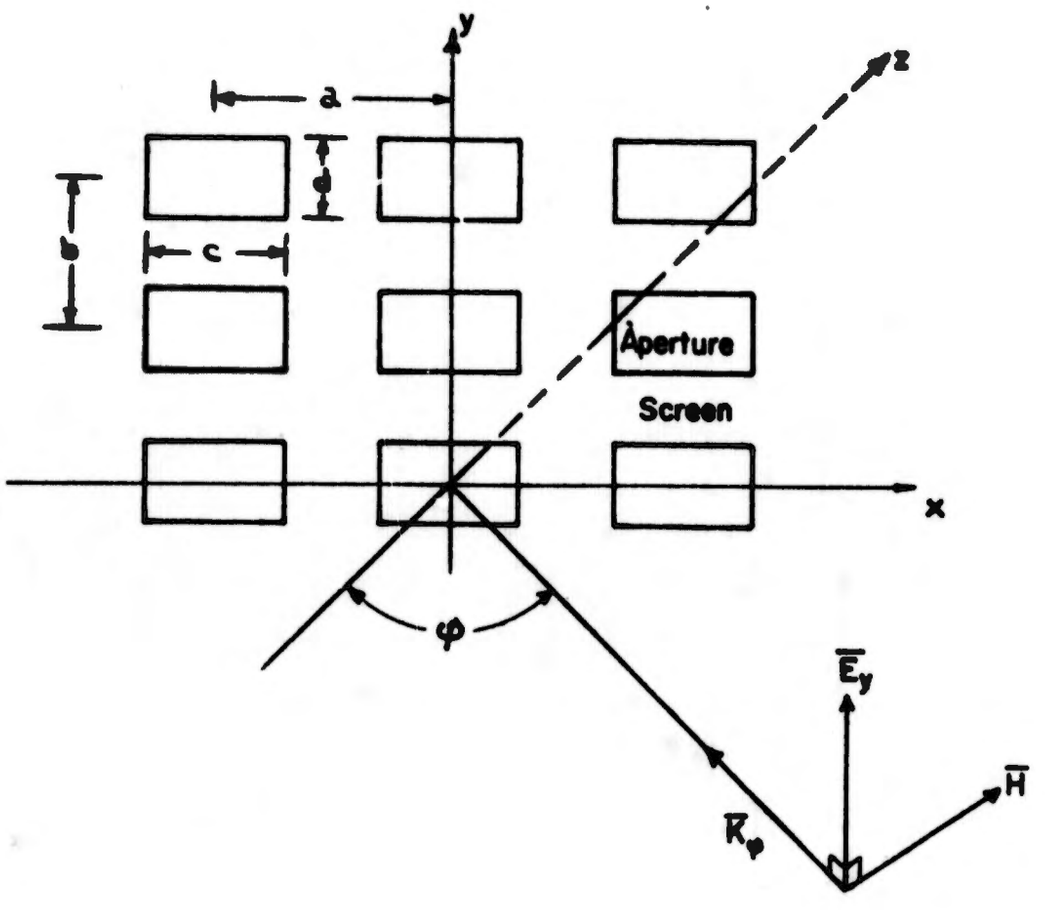

Fig. 1: Electric Field Perpendicular to the Plane of Incidence (Normal Polarization)

AD 1546 D

From the Poynting theorem, the energy integral equation in the variational form is obtained and given below.

$$\frac{\omega (W_h - W_e)}{P} = \frac{\iint_{ap.}\iint_{ap.} \bar{E}(x,y)\cdot\bar{K}_2(x,y,x',y')\cdot\bar{E}^*(x',y')\,dx'dy'dxdy}{\iint_{ap.}\iint_{ap.} \bar{E}(x,y)\cdot\bar{K}_1(x,y,x',y')\cdot\bar{E}^*(x',y')\,dx'dy'dxdy} \qquad (1)$$

where w = $2\pi f$, and f = frequency of incident waves

W_h = total magnetic energy stored in the screen

W_e = total electric energy stored in the screen

P = total power transmission through the screen

E = electric field in the aperture

$\bar{K}_1$ = real part of the tensor Green's function $\bar{K}$

$\bar{K}_2$ = imaginary part of the tensor Green's function $\bar{K}$

$*$ = conjugate

A transmission line model is set up to show that the eigenvalues of the energy integral equation can be treated as a shunt admittance across the transmission line (Fig. 2). For simplicit,, $\bar{K}_2$ is expressed below as a summation of a positive ($\bar{K}_2^+$) and a negative ($\bar{K}_2^-$) part which correspond to the evaluation of the positive and negative parts of the shunt admittance,

$$\bar{K}_2 = \bar{K}_2^+ + \bar{K}_2^- \qquad (2)$$

Assuming the screen is lossless, the shunt admittance becomes purely susceptance. Since half of the energy is stored on each side of the screen, a factor of 2 has to be introduced into Equation (1) to evaluate the total susceptancy B_t of the equivalent circuit.

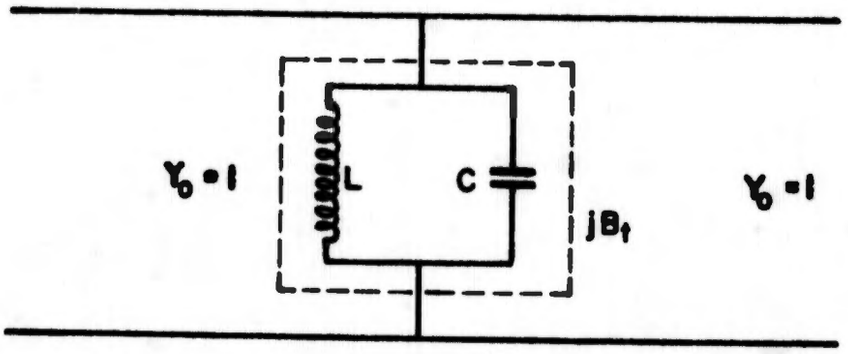

Fig. 2: A Transmission Line Model of a Lossless Periodically Apertured Conducting Screen

Substituting Equation (2) into Equation (1) and replacing the energy operator by susceptance, Equation (1) becomes

$$B^{+} = \frac{\iint_{ap.}\iint_{ap.} \bar{E}(x,y) \cdot \bar{\bar{K}}_2^{+}(x,y,x',y') \cdot \bar{E}^{*}(x',y')\, dx'\, dy'\, dx\, dy}{\iint_{ap.}\iint_{ap.} \bar{E}(x,y) \cdot \bar{\bar{K}}_1(x,y,x',y') \cdot \bar{E}^{*}(x',y')\, dx'\, dy'\, dx\, dy} \tag{3}$$

and

$$B^{-} = \frac{\iint_{ap.}\iint_{ap.} \bar{E}(x,y) \cdot \bar{\bar{K}}_2^{-}(x,y,x',y') \cdot \bar{E}^{*}(x',y')\, dx'\, dy'\, dx\, dy}{\iint_{ap.}\iint_{ap.} \bar{E}(x,y) \cdot \bar{\bar{K}}_1(x,y,x',y') \cdot \bar{E}^{*}(x',y')\, dx'\, dy'\, dx\, dy} \tag{4}$$

The total susceptance is then given by

$$B_t = 2\,(B^{+} + B^{-}) \tag{5}$$

To evaluate the total susceptance B_t from Equations (3) and (4), tensor Green's functions $\bar{\bar{K}}_1$, $\bar{\bar{K}}_2^{+}$ and $\bar{\bar{K}}_2^{-}$ have to be constructed. It is assumed that the only propagating mode of the incident plane E-M waves in the TEM mode. The wave admittance coefficient for this mode is given by

$$Y_{TEM} = \frac{1}{\eta} \cos\varphi \tag{6}$$

Where η = wave impedance
φ = angle between wave vector $\bar{K}_g$ and z-axis
$K = 2\pi/\lambda$

Tensor Green's function $\bar{\bar{K}}$ has been defined as (Appendix)

$$\bar{\bar{K}} = \sum_{m,n} Y_{mn}^{*}\, \bar{\Phi}_{mn}^{*}(x, y)\, \bar{\Phi}_{mn}(x', y') \tag{7}$$

and $$\bar{\bar{K}} = \bar{\bar{K}}_1 + j\bar{\bar{K}}_2 \tag{8}$$

where $\bar{\phi}$ = field function
m,n = integers

The normalized transverse electric field in an aperture is given by

$$\bar{\phi}_{TEM} = (\bar{a}_x + \bar{a}_y)\frac{1}{\sqrt{ab}}\, e^{-j(k_\varphi \sin\varphi)x} \tag{9}$$

where $\bar{a}_x$ and $\bar{a}_y$ are unit vectors along x and y axes respectively.

From Equations (6), (7), (8) and (9), the real part of tensor Green's function is found to be

$$\bar{\bar{K}}_1 = \frac{1}{ab\eta}\cos\varphi\, e^{j(k_\varphi \sin\varphi)(x-x')} \begin{bmatrix} 1 & 1 \\ 1 & 1 \end{bmatrix} \tag{10}$$

where a and b are aperture spacings along x and y axes correspondingly.

Since it has been assumed that the TEM mode is the only propagating mode, the TE and TM modes have to be evanescent. In other words, the propagation constant r_{mn} is real. For the TE mode, the wave admittance coefficients are

$$Y_{mn\,TE} = -j\frac{r_{mn}}{k_\varphi \eta} \tag{11}$$

where $r_{mn} = \left[\left(\frac{2m\pi}{a} - k_\varphi \sin\varphi\right)^2 + \left(\frac{2n\pi}{b}\right)^2 - k_\varphi^2\right]^{1/2}$

The normalized transverse electric field in an aperture is given by

$$\bar{\phi}_{mn\,TE} = \left[\frac{an}{\sqrt{a^2n^2 + b^2(m - k_\varphi a \sin\varphi/2\pi)^2}}\,\bar{a}_x - \frac{b(m - k_\varphi a \sin\varphi/2\pi)}{\sqrt{a^2n^2 + b^2(m - k_\varphi a \sin\varphi/2\pi)^2}}\,\bar{a}_y\right] \cdot \frac{1}{\sqrt{ab}}\, e^{j\left(\frac{2m\pi}{a} - k_\varphi \sin\varphi\right)x}\, e^{j\left(\frac{2n\pi}{b}\right)y} \tag{12}$$

From Equations (7), (8), (11) and (12), the positive imaginary part of tensor Green's function is found to be

$$\bar{\bar{K}}_z^+ = \frac{1}{ab\eta K_\varphi} \sum_{m,n} \Gamma_{mn}\, e^{-j\left(\frac{2m\pi}{a} - K_\varphi \sin\varphi\right)(x-x')}\, e^{-j\left(\frac{2n\pi}{b}\right)(y-y')}$$

$$\begin{bmatrix} \dfrac{a^2n^2}{b^2\left(m - \frac{K_\varphi a \sin\varphi}{2\pi}\right)^2 + a^2n^2} & \dfrac{-abn\left(m - \frac{K_\varphi a \sin\varphi}{2\pi}\right)}{b^2\left(m - \frac{K_\varphi a \sin\varphi}{2\pi}\right)^2 + a^2n^2} \\ \dfrac{-abn\left(m - \frac{K_\varphi a \sin\varphi}{2\pi}\right)}{b^2\left(m - \frac{K_\varphi a \sin\varphi}{2\pi}\right)^2 + a^2n^2} & \dfrac{b^2\left(m - \frac{K_\varphi a \sin\varphi}{2\pi}\right)^2}{b^2\left(m - \frac{K_\varphi a \sin\varphi}{2\pi}\right)^2 + a^2n^2} \end{bmatrix} \qquad (13)$$

For the TM mode, the wave admittance coefficients are

$$Y_{mn\,TM} = j\frac{K_\varphi}{\Gamma_{mn}\eta} \qquad (14)$$

The normalized transverse electric field in an aperture is given by

$$\bar{\Phi}_{mn\,TM} = \left[\frac{b\left(m - \frac{K_\varphi a \sin\varphi}{2\pi}\right)}{\sqrt{b^2\left(m - \frac{K_\varphi a \sin\varphi}{2\pi}\right)^2 + a^2n^2}}\,\bar{a}_x + \frac{an}{\sqrt{b^2\left(m - \frac{K_\varphi a \sin\varphi}{2\pi}\right)^2 + a^2n^2}}\,\bar{a}_y\right] \cdot \qquad (15)$$

$$\frac{1}{\sqrt{ab}}\, e^{j\left(\frac{2m\pi}{a} - K_\varphi \sin\varphi\right)}\, e^{j\left(\frac{2n\pi}{b}\right)y}$$

From Equations (7), (8), (14) and (15) the negative imaginary part of tensor Green's function is found to be

$$\bar{\bar{K}}_2^- = -\frac{K_\varphi}{ab\eta}\sum_{m,n} e^{-j\left(\frac{2m\pi}{a} - K_\varphi \sin\varphi\right)(x-x')} e^{-j\left(\frac{2n\pi}{b}\right)(y-y')}$$

$$\begin{bmatrix} \frac{b^2\left(m - \frac{K_\varphi a \sin\varphi}{2\pi}\right)^2}{b^2\left(m - \frac{K_\varphi a \sin\varphi}{2\pi}\right)^2 + a^2 n^2} & \frac{abn\left(m - \frac{K_\varphi a \sin\varphi}{2\pi}\right)}{b^2\left(m - \frac{K_\varphi a \sin\varphi}{2\pi}\right)^2 + a^2 n^2} \\ \frac{abn\left(m - \frac{K_\varphi a \sin\varphi}{2\pi}\right)}{b^2\left(m - \frac{K_\varphi a \sin\varphi}{2\pi}\right)^2 + a^2 n^2} & \frac{a^2 n^2}{b^2\left(m - \frac{K_\varphi a \sin\varphi}{2\pi}\right)^2 + a^2 n^2} \end{bmatrix} \quad (16)$$

An electric field along the y-axis in an aperture is assumed under boundary conditions, such as[3]

$$\bar{E}(x,y) = \left[1 - \left(\frac{2x}{c}\right)^2\right]^{-1/2}\left[1 - \left(\frac{2y}{d}\right)^2\right]^{-1/2} e^{-j(K_\varphi \sin\varphi)x}\,\bar{a}_y \quad (17)$$

where c and d are the dimensions of apertures.

From Equations (3), (11), (13) and (17) the positive part of the inductance is found to be

$$B^+ = \sum_{m,n} \frac{2\pi \sec\varphi}{K_\varphi a}\left[\left(m - \frac{K_\varphi a \sin\varphi}{2\pi}\right)^2 + \left(\frac{a}{b}\right)^2 n^2 - \left(\frac{K_\varphi a}{2\pi}\right)^2\right]^{-1/2} \quad (18)$$

$$\frac{\left(\frac{b}{a}\right)^2\left(m - \frac{K_\varphi a \sin\varphi}{2\pi}\right)^2}{\left(\frac{b}{a}\right)^2\left(m - \frac{K_\varphi a \sin\varphi}{2\pi}\right)^2 + n^2}\left[\frac{J_1\left(\frac{m\pi c}{a}\right)}{\frac{m\pi c}{2a}}\right]^2\left[\frac{J_1\left(\frac{n\pi d}{b}\right)}{\frac{n\pi d}{2b}}\right]^2$$

where J_1 is the Bessel function of first order of the first kind.

Similarly, from Equations (4), (11), (16) and (17), the negative part of the susceptance is found to be

$$B^{-} = -\sum_{m,n} \frac{K_\varphi a \sec\varphi}{2\pi\left[\left(m - \frac{K_\varphi a \sin\varphi}{2\pi}\right)^2 + \left(\frac{a}{b}\right)^2 n^2 - \left(\frac{K_\varphi a}{2\pi}\right)^2\right]^{1/2}} \tag{19}$$

$$\frac{n^2}{n^2 + \left(\frac{b}{a}\right)^2 \left(m - \frac{K_\varphi a \sin\varphi}{2\pi}\right)^2} \left[\frac{J_1\left(\frac{m\pi c}{a}\right)}{\frac{m\pi c}{2a}}\right]^2 \left[\frac{J_1\left(\frac{n\pi d}{b}\right)}{\frac{n\pi d}{2b}}\right]^2$$

Total susceptance B_t can be found from Equations (5), (18) and (19).

From the transmission line model, the voltage transmission coefficient of the screen is found to be

$$T = \frac{2}{2 + jB_t} \tag{20}$$

III. FIELD PARALLEL TO THE PLANE OF INCIDENCE (Parallel Polarization)

In this case, the plane of incidence is the yz plane (Fig. 3). Analysis here is similar to that in the preceding section.

To construct $\bar{K}_1$, it is again assumed that the only propagating mode is the TEM mode. The wave admittance coefficient is given by

$$Y_{TEM} = \frac{1}{\eta \cos\theta} \tag{21}$$

Where θ is the angle between wave vector K_θ and z-axis, and $K_\theta = 2\pi/\lambda$

The normalized transverse electric field in an aperture is given by

$$\bar{\Phi}_{TEM} = (\bar{a}_x + \bar{a}_y) \frac{1}{\sqrt{ab}} e^{-j(K_\theta \sin\theta)\, y} \tag{22}$$

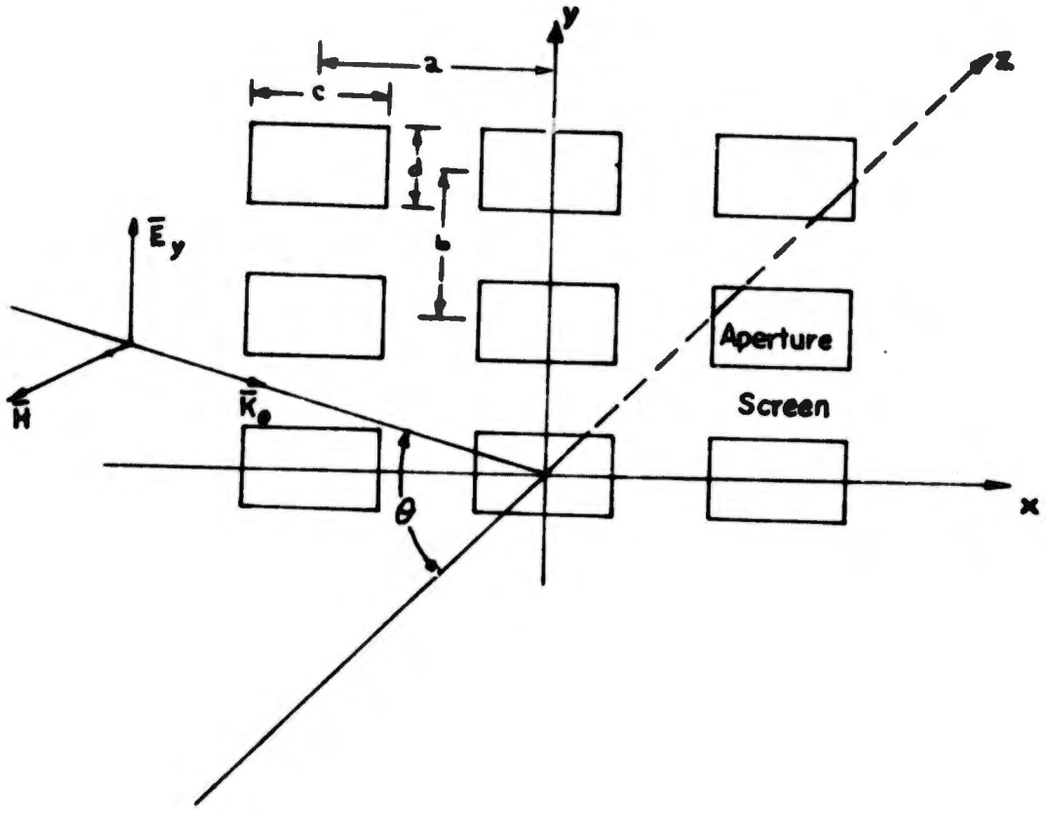

Fig. 3: Electric Field Parallel to the Plane of Incidence (Parallel Polarization)

From Equations (7), (21) and (22), the real part of the tensor Green's function $\bar{\bar{K}}_1$ is found to be

$$\bar{\bar{K}}_1 = \frac{1}{ab\eta\cos\theta} e^{j(K_0 \sin\theta)y} e^{-j(K_0 \sin\theta)y'} \begin{bmatrix} 1 & 1 \\ 1 & 1 \end{bmatrix} \tag{23}$$

Since the TE and TM modes are envanescent, r_{mn} is real. For the TE mode, the wave admittance coefficients are

$$Y_{mn\,TE} = -j\frac{r_{mn}}{K_0\eta} \tag{24}$$

where $r_{mn} = \left[\left(\frac{2m\pi}{a}\right)^2 + \left(\frac{2n\pi}{b} - K_0 \sin\theta\right)^2 - K_0^2 \right]^{1/2}$

The normalized transverse electrical field in an aperture is given by

$$\bar{f}_{mn\,TE} = \left[\frac{a\left(n - \frac{K_0 b \sin\theta}{2\pi}\right)}{\sqrt{m^2b^2 + a^2\left(n - \frac{K_0 b \sin\theta}{2\pi}\right)^2}} \bar{a}_x - \frac{mb}{\sqrt{m^2b^2 + a^2\left(n - \frac{K_0 b \sin\theta}{2\pi}\right)^2}} \bar{a}_y \right] \cdot \frac{1}{\sqrt{ab}} e^{j\left(\frac{2m\pi}{a}\right)x} e^{j\left(\frac{2n\pi}{b} - K_0 \sin\theta\right)y} \tag{25}$$

From Equations (7), (24) and (25), the positive imaginary part of the tensor Green's function is found to be

$$\bar{\bar{K}}_2^+ = \sum_{m,n} \frac{r_{mn}}{ab\eta K_0} e^{-j\left(\frac{2m\pi}{a}\right)(x-x')} e^{-j\left(\frac{2n\pi}{b} - K_0 \sin\theta\right)(y-y')} \begin{bmatrix} \frac{a^2\left(n - \frac{K_0 b \sin\theta}{2\pi}\right)^2}{m^2b^2 + a^2\left(n - \frac{K_0 b \sin\theta}{2\pi}\right)^2} & \frac{abm\left(n - \frac{K_0 b \sin\theta}{2\pi}\right)}{m^2b^2 + a^2\left(n - \frac{K_0 b \sin\theta}{2\pi}\right)^2} \\ \frac{abm\left(n - \frac{K_0 b \sin\theta}{2\pi}\right)}{m^2b^2 + a^2\left(n - \frac{K_0 b \sin\theta}{2\pi}\right)^2} & \frac{m^2b^2}{m^2b^2 + a^2\left(n - \frac{K_0 b \sin\theta}{2\pi}\right)^2} \end{bmatrix} \tag{26}$$

For the TM mode, the wave admittance coefficients are

$$Y_{mn\,TM} = j\frac{K_0}{\eta r_{mn}} \tag{27}$$

The normalized transverse electric field in an aperture is given by

$$\bar{f}_{mn\,TM} = \left[\frac{bm}{\sqrt{m^2b^2 + a^2\left(n - \frac{K_0 b \sin\theta}{2\pi}\right)^2}} \bar{a}_x - \frac{a\left(n - \frac{K_0 b \sin\theta}{2\pi}\right)}{\sqrt{m^2b^2 + a^2\left(n - \frac{K_0 b \sin\theta}{2\pi}\right)^2}} \bar{a}_y \right] \frac{1}{\sqrt{ab}} e^{j\left(\frac{2m\pi}{a}\right)x} e^{j\left(\frac{2n\pi}{b} - K_0 \sin\theta\right)y} \tag{28}$$

From Equations (7), (27) and (28), the negative imaginary part of the tensor Green's function is found to be

$$\bar{K}_z^- = -\sum_{m,n} \frac{K_0}{ab\eta\,\Gamma_{mn}} e^{-j\left(\frac{2m\pi}{a}\right)(x-x')} e^{-j\left(\frac{2n\pi}{b} - K_0\sin\theta\right)(y-y')} \begin{bmatrix} \frac{b^2m^2}{b^2m^2 + a^2\left(n - \frac{K_0 b\sin\theta}{2\pi}\right)^2} & \frac{abm\left(n - \frac{K_0 b\sin\theta}{2\pi}\right)}{b^2m^2 + a^2\left(n - \frac{K_0 b\sin\theta}{2\pi}\right)^2} \\ \frac{abm\left(n - \frac{K_0 b\sin\theta}{2\pi}\right)}{b^2m^2 + a^2\left(n - \frac{K_0 b\sin\theta}{2\pi}\right)^2} & \frac{a^2\left(n - \frac{K_0 b\sin\theta}{2\pi}\right)^2}{b^2m^2 + a^2\left(n - \frac{K_0 b\sin\theta}{2\pi}\right)^2} \end{bmatrix} \tag{29}$$

An electric field along the y-axis in an aperture is assumed under boundary conditions and is given by

$$\bar{E}(x,y) = \left[1 - \left(\frac{2x}{c}\right)^2\right]^{1/2} \left[1 - \left(\frac{2y}{d}\right)^2\right]^{1/2} e^{-j(K_0\sin\theta)y}\, \bar{a}_y \tag{30}$$

From Equations (3), (23), (26) and (30), the positive part of the susceptance is found to be

$$B^+ = \sum_{m,n} \frac{2\pi\cos\theta}{K_0 b} \left[\left(\frac{b}{a}\right)^2 m^2 + \left(n - \frac{K_0 b\sin\theta}{2\pi}\right)^2 - \left(\frac{K_0 b}{2\pi}\right)^2 \right]^{1/2} \frac{m^2}{m^2 + \left(\frac{a}{b}\right)^2\left(n - \frac{K_0 b\sin\theta}{2\pi}\right)^2} \left[\frac{J_1\left(\frac{m\pi c}{a}\right)}{\frac{m\pi c}{2a}} \right]^2 \left[\frac{J_1\left(\frac{n\pi d}{b}\right)}{\frac{n\pi d}{2b}} \right]^2 \tag{31}$$

From Equations (4), (23), (29) and (30), the negative part of the susceptance is found to be

$$B^- = -\sum_{m,n} \frac{K_0 b \cos\theta}{2\pi\left[\left(\frac{b}{a}\right)^2 m^2 + \left(n - \frac{K_0 b \sin\theta}{2\pi}\right)^2 - \left(\frac{K_0 b}{2\pi}\right)^2\right]^{1/2}} \tag{32}$$

$$\frac{\left(\frac{a}{b}\right)^2\left(n - \frac{K_0 b \sin\theta}{2\pi}\right)^2}{m^2 + \left(\frac{a}{b}\right)^2\left(n - \frac{K_0 b \sin\theta}{2\pi}\right)^2}\left[\frac{J_1\left(\frac{m\pi c}{a}\right)}{\frac{m\pi c}{2a}}\right]^2\left[\frac{J_1\left(\frac{n\pi d}{b}\right)}{\frac{n\pi d}{2b}}\right]^2$$

IV. NORMAL INCIDENCE

If plane E-M waves are incident normally to the screen, the angle φ or θ should be zero (Fig. 4). Equations to evaluate the susceptances of positive and negative parts for this case can be easily obtained from Equations (18) and (19), or (31) and (32) by setting φ or θ equal to zero. For completeness, these equations are also given below

$$B^+ = \sum_{m,n} \frac{2\pi}{K_n a}\left[m^2 + \left(\frac{a}{b}\right)^2 n^2 - \left(\frac{K_n a}{2\pi}\right)^2\right]^{1/2} \tag{33}$$

$$\frac{\left(\frac{b}{a}\right)^2 m^2}{\left(\frac{b}{a}\right)^2 m^2 + n^2}\left[\frac{J_1\left(\frac{m\pi c}{a}\right)}{\frac{m\pi c}{2a}}\right]^2\left[\frac{J_1\left(\frac{n\pi d}{b}\right)}{\frac{n\pi d}{2b}}\right]^2$$

and

$$B^- = -\sum_{m,n} \frac{K_n a}{2\pi\left[m^2 + \left(\frac{a}{b}\right)^2 n^2 - \left(\frac{K_0 a}{2\pi}\right)^2\right]^{1/2}} \tag{34}$$

$$\frac{n^2}{\left(\frac{b}{a}\right)^2 m^2 + n^2}\left[\frac{J_1\left(\frac{m\pi c}{a}\right)}{\frac{m\pi c}{2a}}\right]^2\left[\frac{J_1\left(\frac{n\pi d}{b}\right)}{\frac{n\pi d}{2b}}\right]^2$$

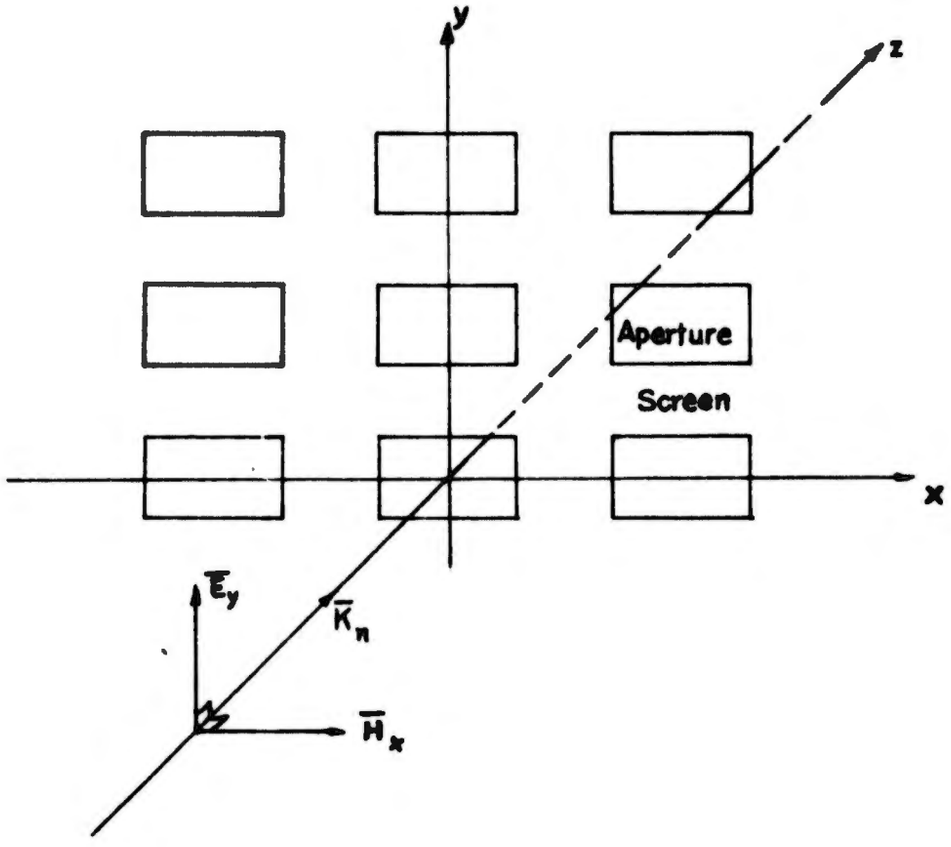

Fig. 4: Electromagnetic Wave Incident Normally to the Apertured Conducting Screen (Normal Incidence)

V. NUMERICAL RESULTS

A. Normal Polarization

The voltage transmission coefficient, T, of normal polarization was calculated (by computer) as a function of wave number (or vector) K_φ and aperture spacing a for each incident angle φ. To compare calculations with measurements, T was converted into attenuation (-db) and $K_\varphi a$ into frequency f (Figs. 5-18).

Several interesting phenomena are observed from calculations. It is seen that the larger the aperture, the broader is the bandwidth of frequency (Figs. 5-18). As the aperture spacings get smaller, the peak of transmission shifts toward the higher frequency. As the incident angle, φ, is increased, the peak of transmission also shifts toward the higher frequency. In addition, the amplitude of the peak will first decrease (from 0° to 5°) and then increase ($> 5^\circ$).

The Wood anomalies[8] are noticed (Fig. 5). That is, a peak of transmission will decrease sharply with exceedingly slight change of the incident frequency. Surprisingly enough, this dip of transmission occurs at the wavelength close to the spacing of apertures as it has been reported by Wood[11] (Figs. 5-10).

Another very important phenomenon is noticed here, also. That is, all of the power of the incident waves will not be able to pass through an apertured conducting screen at all incident angles within a certain frequency range (for example, from 7 to 11 Gc/s). Full transmission of power occurs only at the frequency at which the reflected power from conducting surfaces is all cancelled by the re-radiation from the apertures. This phenomenon is different from a single aperture resonance that will give maximum transmission cross section.

Experimental verification for the voltage transmission coefficient of normal polarization was obtained with the aid of a transmitting

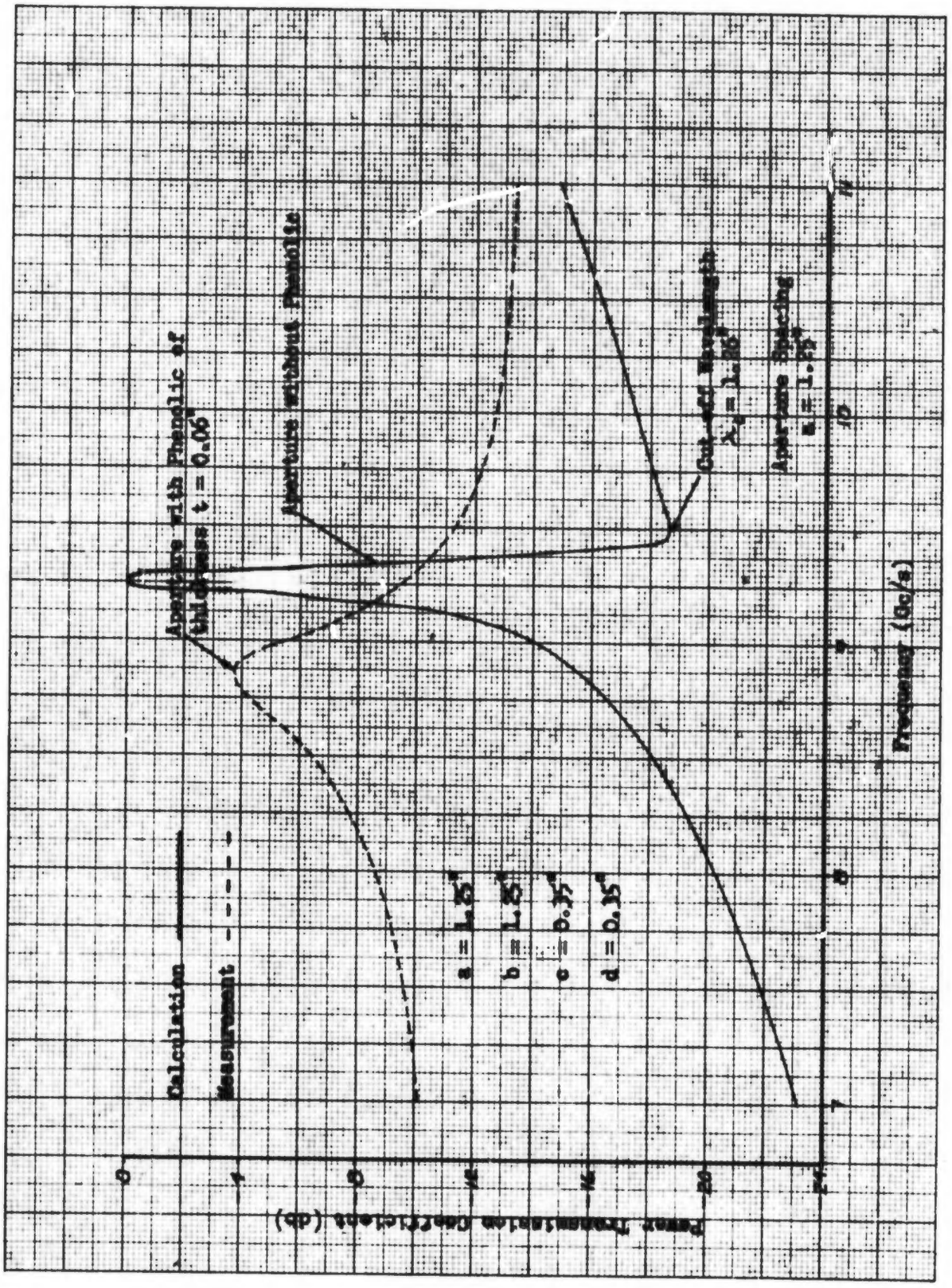

Fig. 5: Power Transmission Coefficient vs. Frequency for Normal Polarization. $\psi = 0^{\circ}$

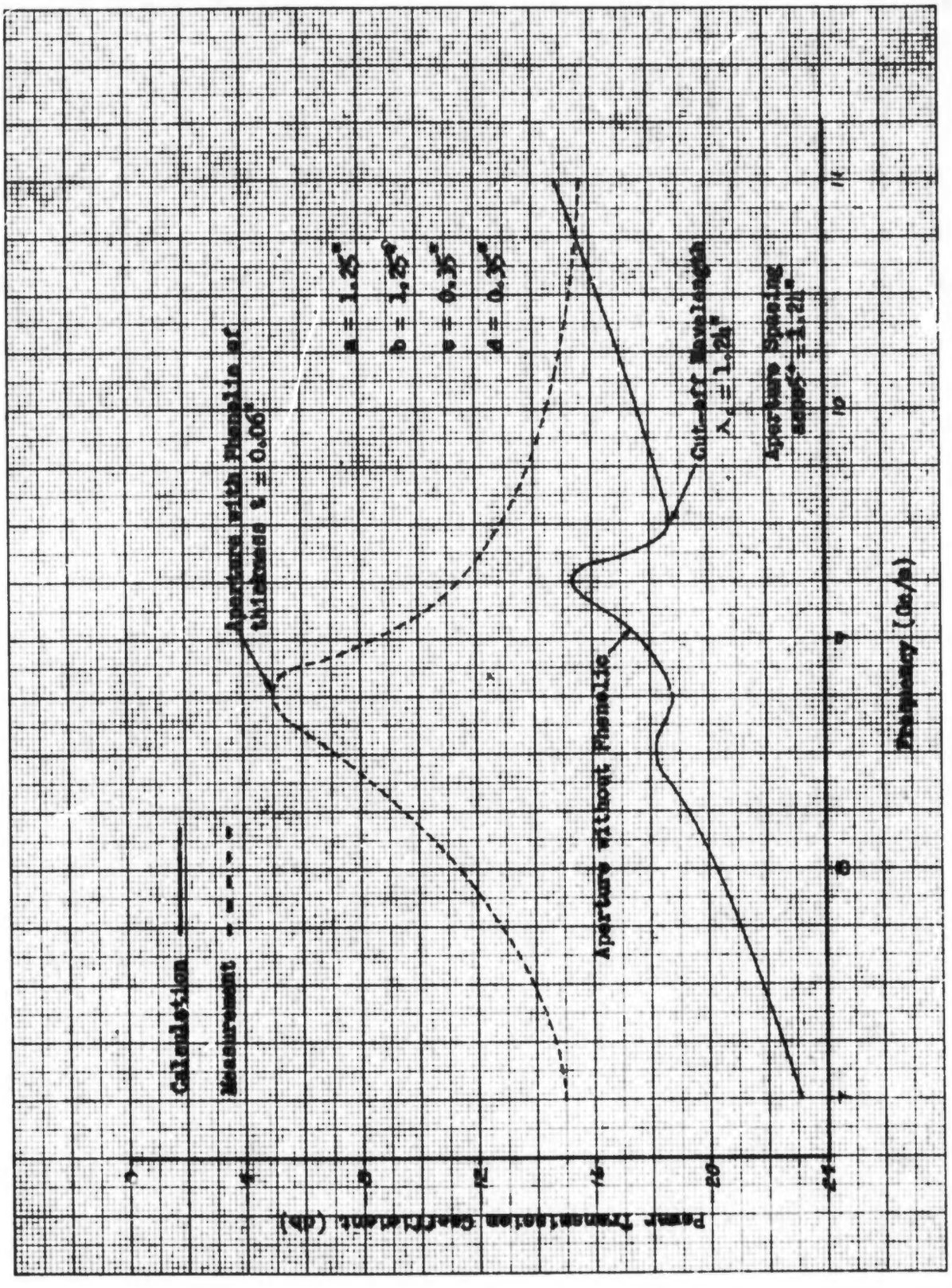

Fig. 6: Power Transmission Coefficient vs. Frequency for Normal Polarization. $\psi = 5°$

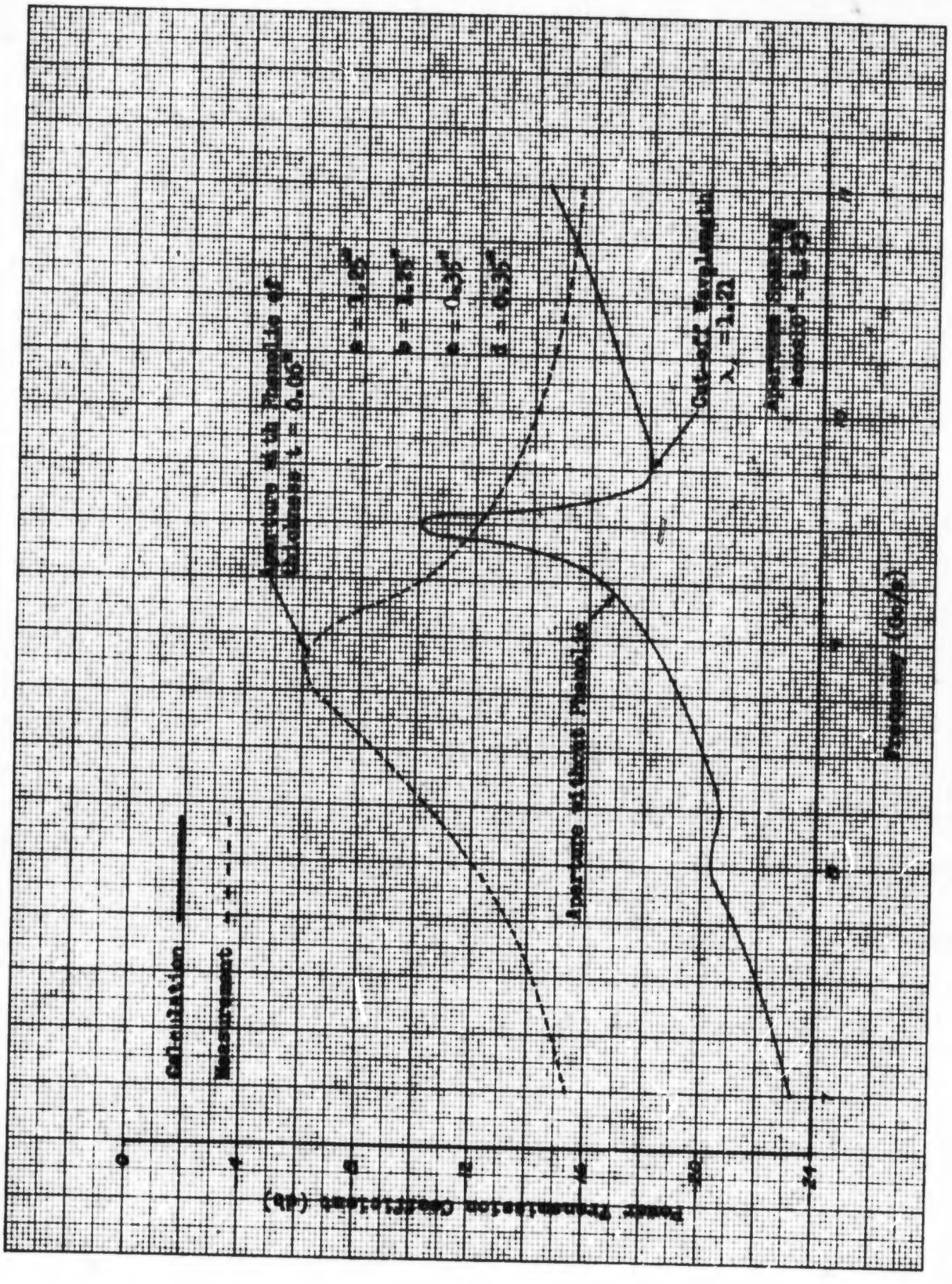

Fig. 7: Power Transmission Coefficient vs. Frequency for Normal Polarization. $\psi = 10°$

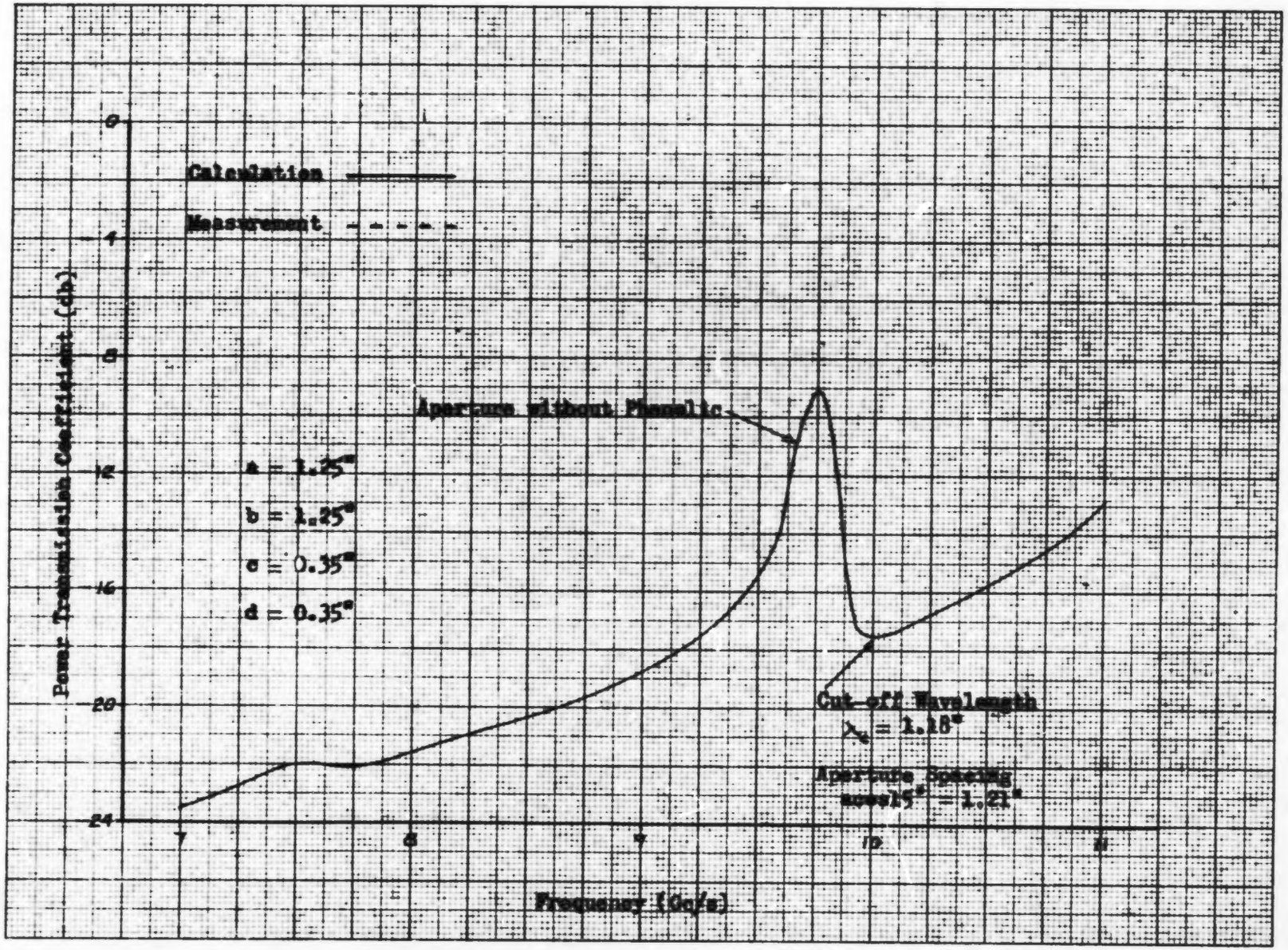

Fig. 8: Power Transmission Coefficient vs. Frequency for Normal Polarization. $\varphi = 15°$

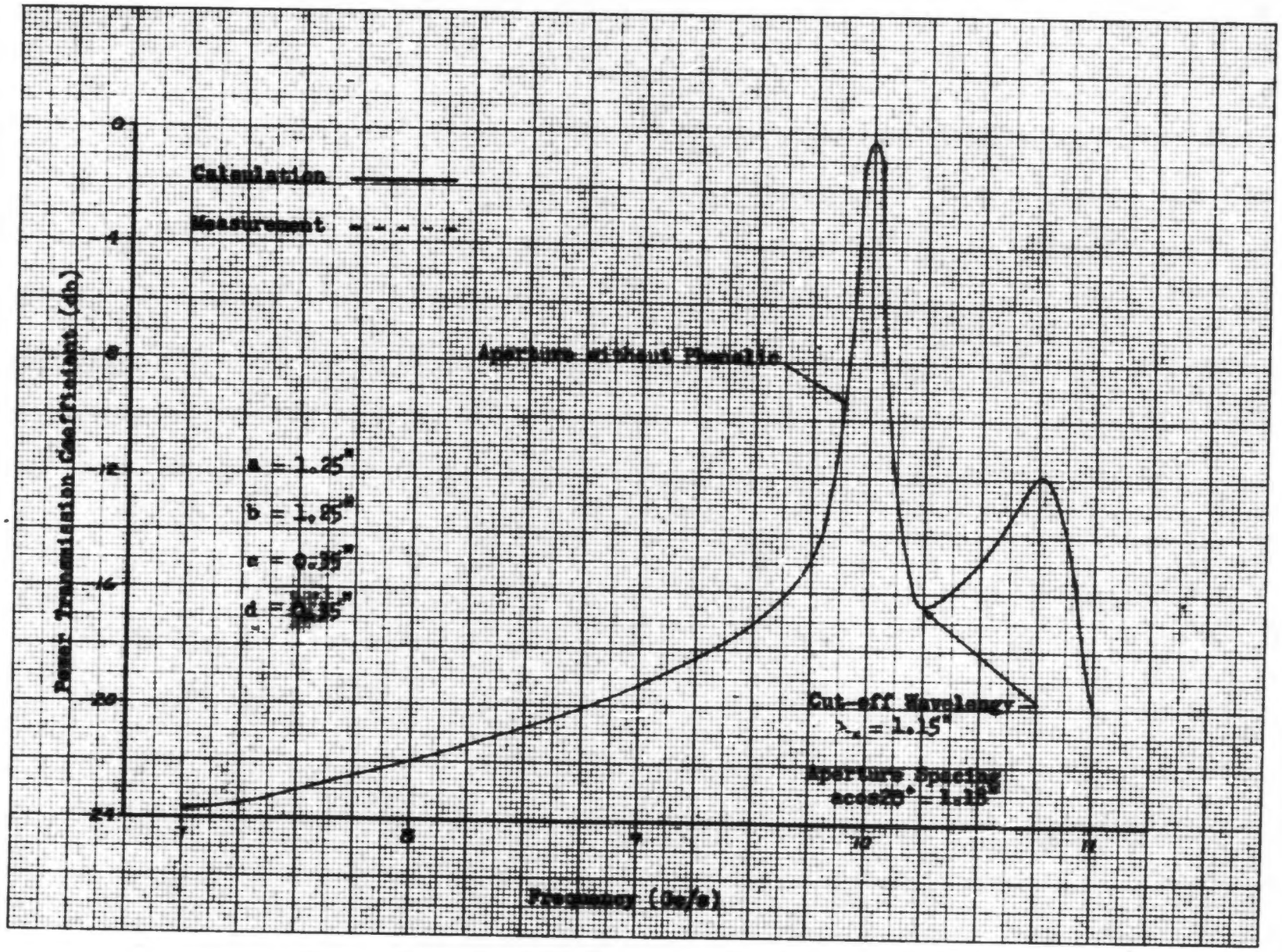

Fig. 9: Power Transmission Coefficient vs. Frequency for Normal Polarization. $\varphi = 20°$

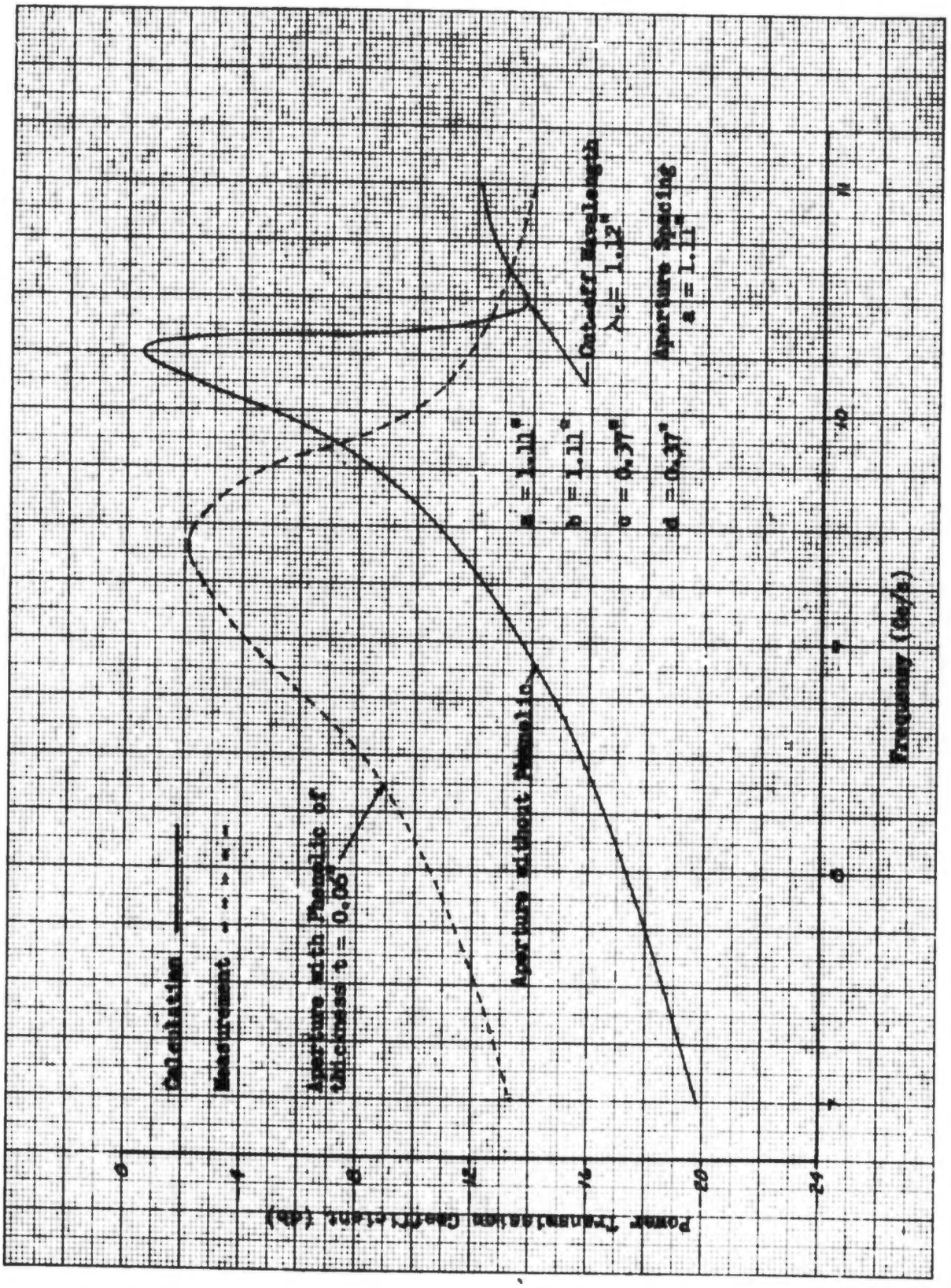

Fig. 10: Power Transmission Coefficient vs. Frequency for Normal Polarization. $\varphi = 0°$

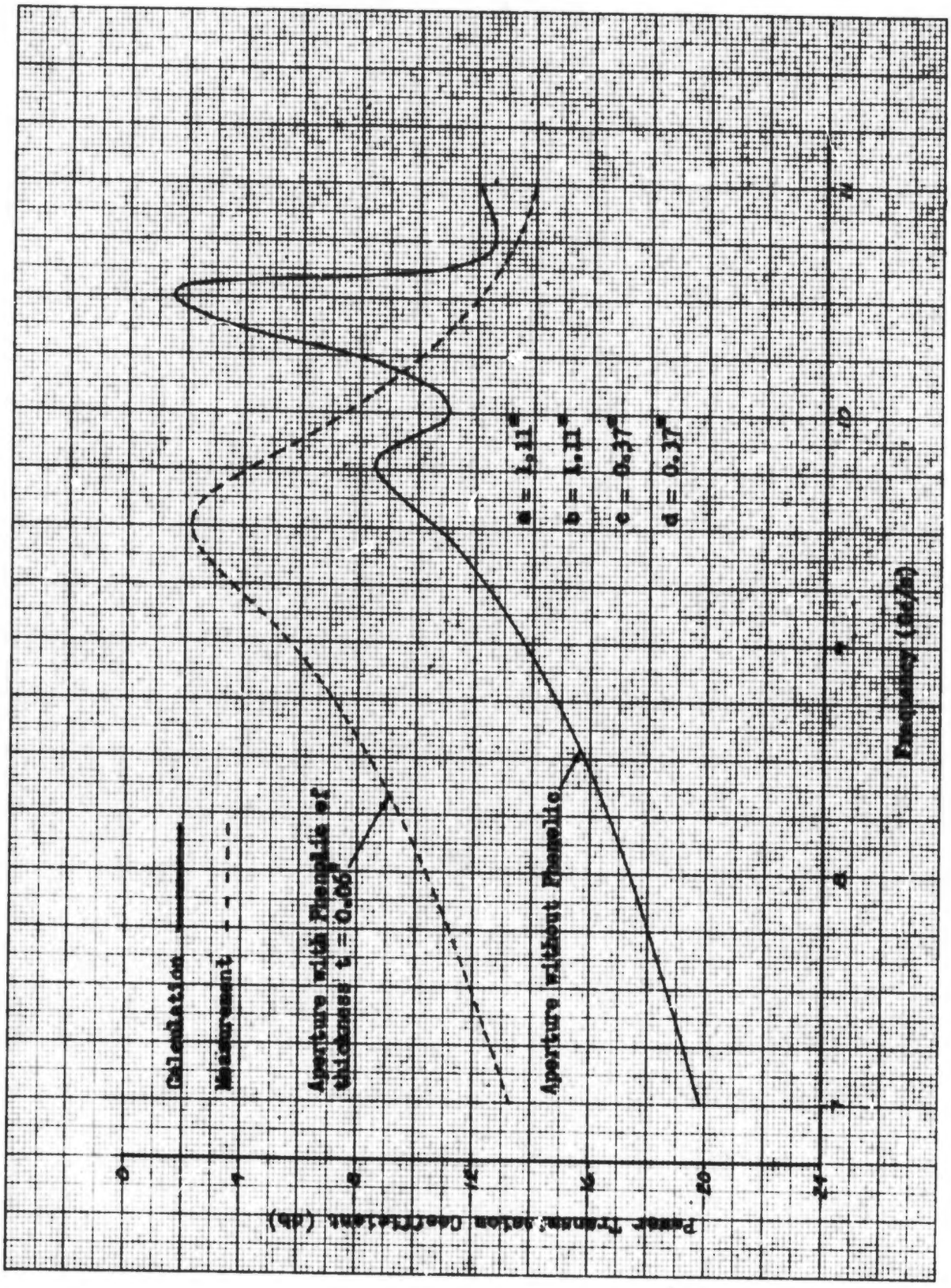

Fig. 11: Power Transmission Coefficient vs. Frequency for Normal Polarization. $\varphi = 5°$

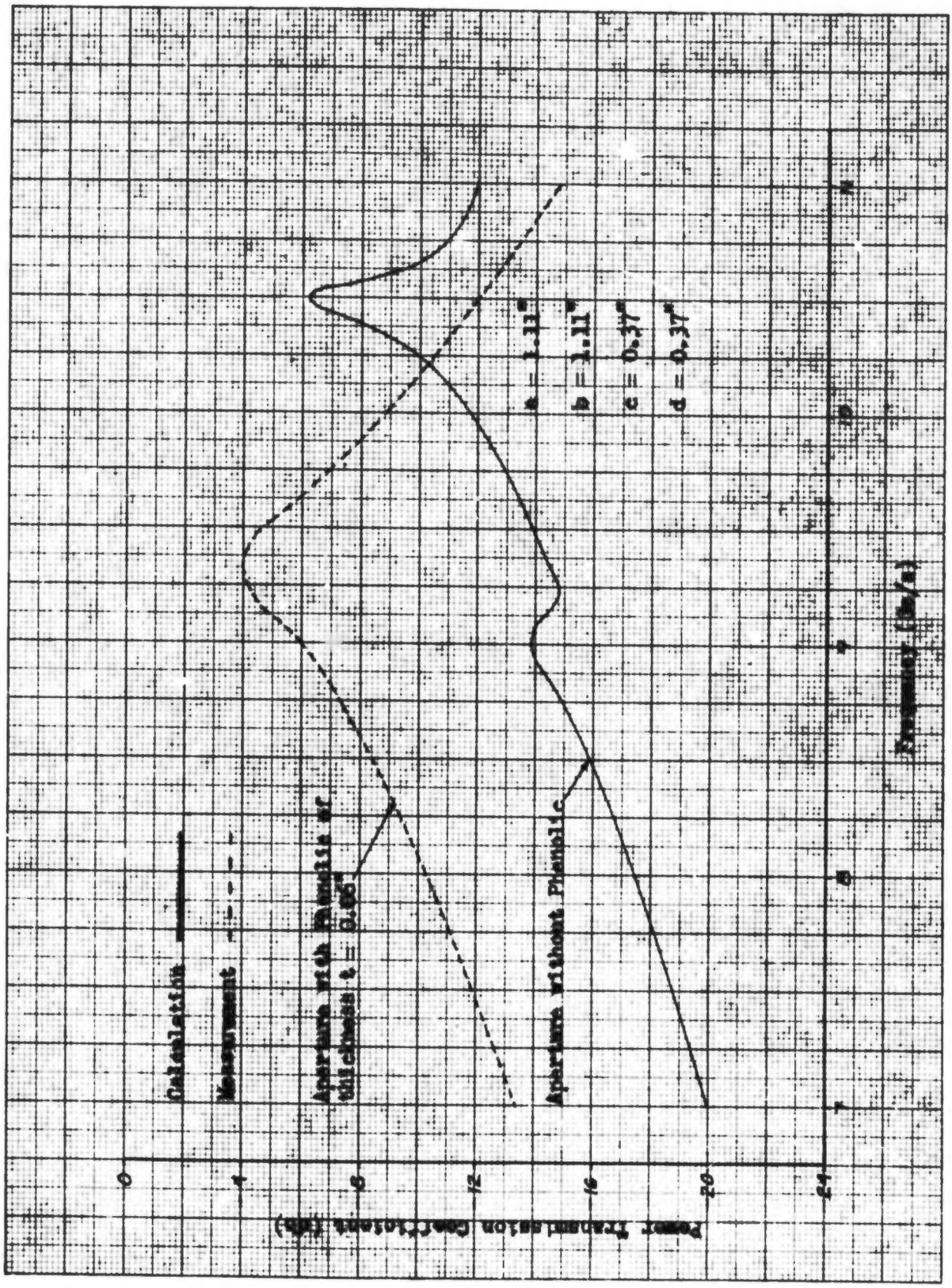

Fig. 12: Power Transmission Coefficient vs. Frequency for Normal Polarization. $\psi = 10°$

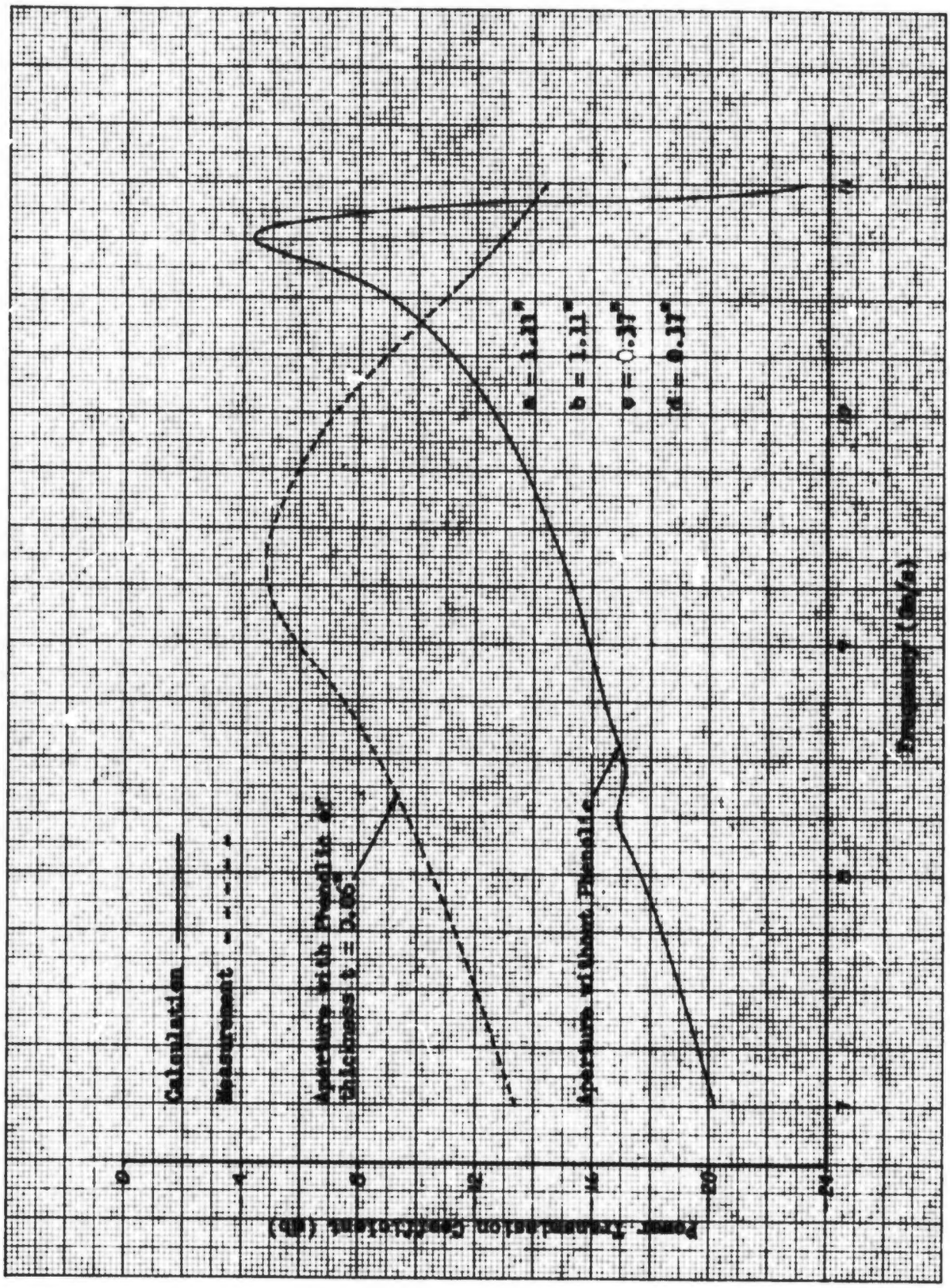

Fig. 13: Power Transmission Coefficient vs. Frequency for Normal Polarization. $\varphi = 15°$

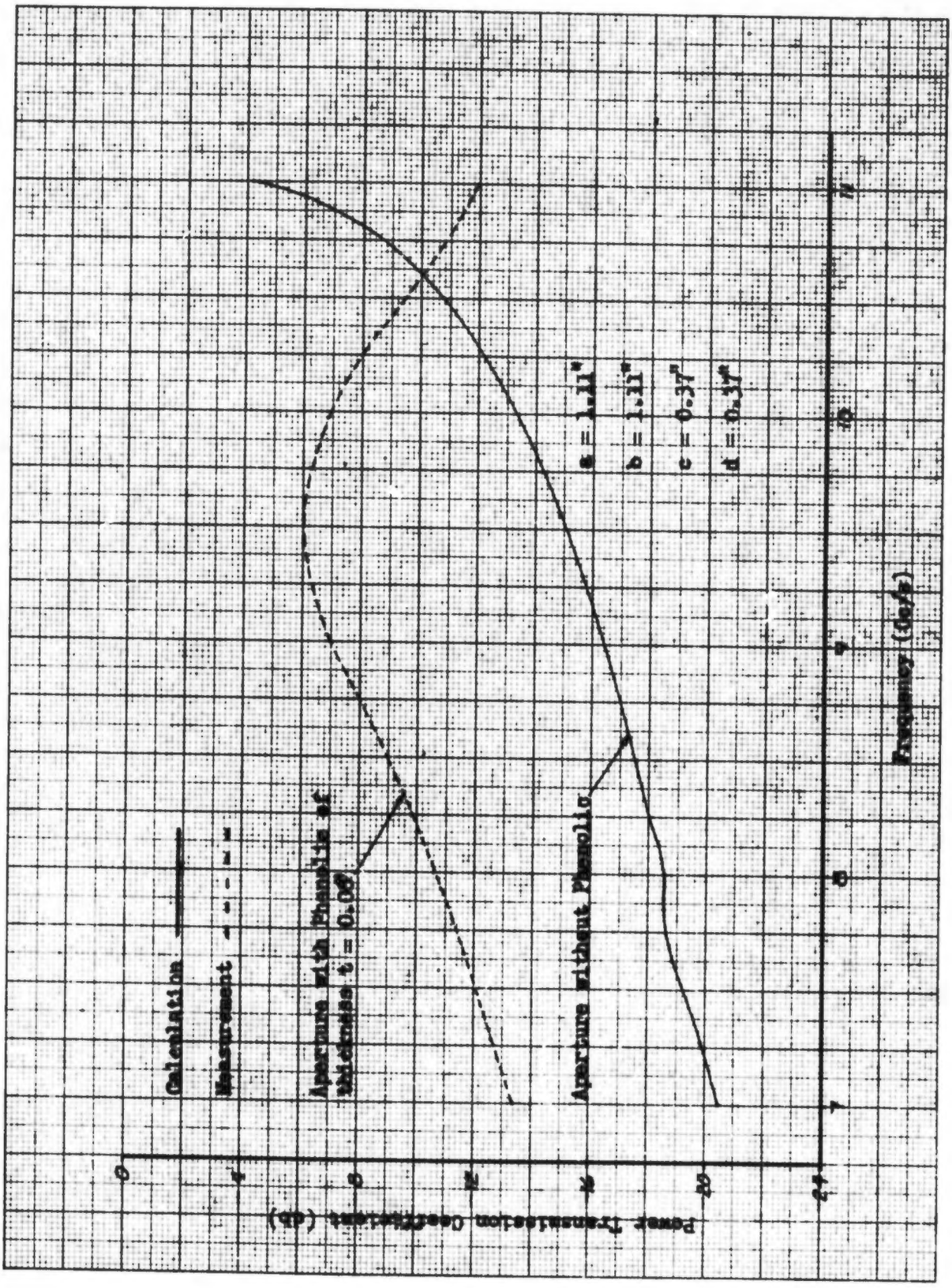

Fig. 14: Power Transmission Coefficient vs. Frequency for Normal Polarization. $\psi = 20°$

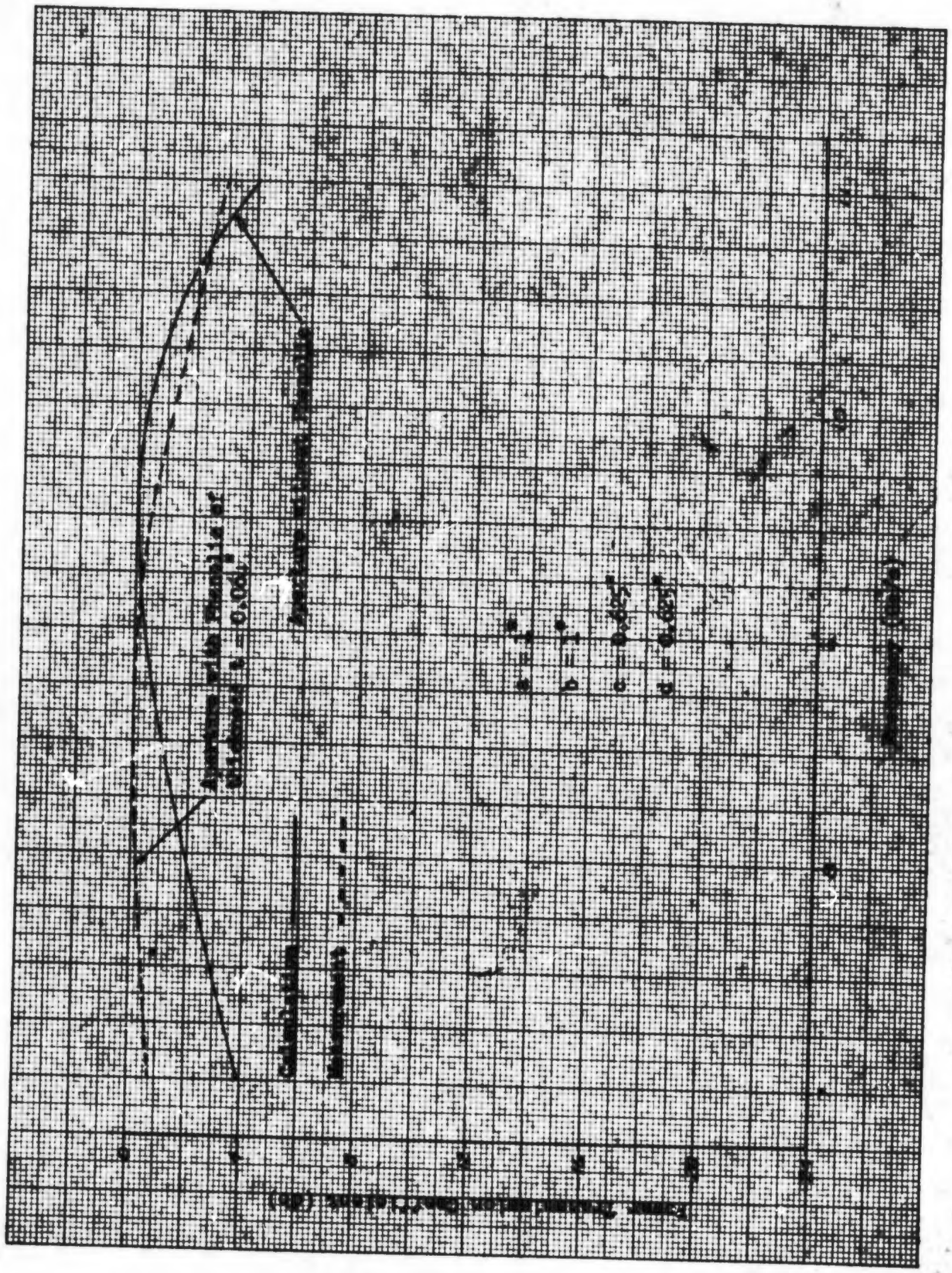

Fig. 15: Power Transmission Coefficient vs. Frequency for Normal Polarization. $\psi = 0°$

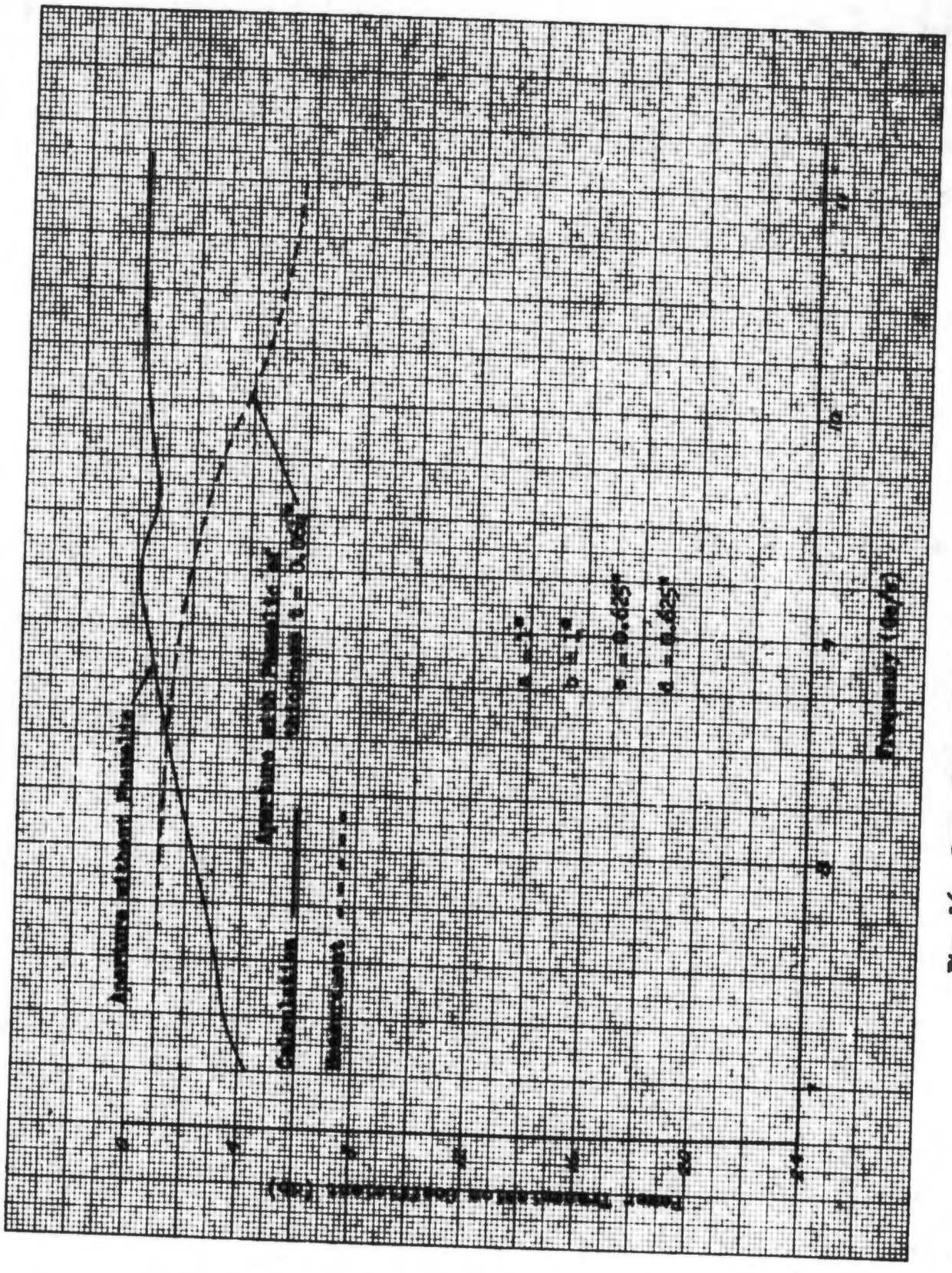

Fig. 16: Power Transmission Coefficient vs. Frequency for Normal Polarization. $\varphi = 15°$

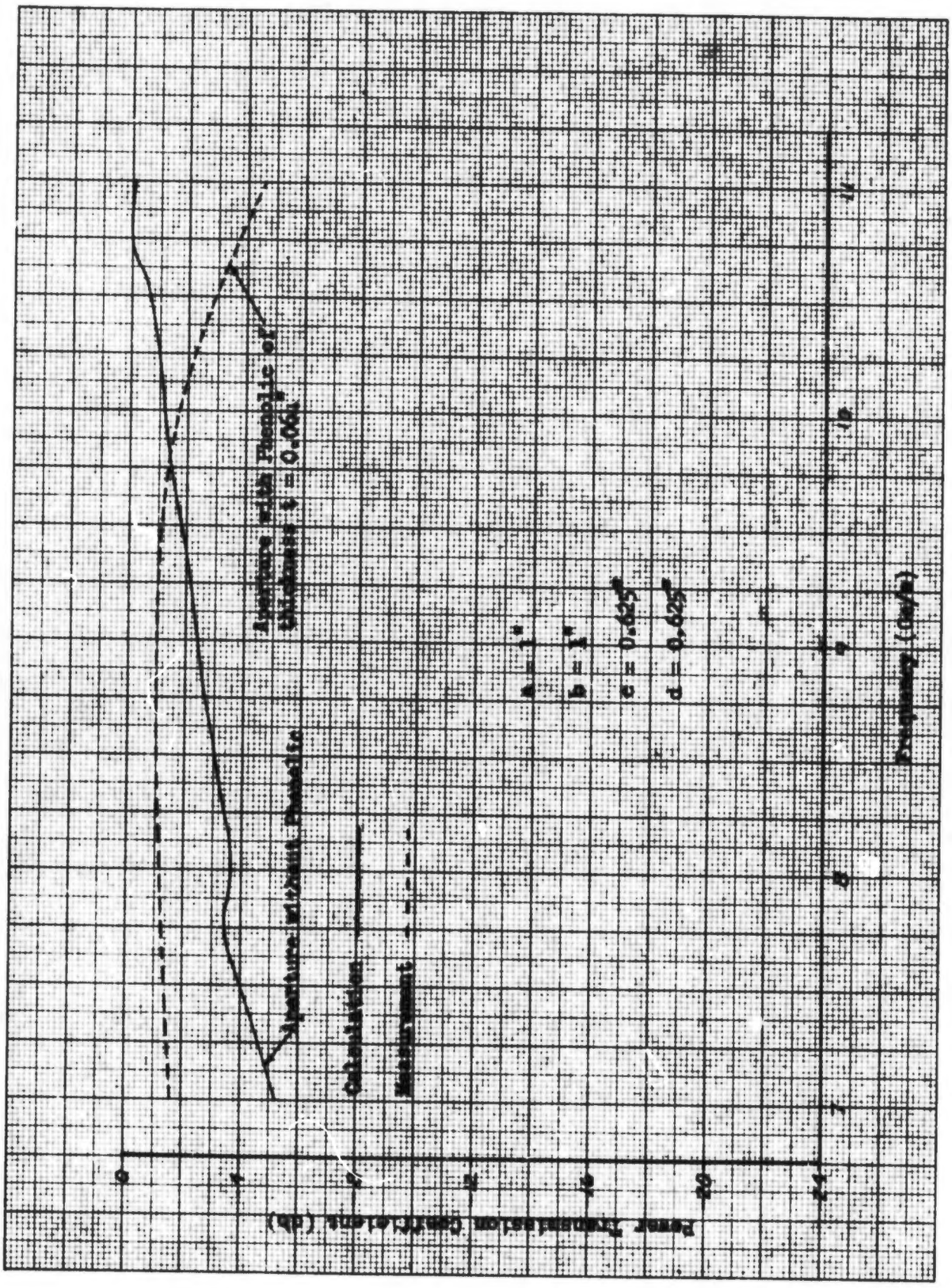

Fig. 17: Power Transmission Coefficient vs. Frequency for Normal Polarization. $\varphi = 30°$

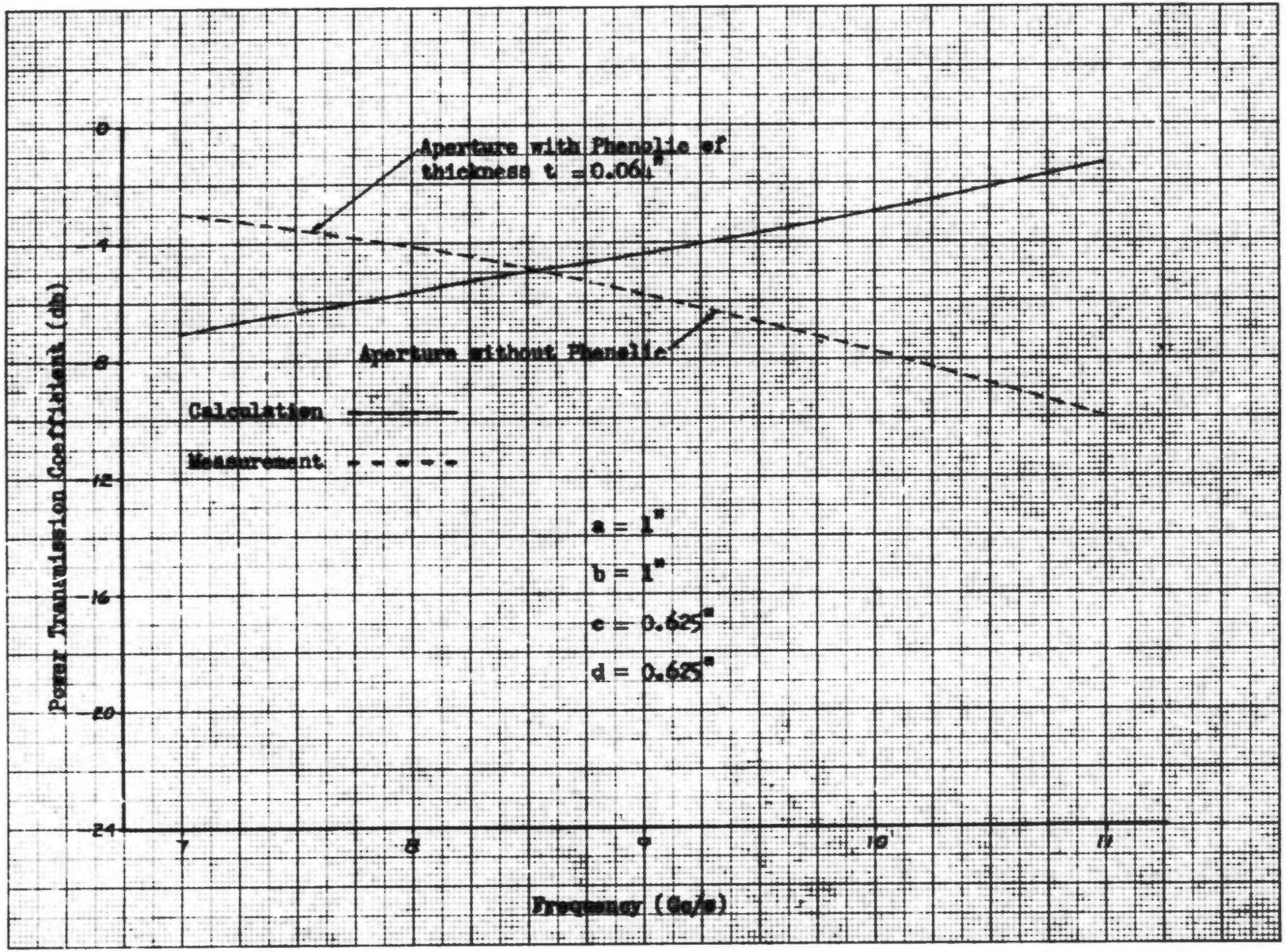

Fig. 18: Power Transmission Coefficient vs. Frequency for Normal Polarization. $\varphi = 45°$

horn and a receiving parabolic antenna placed about 25 feet apart. The apertured screen and receiving antenna are shown in Fig. 19. It must be pointed out that the apertures of the conducting screen were phenolic, while for calculations the apertures were air. It is known that the higher the dielectric constant, the larger is the aperture to E-M waves. As mentioned before, the larger the aperture, the broader is the bandwidth of frequency. This explains why the shift of the peak as a function of incident angle and the Wood anomalies in the measurements are not as explicit as those in the calculations (Figs. 5-18).

B. Parallel Polarization

The voltage transmission coefficient T of parallel polarization was also calculated as a function of wave number K_θ and aperture spacing b for each incident angle θ. Conversion of the voltage transmission coefficient and wave number into the attenuation (-db) and frequency f was also made for the purpose of comparison to that of measurements.

A striking phenomenon is observed which is similar to that noticed by R. W. Wood[8-11] and L. Rayleigh[6] early in the twentieth century. That is, there are two peaks of transmission across a certain frequency band (7-11 Gc/s). As the angle of incidence decreases, the two peaks approach one another and coincide when the incidence is normal (Figs. 20-30). As the angle of incidence increases (from 0° to 5°), the amplitude of the two peaks decreases (Figs. 24-27). With further increase of the incident angle ($>5^\circ$), one peak moves toward the lower frequency band with its amplitude first increasing (from 5° to 10°) and then decreasing ($>10^\circ$), while the other moves toward the higher frequency band with its amplitude increasing. This phenomenon may be caused by the fact that changing the angle of incidence changes the aperture spacing and width which dominate the amplitude and frequency of the peak of transmission. As the angle of incidence increases, the aperture width becomes narrower and spacing smaller, hence the higher order mode tends to pass off. In other words, a transition of the propagating mode takes place.

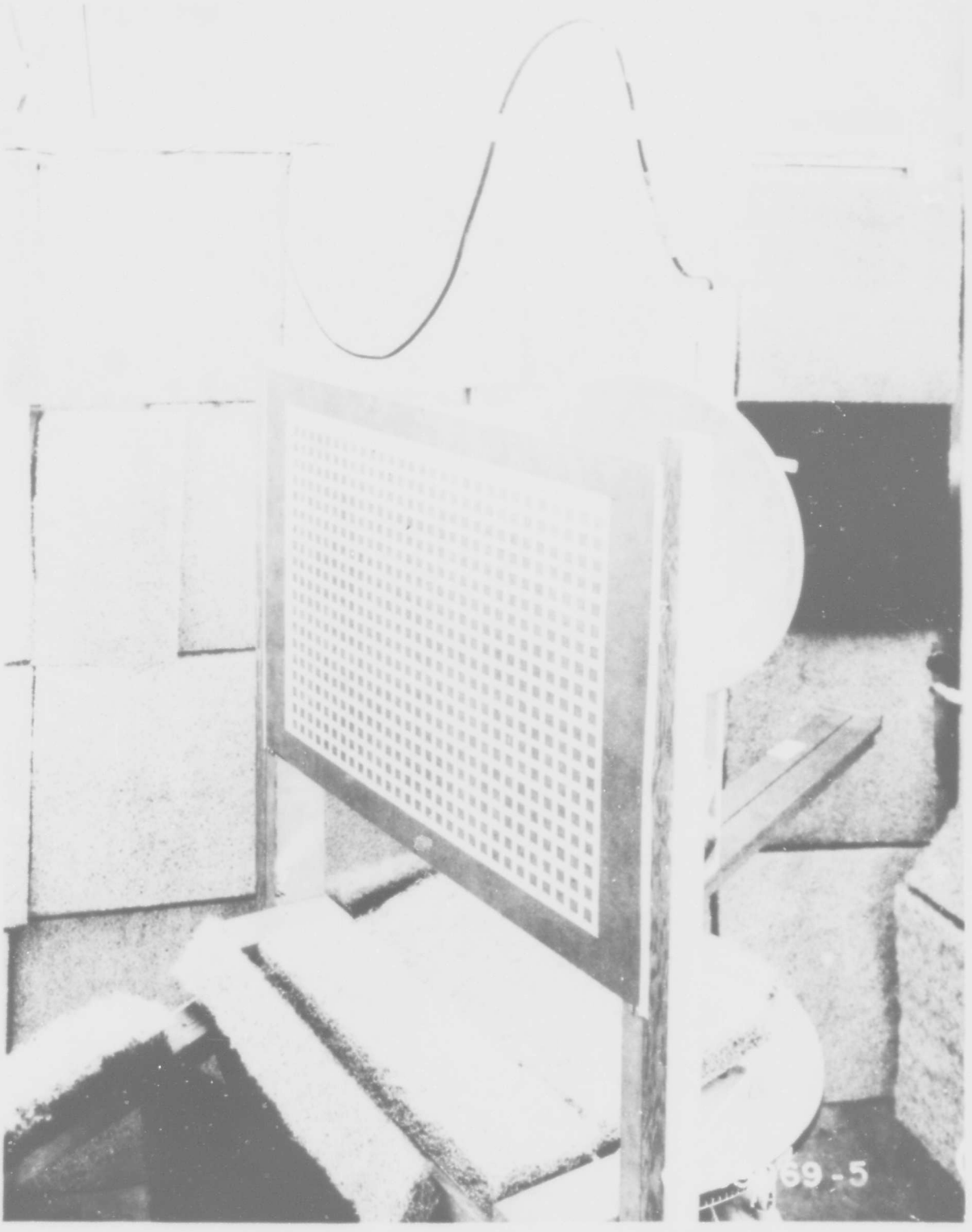

Figure 19 EXPERIMENTAL MEASUREMENT FOR NORMAL POLARIZATION

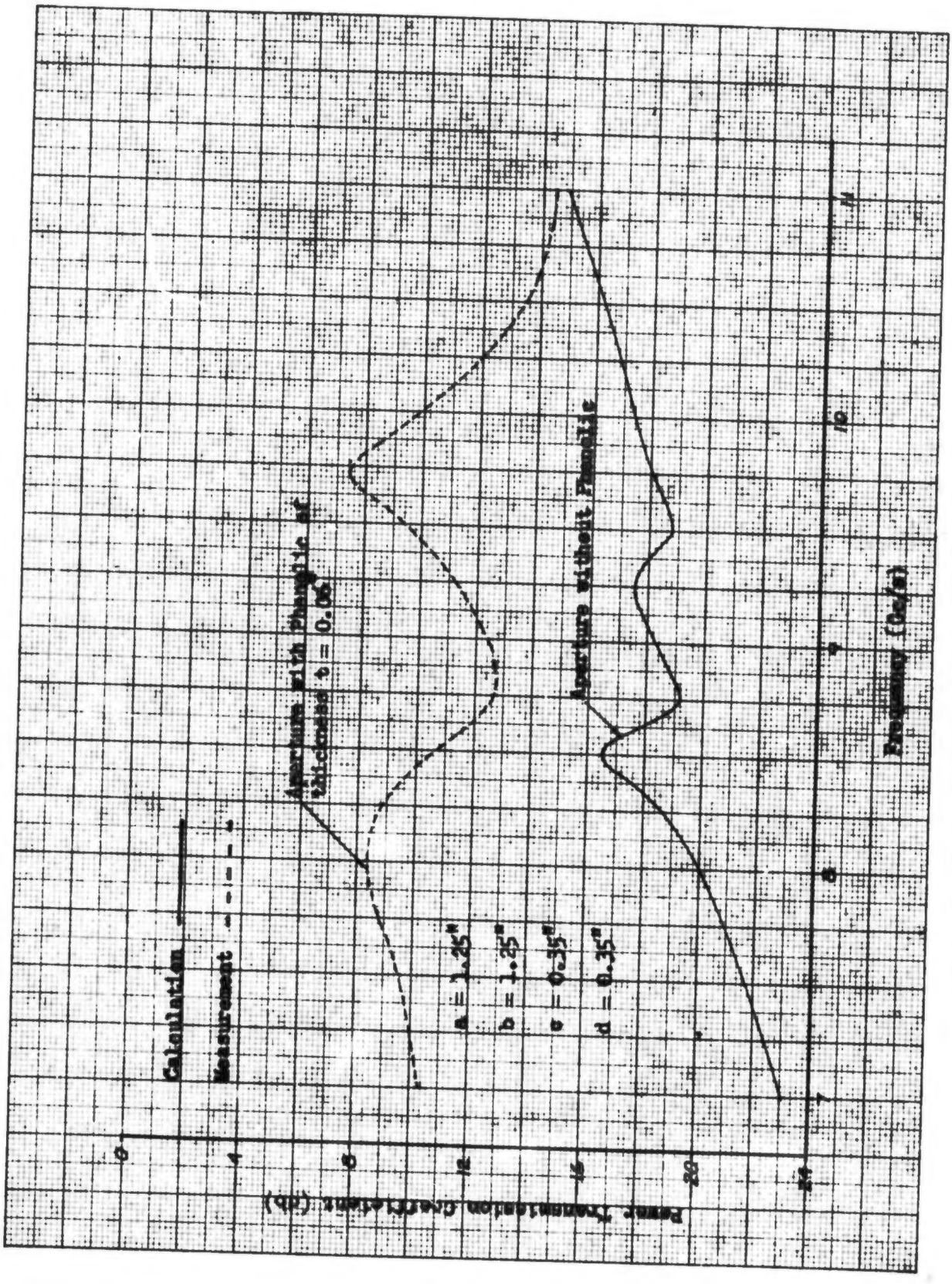

Fig. 20: Power Transmission Coefficient vs. Frequency for Parallel Polarization. $\theta = 5°$

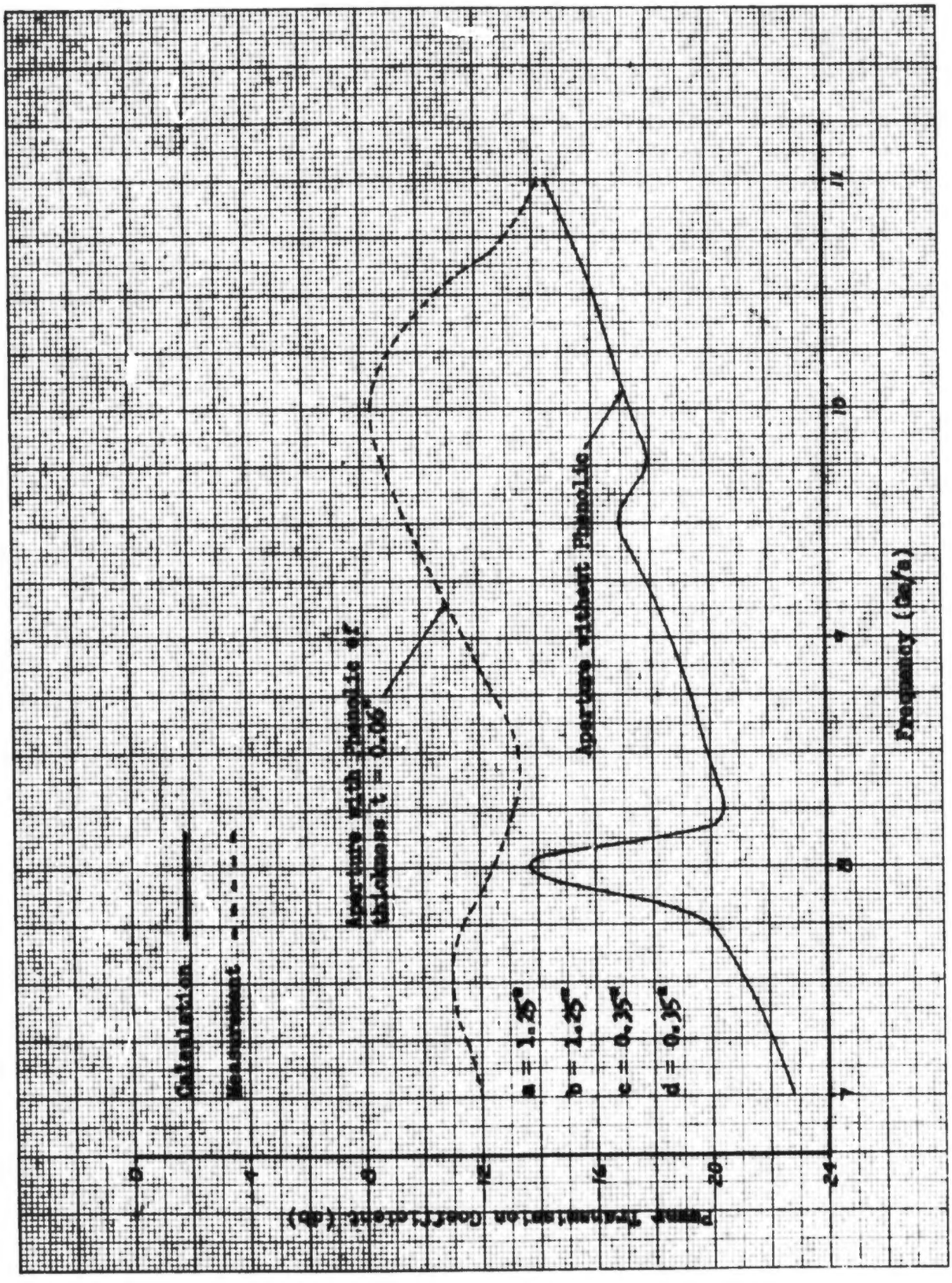

Fig. 21: Power Transmission Coefficient vs. Frequency for Parallel Polarization. $\theta = 10°$

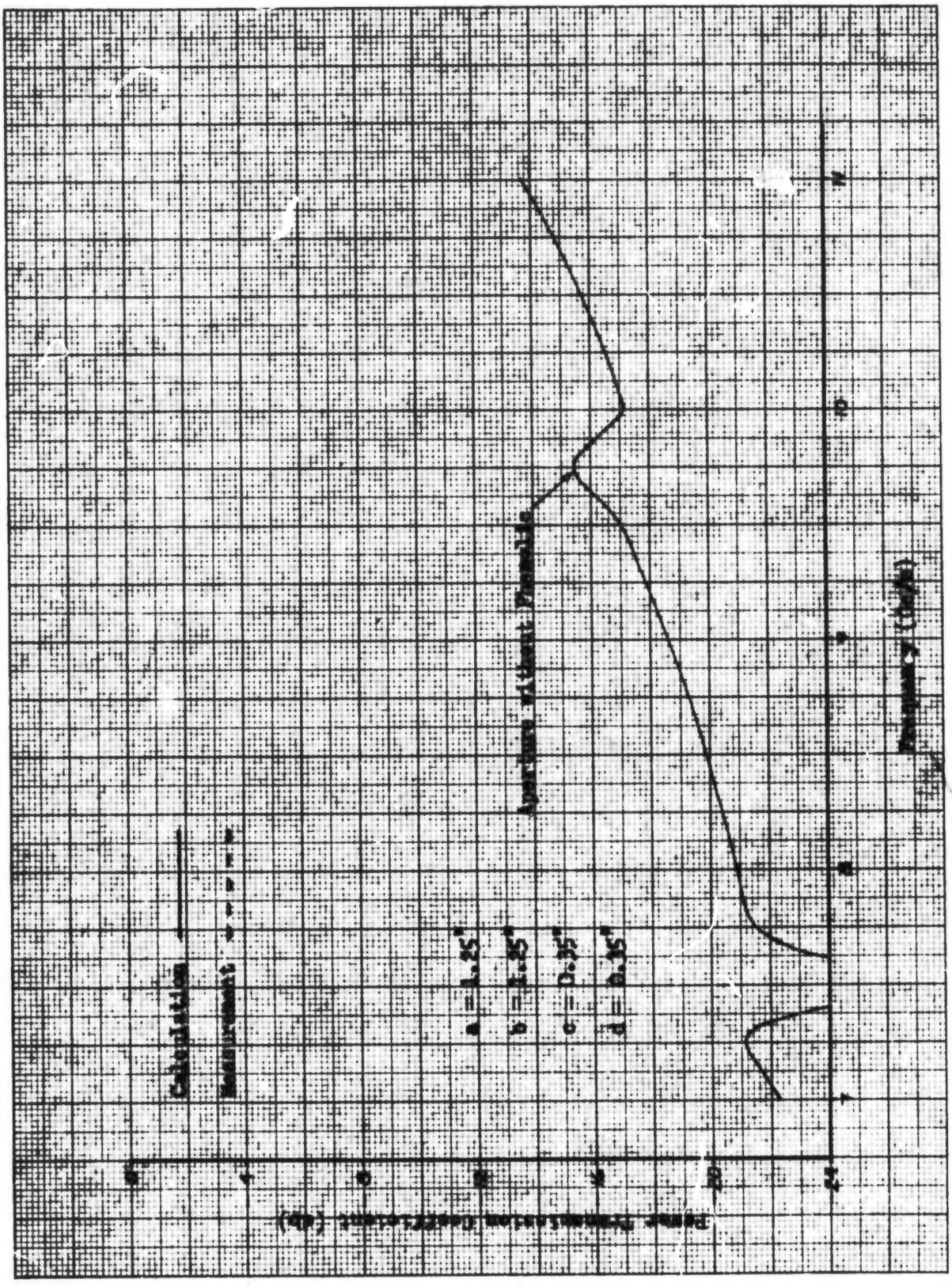

Fig. 22: Power Transmission Coefficient vs. Frequency for Parallel Polarization. $\theta = 15°$

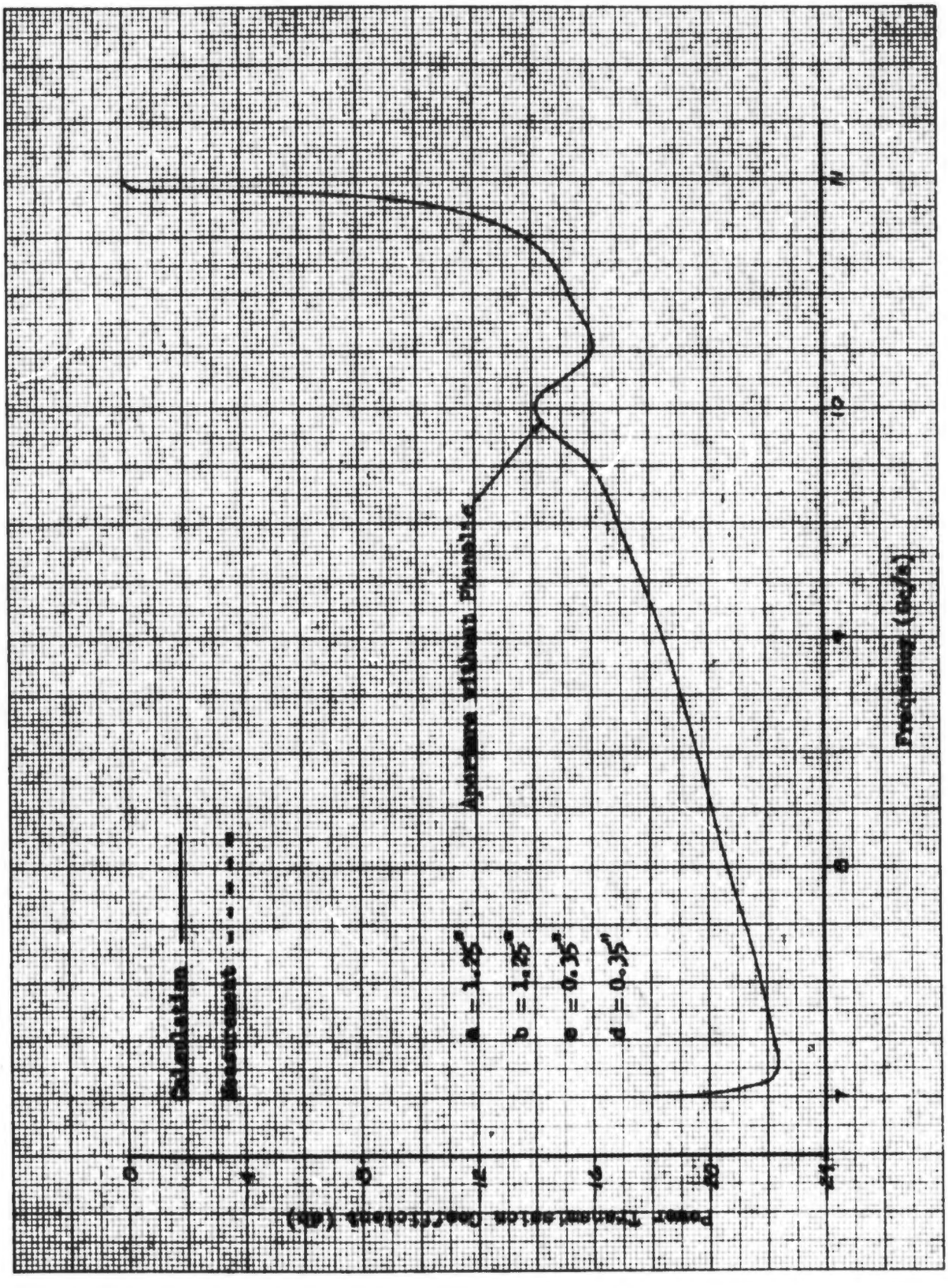

Fig. 23: Power Transmission Coefficient vs. Frequency for Parallel Polarization. $\theta = 20°$

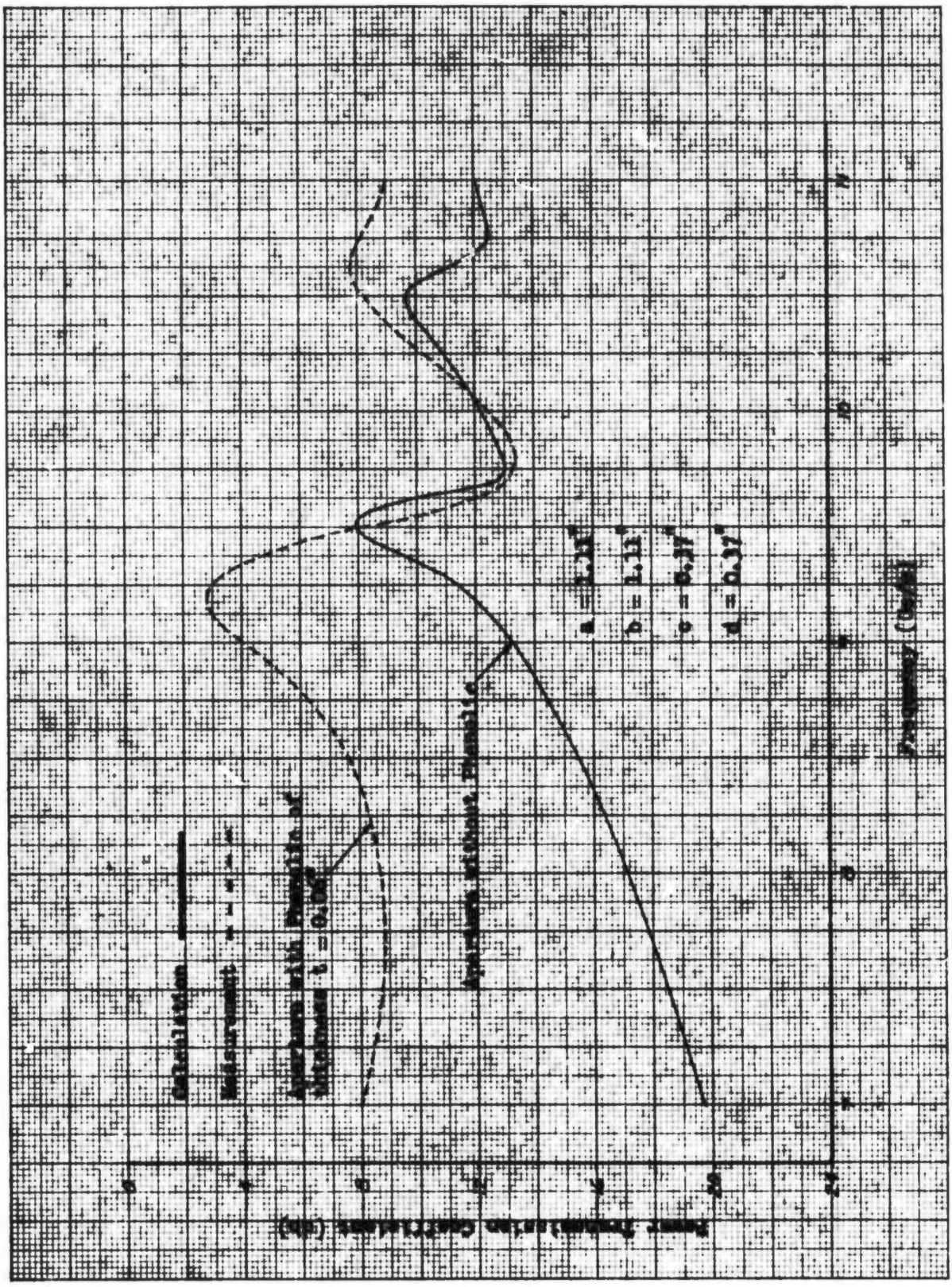

Fig. 24: Power Transmission Coefficient vs. Frequency for Parallel Polarization. $\theta = 5°$

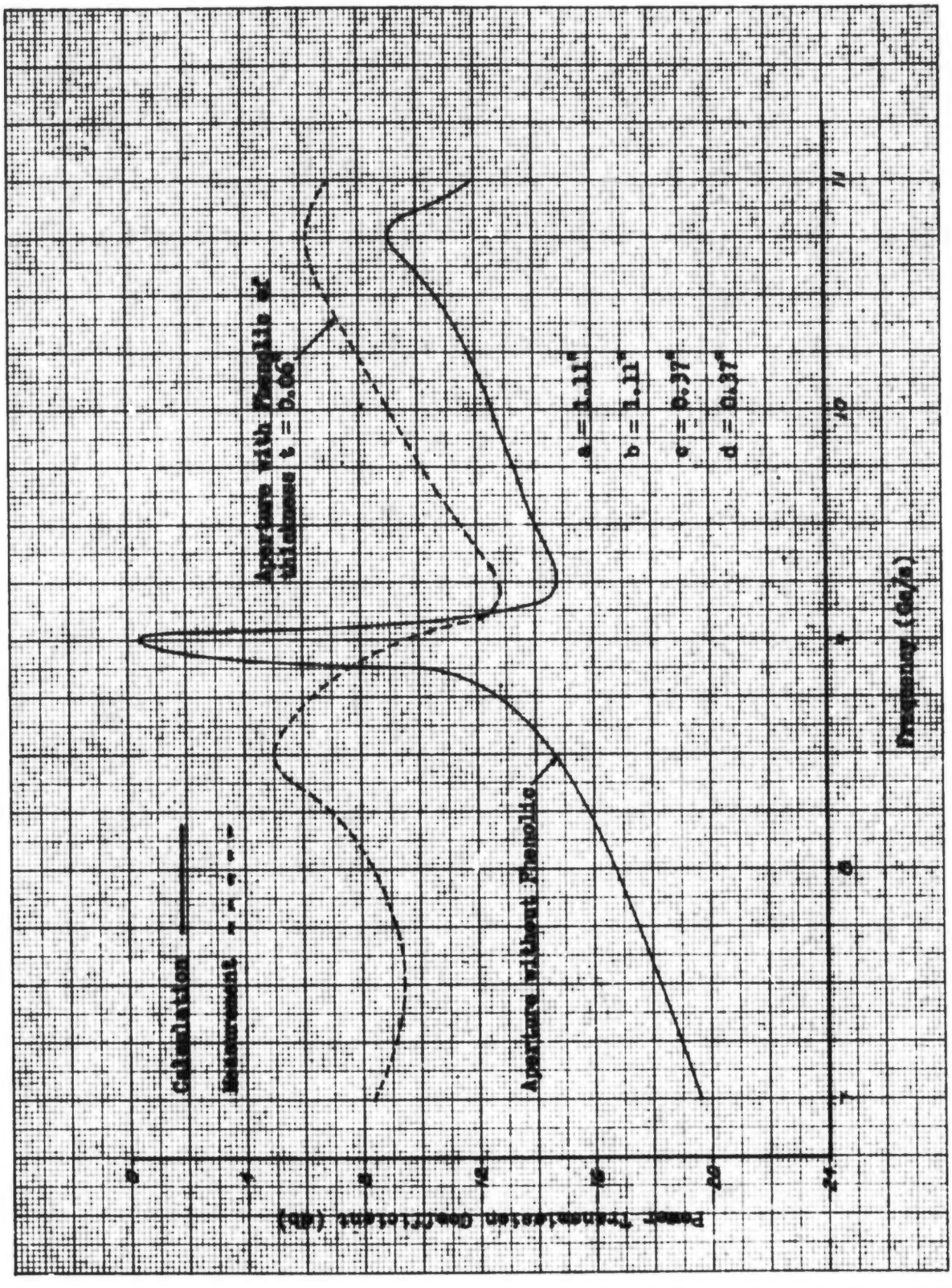

Fig. 25: Power Transmission Coefficient vs. Frequency for Parallel Polarization. $\phi = 10°$

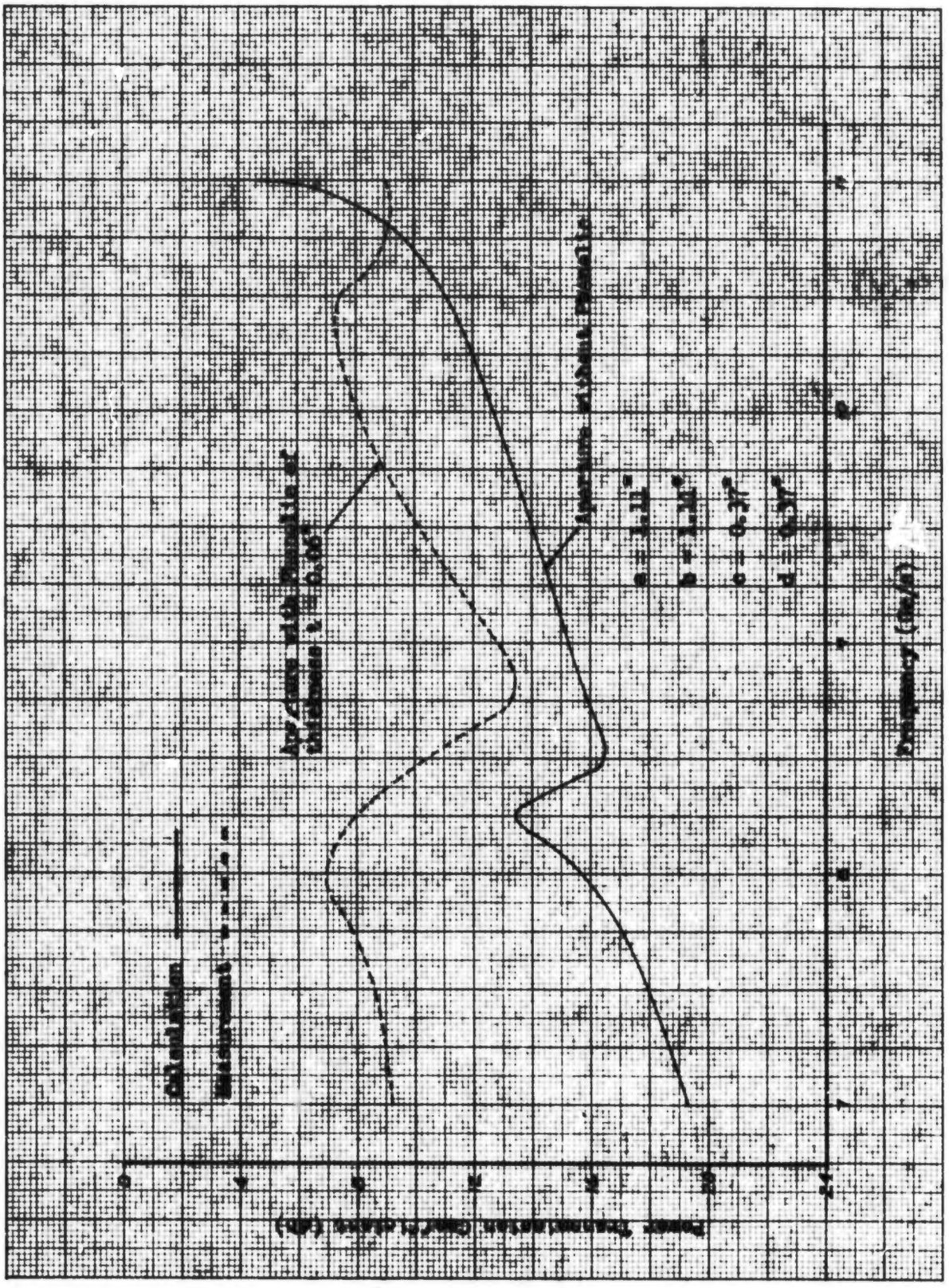

Fig. 26: Power Transmission Coefficient vs. Frequency for Parallel Polarization. $\theta = 15°$

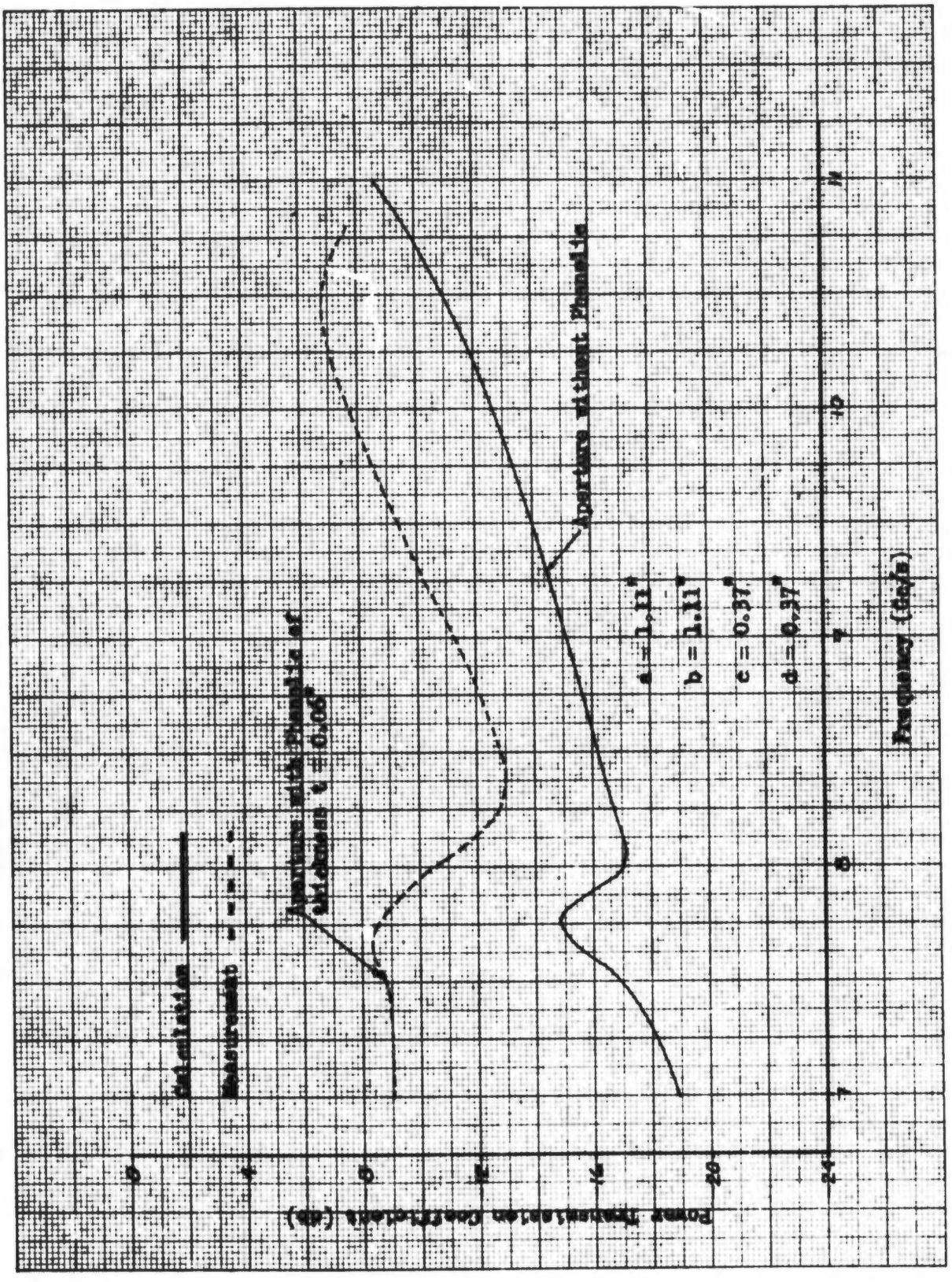

Fig. 27: Power Transmission Coefficient vs. Frequency for Parallel Polarization. $\theta = 20°$

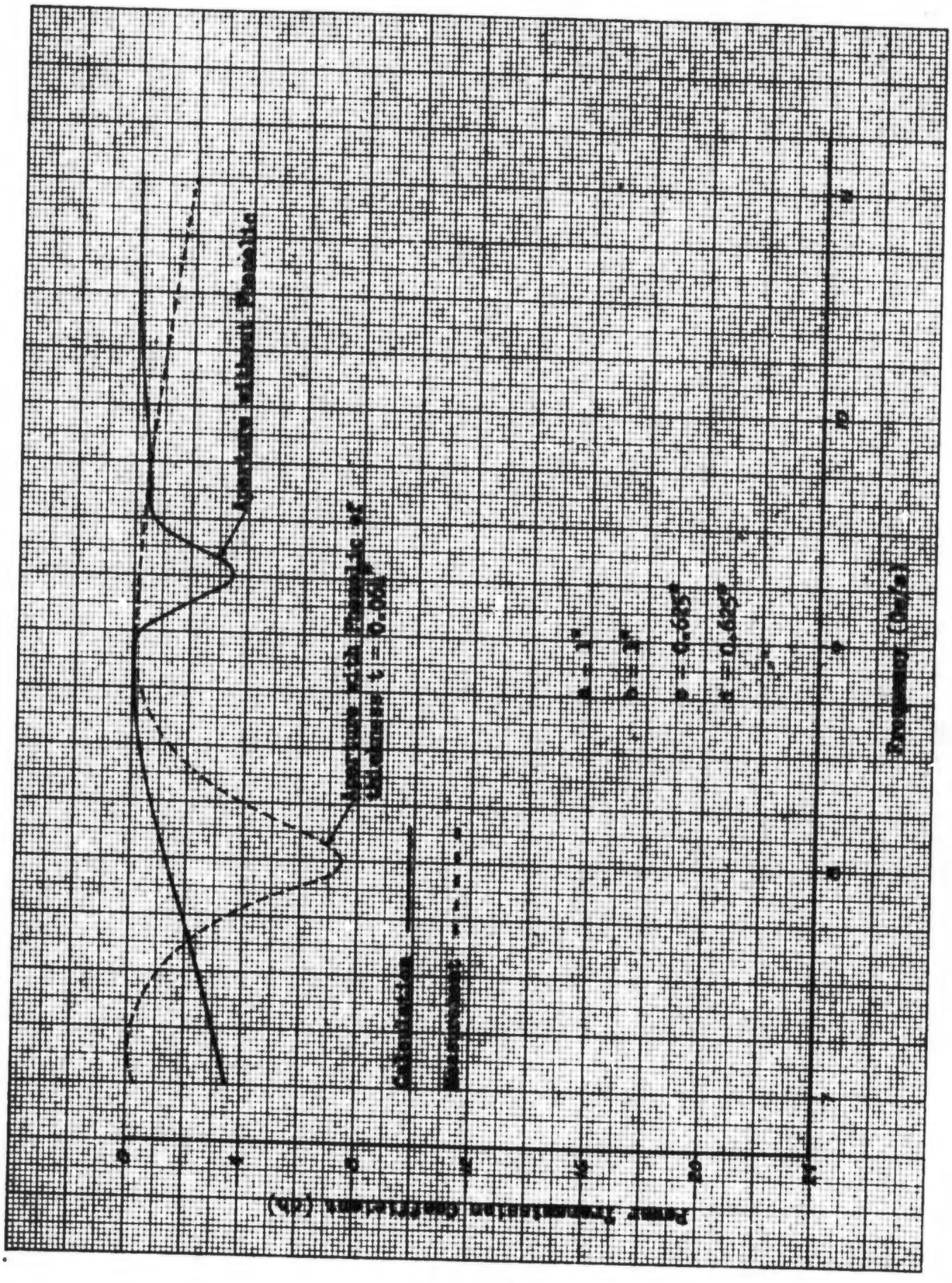

Fig. 28: Power Transmission Coefficient vs. Frequency for parallel Polarization. $\theta = 15°$

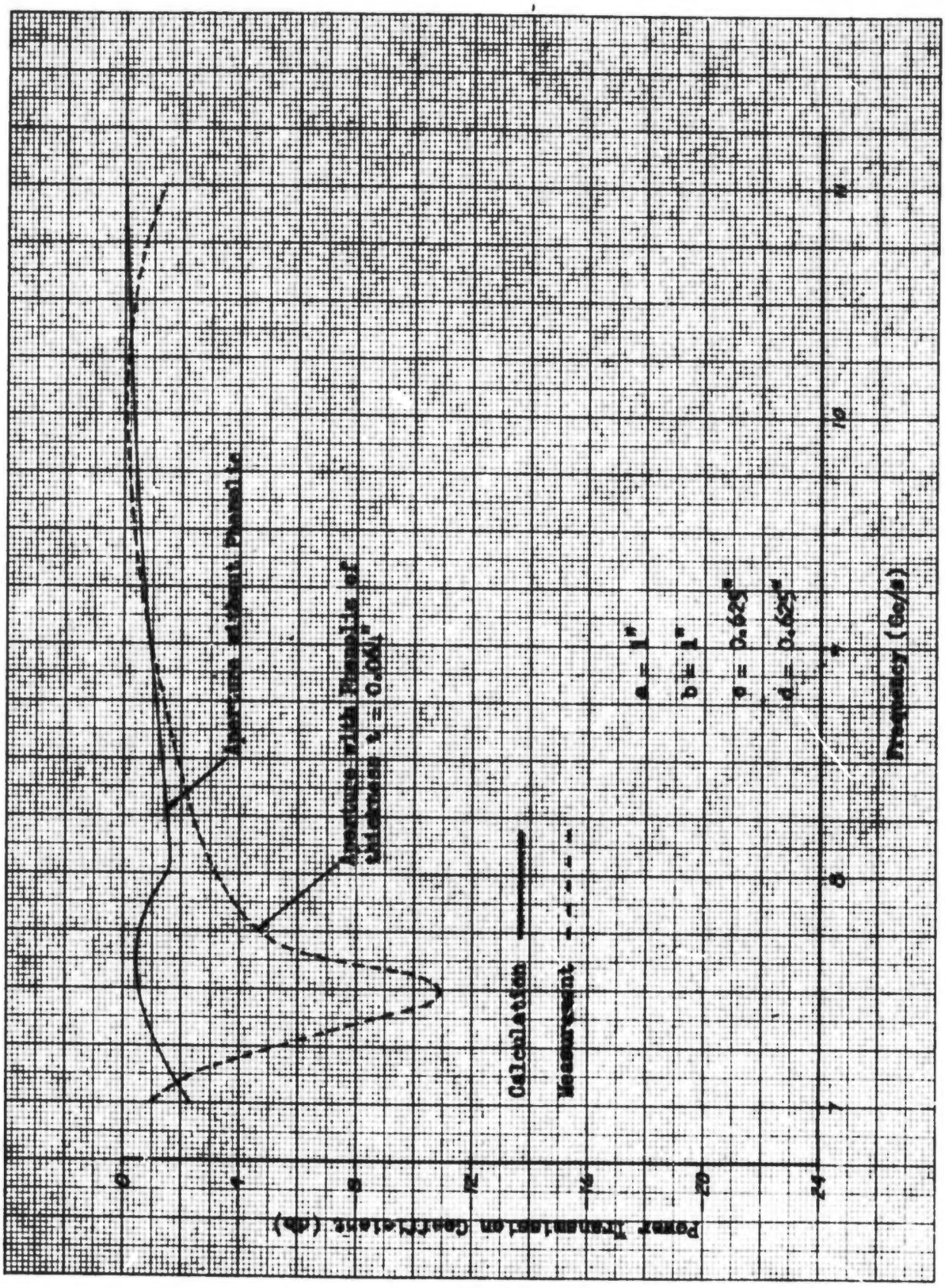

Fig. 29: Power Transmission Coefficient vs. Frequency for Parallel Polarization. $\theta = 30°$

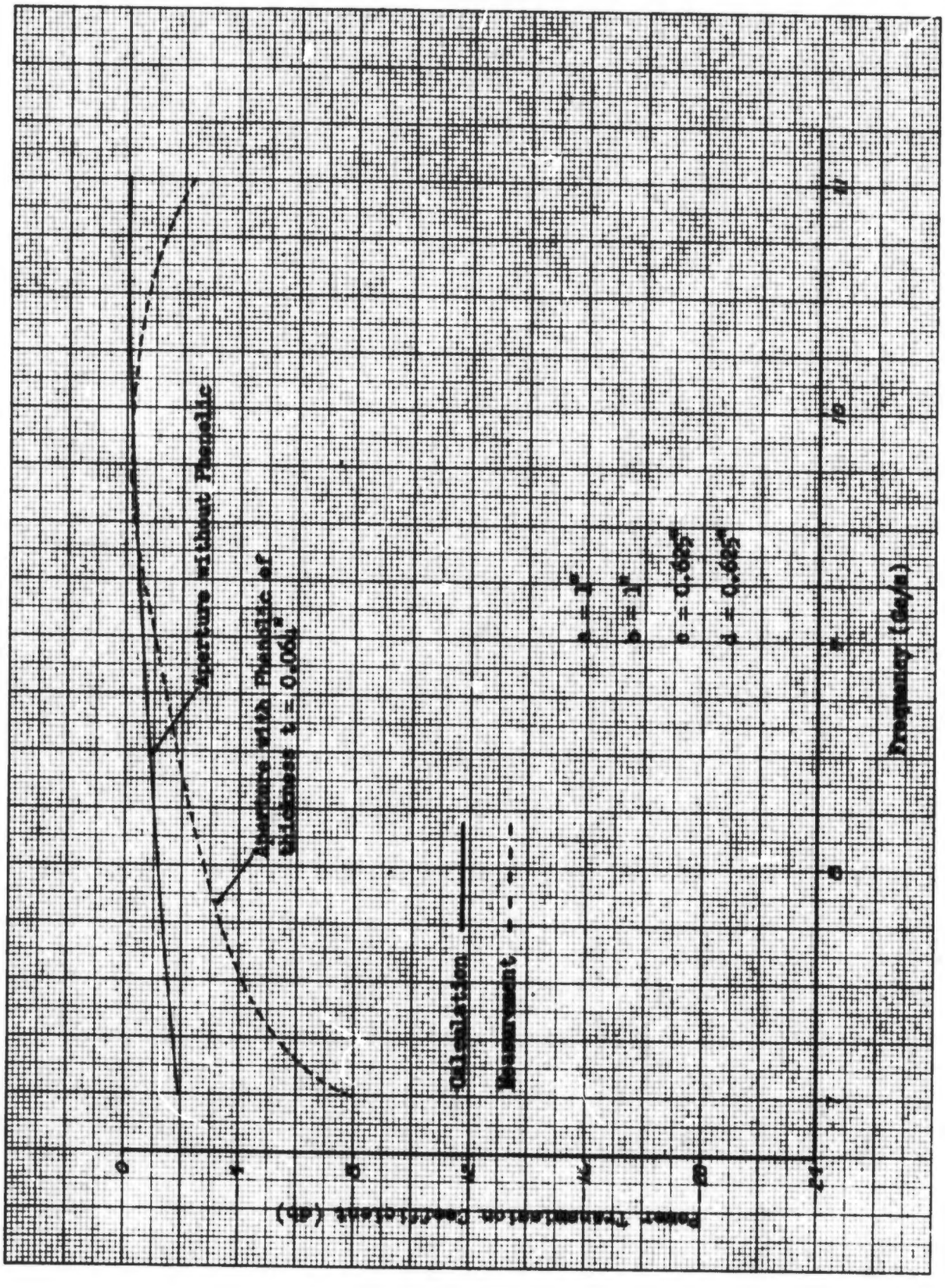

Fig. 30: Power Transmission Coefficient vs. Frequency for Parallel Polarization. $\theta = 45°$

An apertured conducting screen and receiving reflector were shown in Fig. 31 for experimental verification of the parallel polarization calculations. The abnormal energy distributions (two peaks) were obvious as was expected from the calculations (Figs. 20-30). Because of the assumption of a plane wave, infinitesma thickness of the screen, and air aperture which was not possible to achieve in the experiment, difference between calculated and measured results were expected. However, close agreement in the variation of intensity was obtained.

C. Normal Incidence

The voltage transmission coefficient T of normal incidence was also calculated to complete the analysis. Curves T vs. $k_n a$ were obtained for different aperture spacings and dimensions (Figs. 32-49), where k_n is wave number and a is aperture spacing.

Several interesting phenomena were observed. First, by increasing aperture spacing ratio, a/b, (from 1 to 5) with constant ratios of c/a = 1/2 and d/b = 1/3, the peak of transmission is shifted toward the higher value of $k_n a$ and becomes flatter (Figs. 32-36). Second, by increasing the side of aperture c, which is perpendicular to the electric field, with constant ratios of a/b = 2 and d/b = 1/2, the peak (of transmission) is shifted toward the lower value of $k_n a$, and also becomes flatter (Figs. 37-42). Third, by increasing the width of apertures d, which is parallel to the electric field, with constant ratios of a/b = 2 and c/b = 1/2, the peak is not shifted, but does flatten out (Figs. 43-49).

Experimental measurements were also conducted to confirm the calculations. A fenestrated conducting screen with apertures of phenolic and a receiving reflector for normal incidence measurements are shown in Fig. 50. A fenestrated aluminum foil with apertures of air was also made for the measurement. When compared, these showed a close

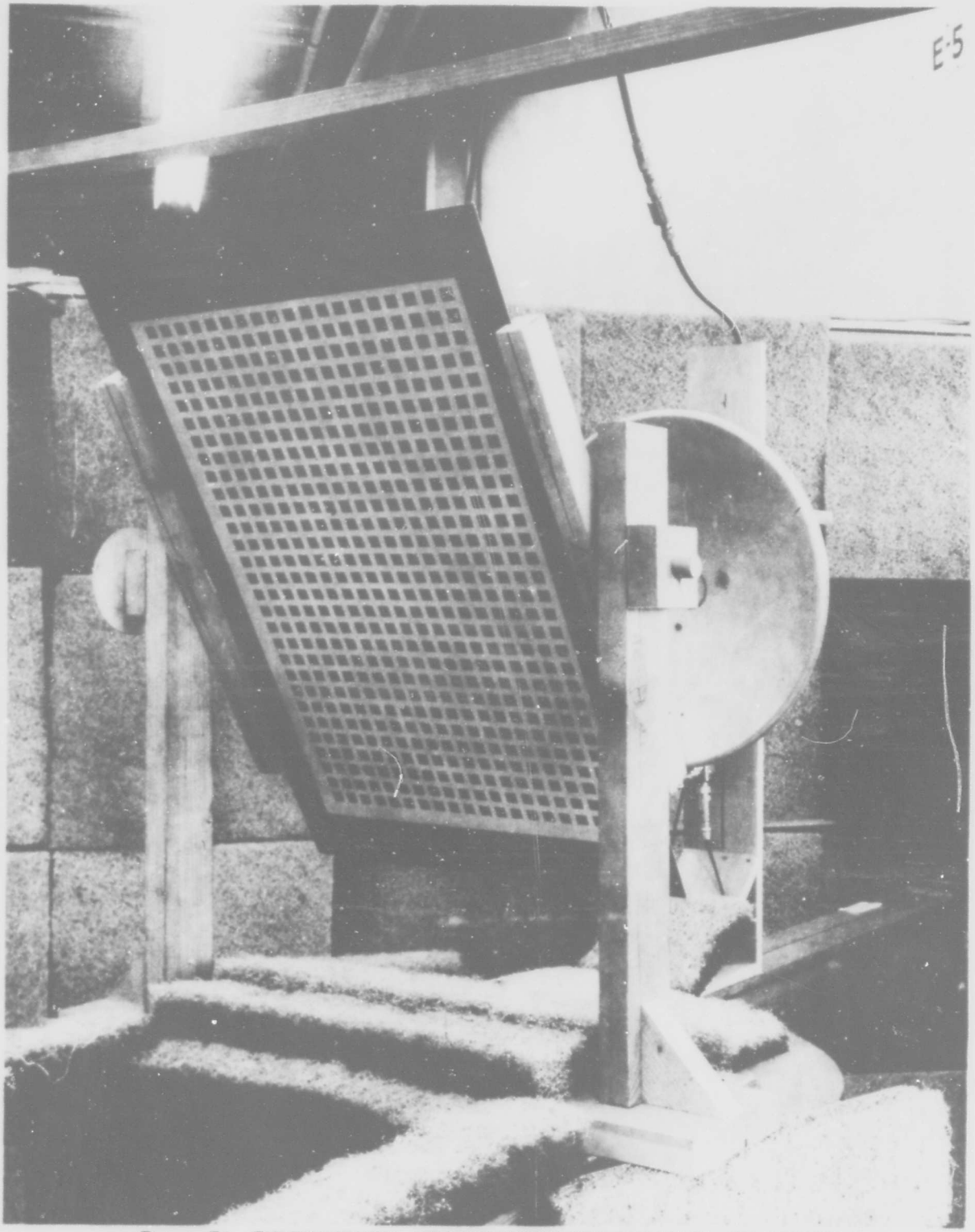

Figure 31 EXPERIMENTAL MEASUREMENT FOR PARALLEL POLARIZATION

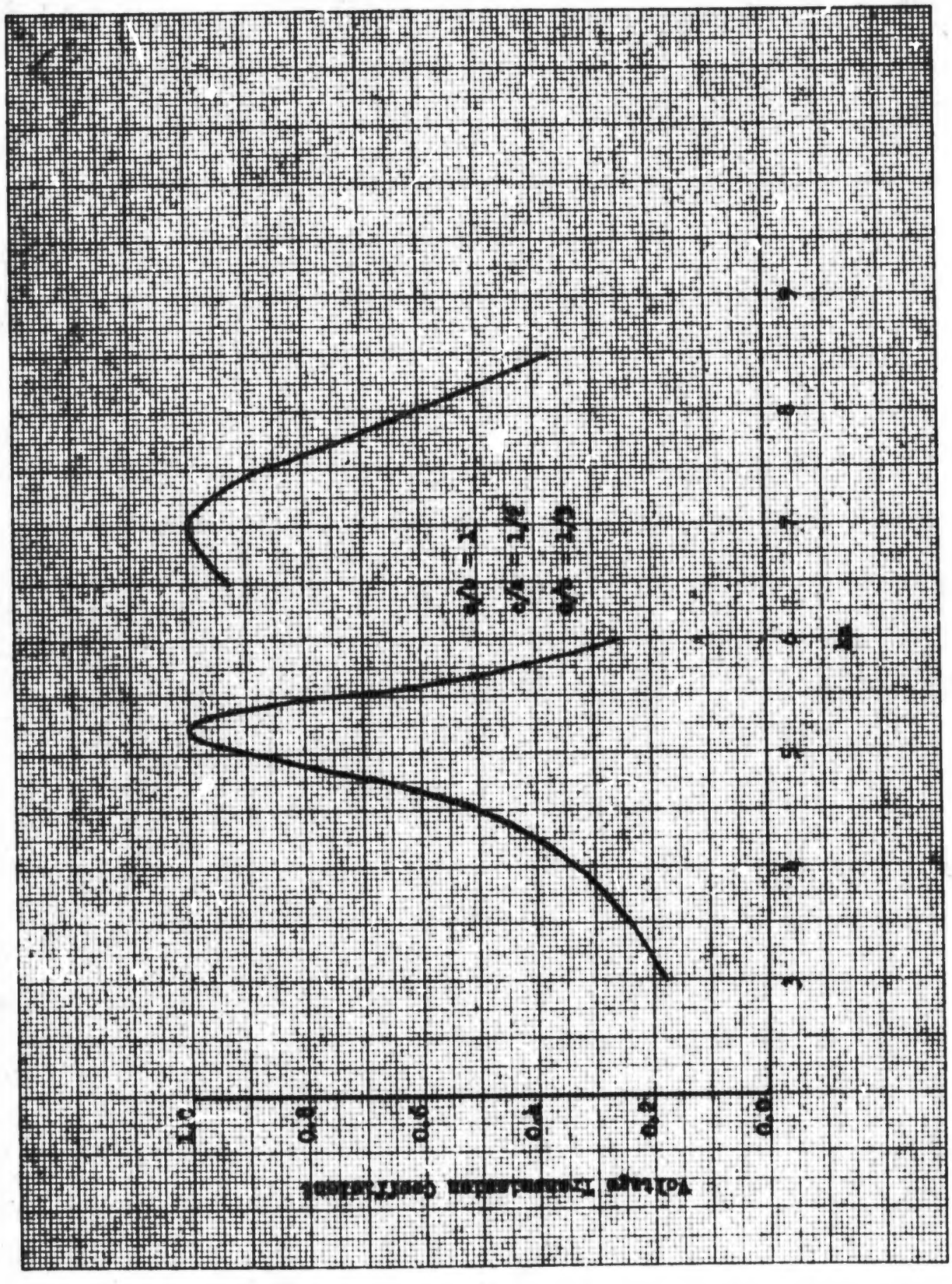

Fig. 32: Voltage Transmission Coefficient vs. k_0 for Normal Incidence

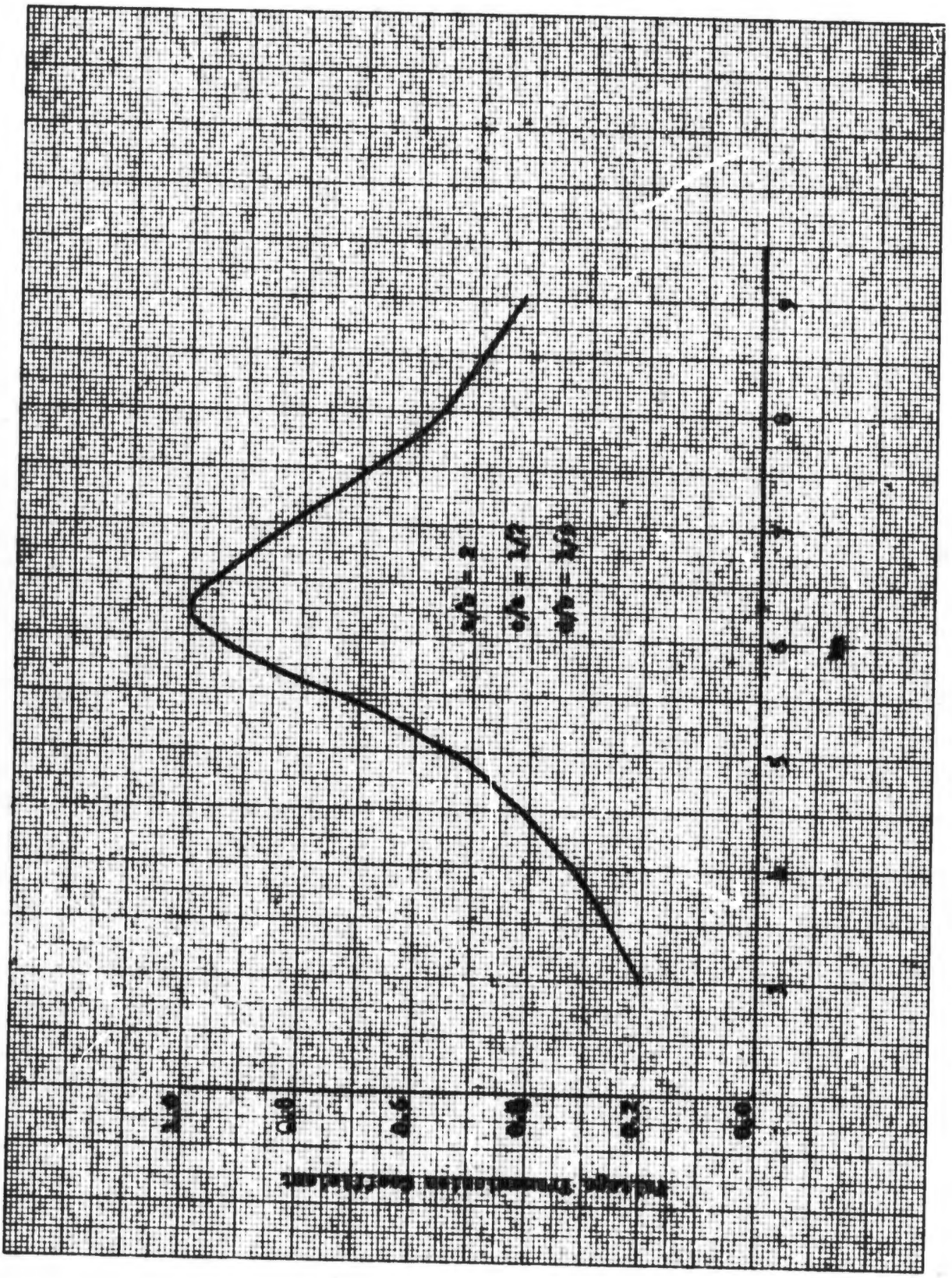

Fig. 33: Voltage Transmission Coefficient vs. $\frac{\Delta}{\lambda_0}$ for Normal Incidence

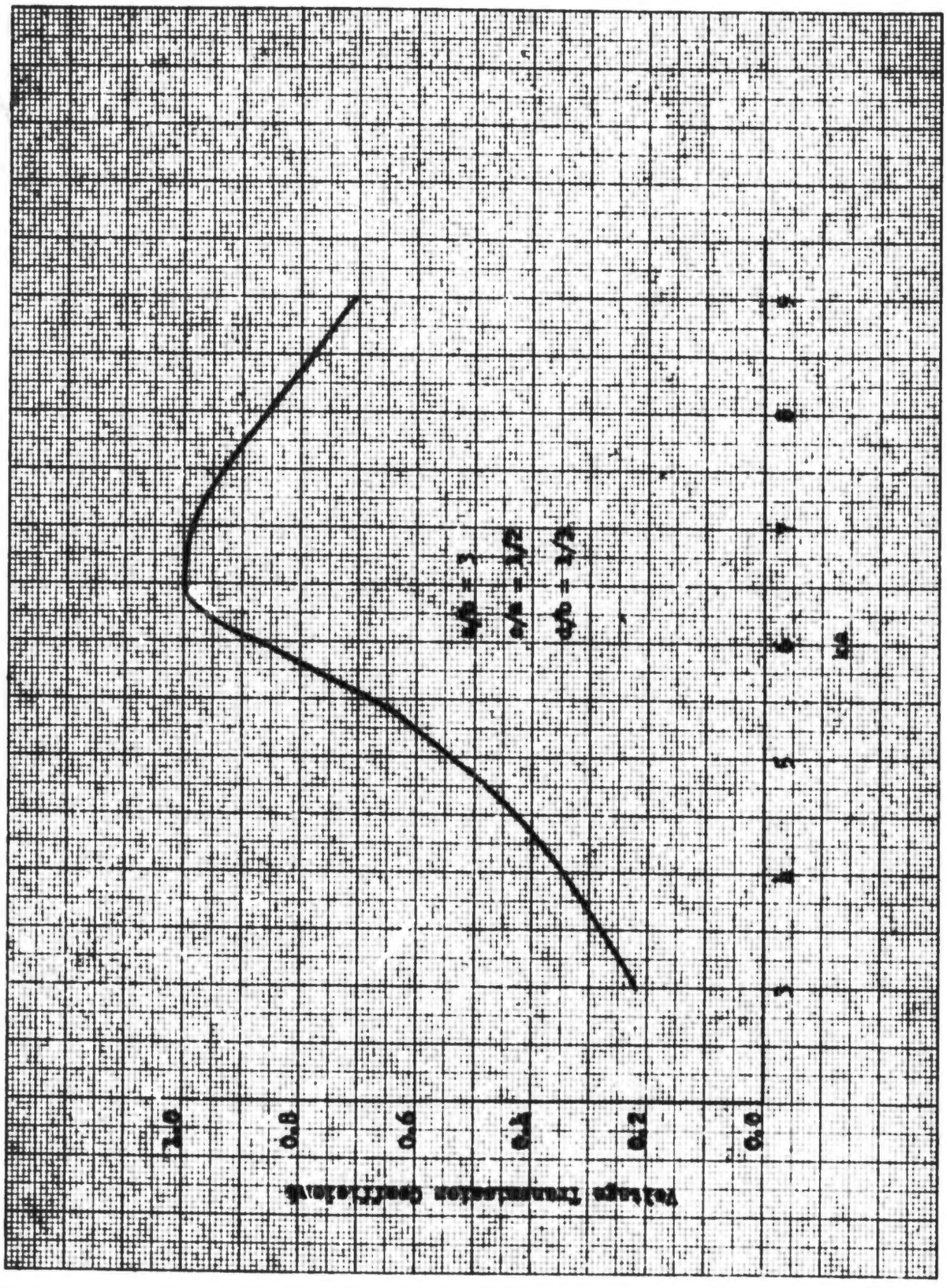

Fig. 34: Voltage Transmission Coefficient vs. ka for Normal Incidence

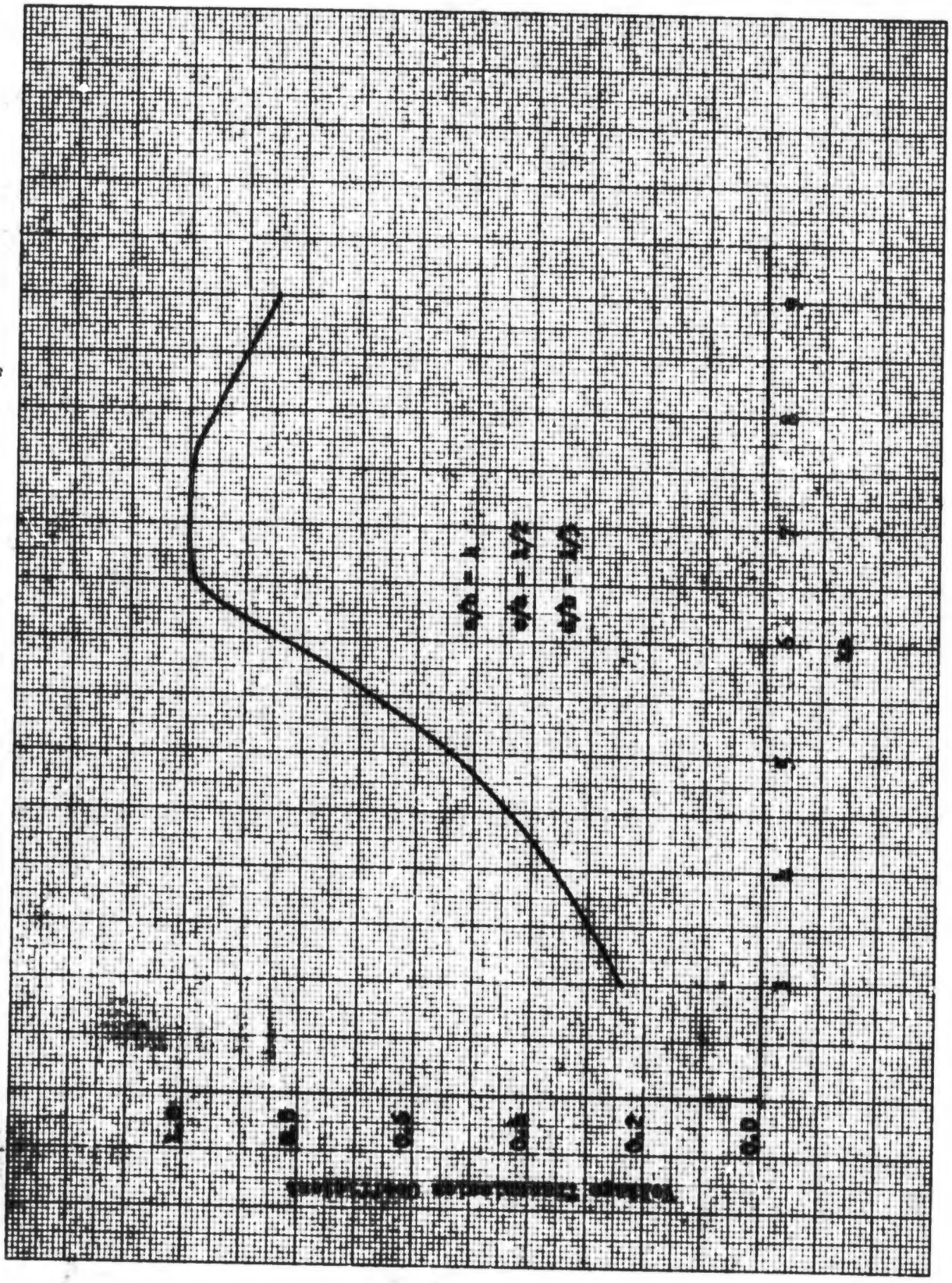

Fig. 35: Voltage Transmission Coefficient vs. ka for Normal Incidence

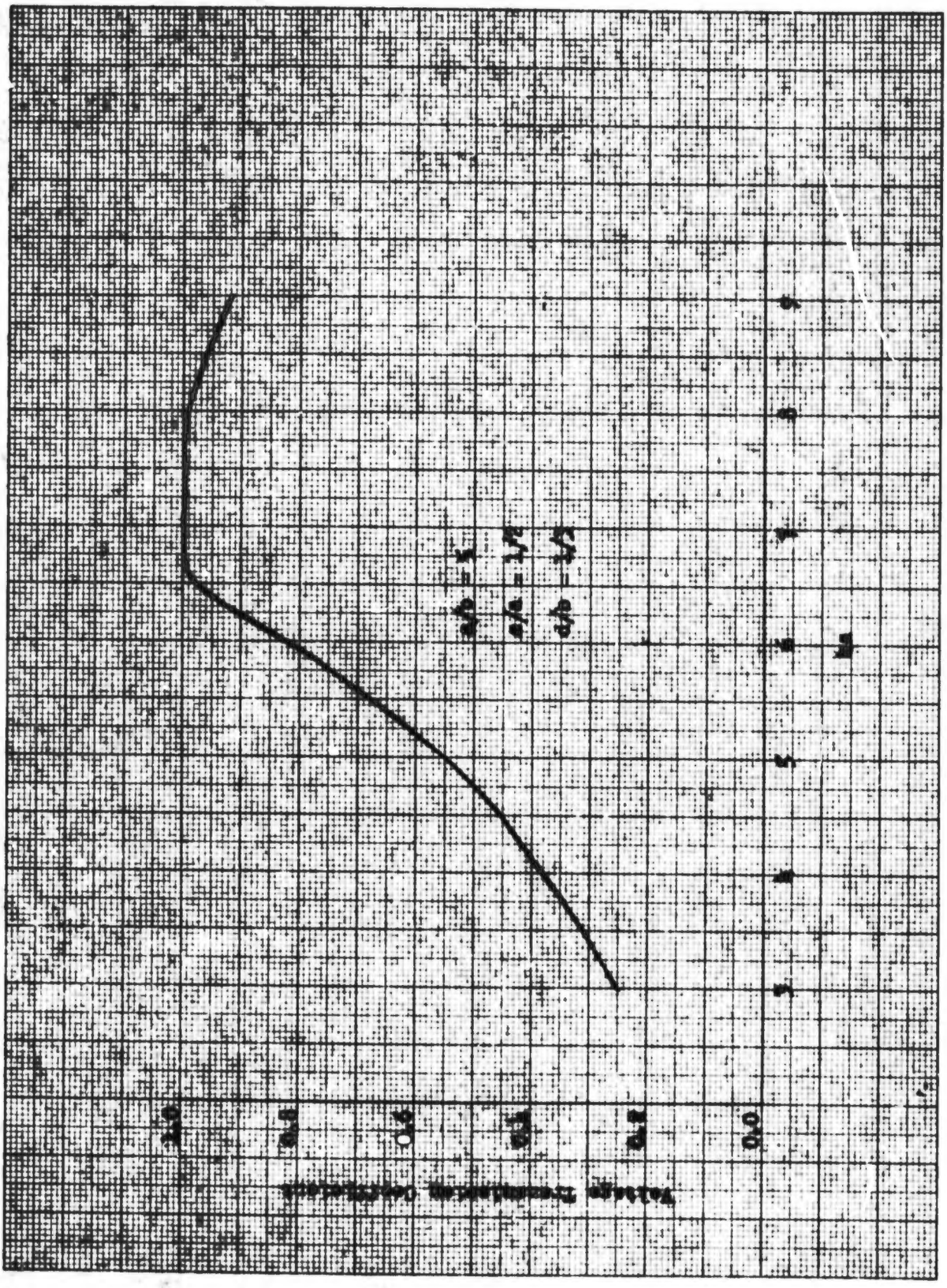

Fig. 36: Voltage Transmission Coefficient vs. ka for Normal Incidence

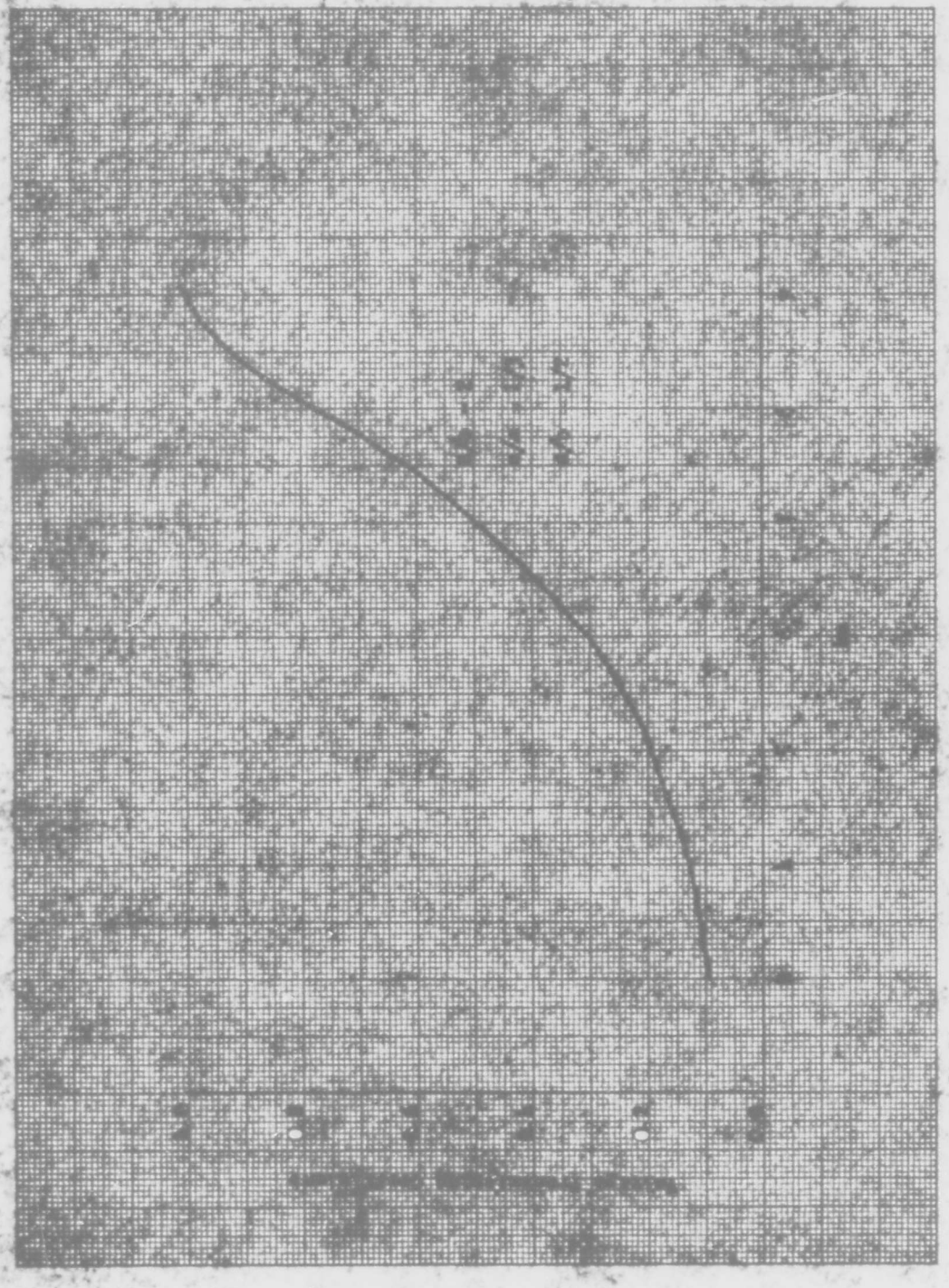

Fig. 37: Voltage Transmission Coefficient vs. ka for Normal Incidence

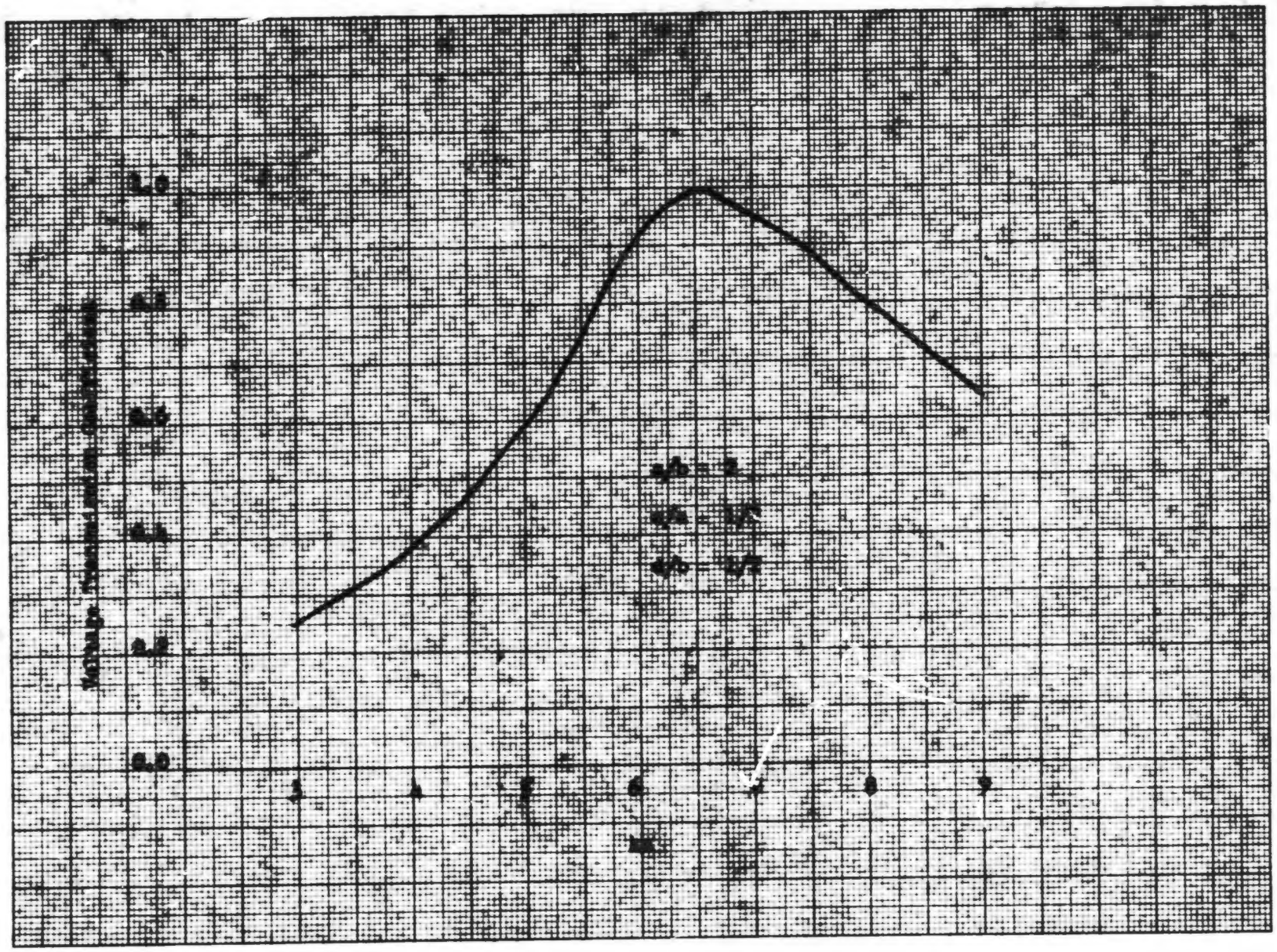

Fig. 38: Voltage Transmission Coefficient vs. k₀ for Normal Incidence

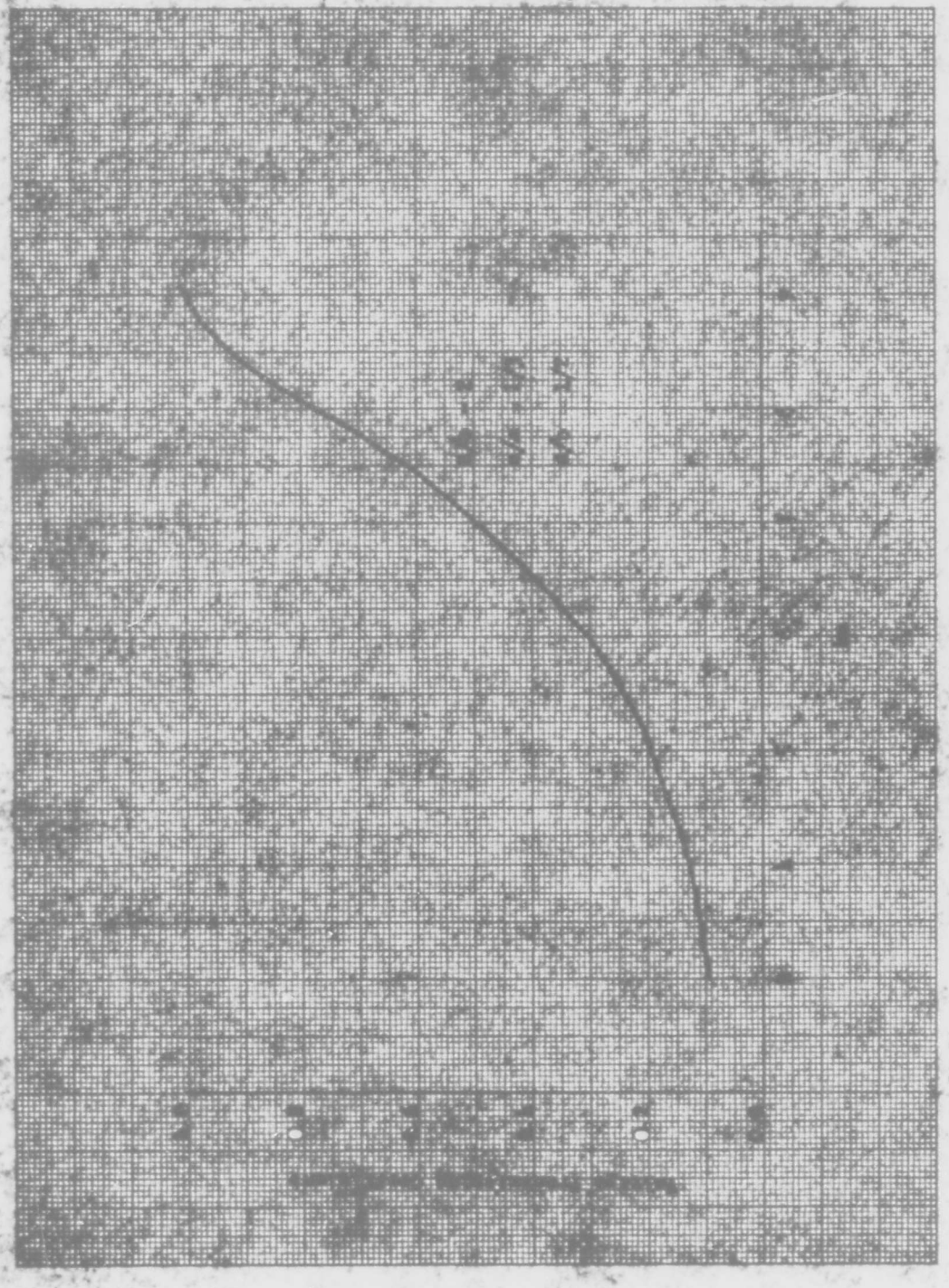

Fig. 37: Voltage Transmission Coefficient vs. ka for Normal Incidence

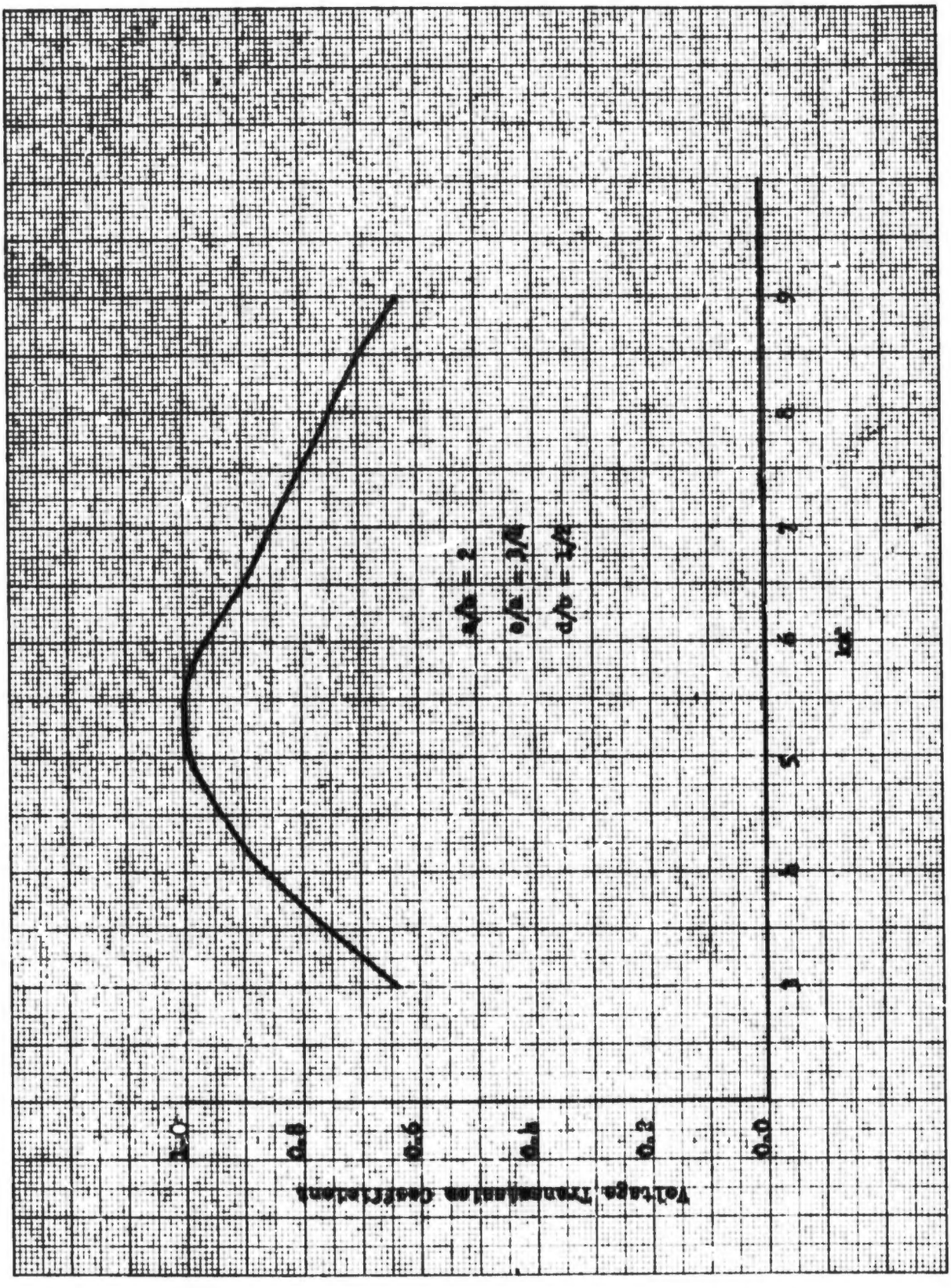

Fig. 40: Voltage Transmission Coefficient vs. ka for Normal Incidence

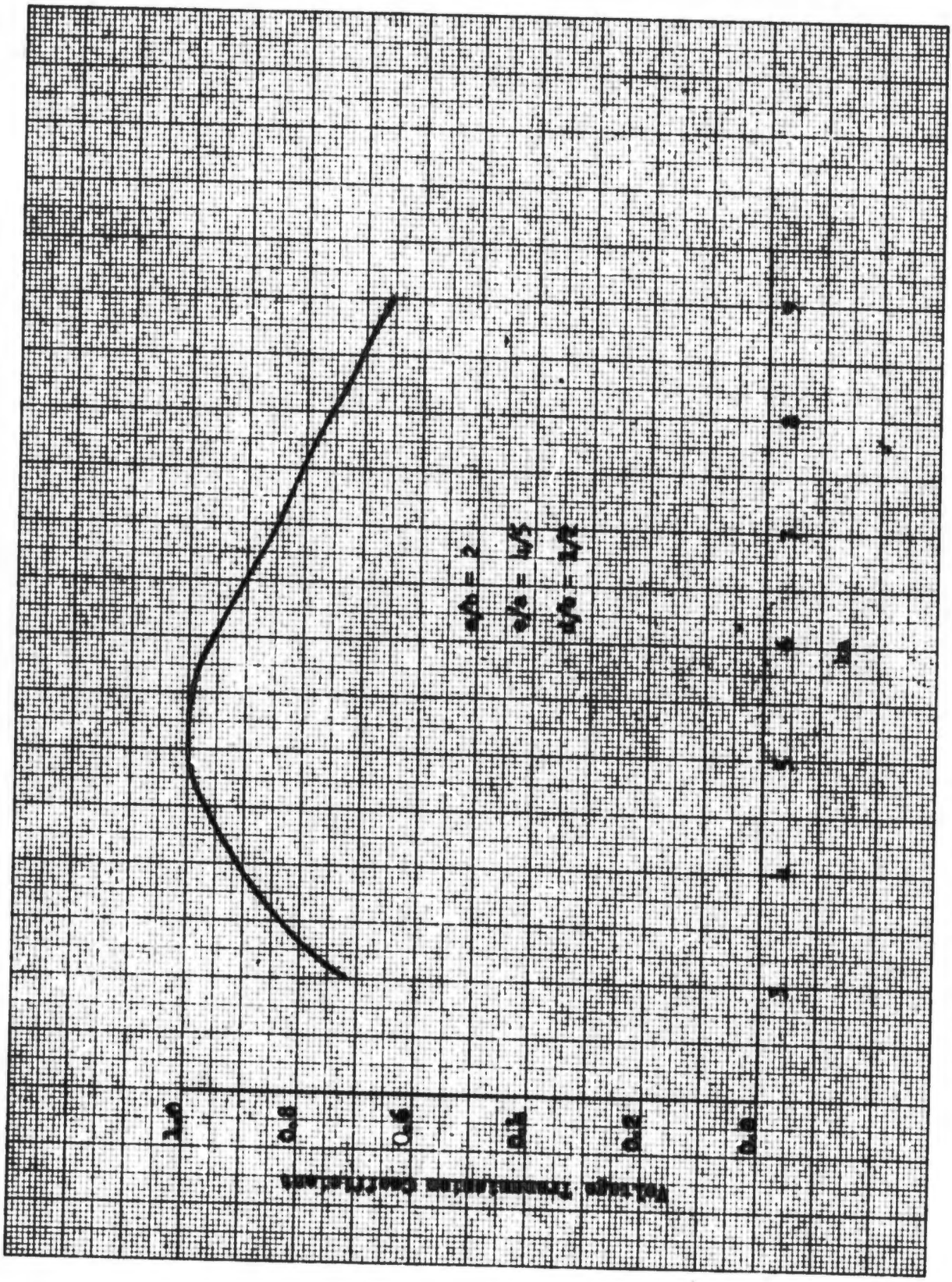

Fig. 41: Voltage Transmission Coefficient vs. ka for Normal Incidence

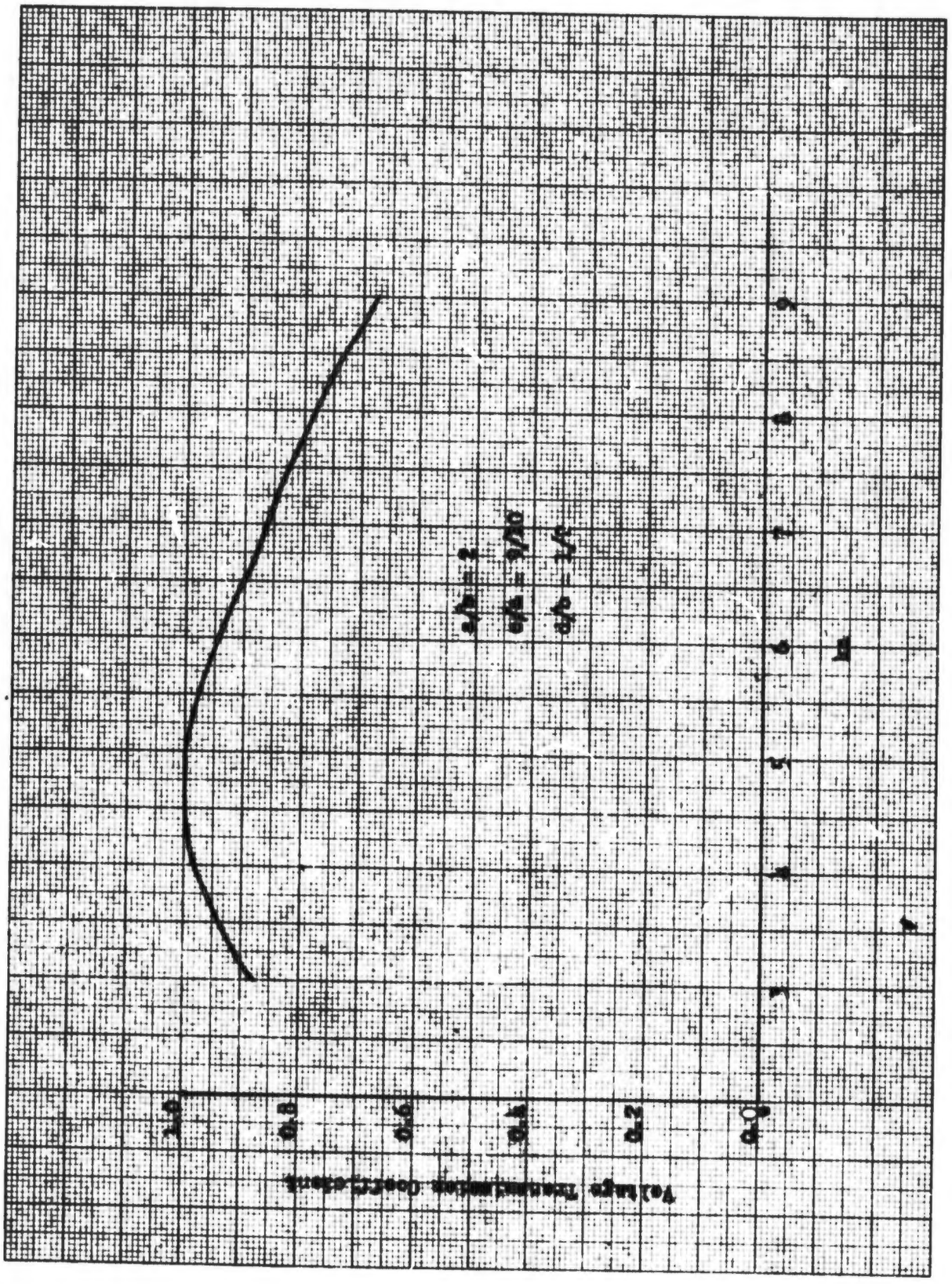

Fig. 42: Voltage Transmission Coefficient vs. k_0 for Normal Incidence

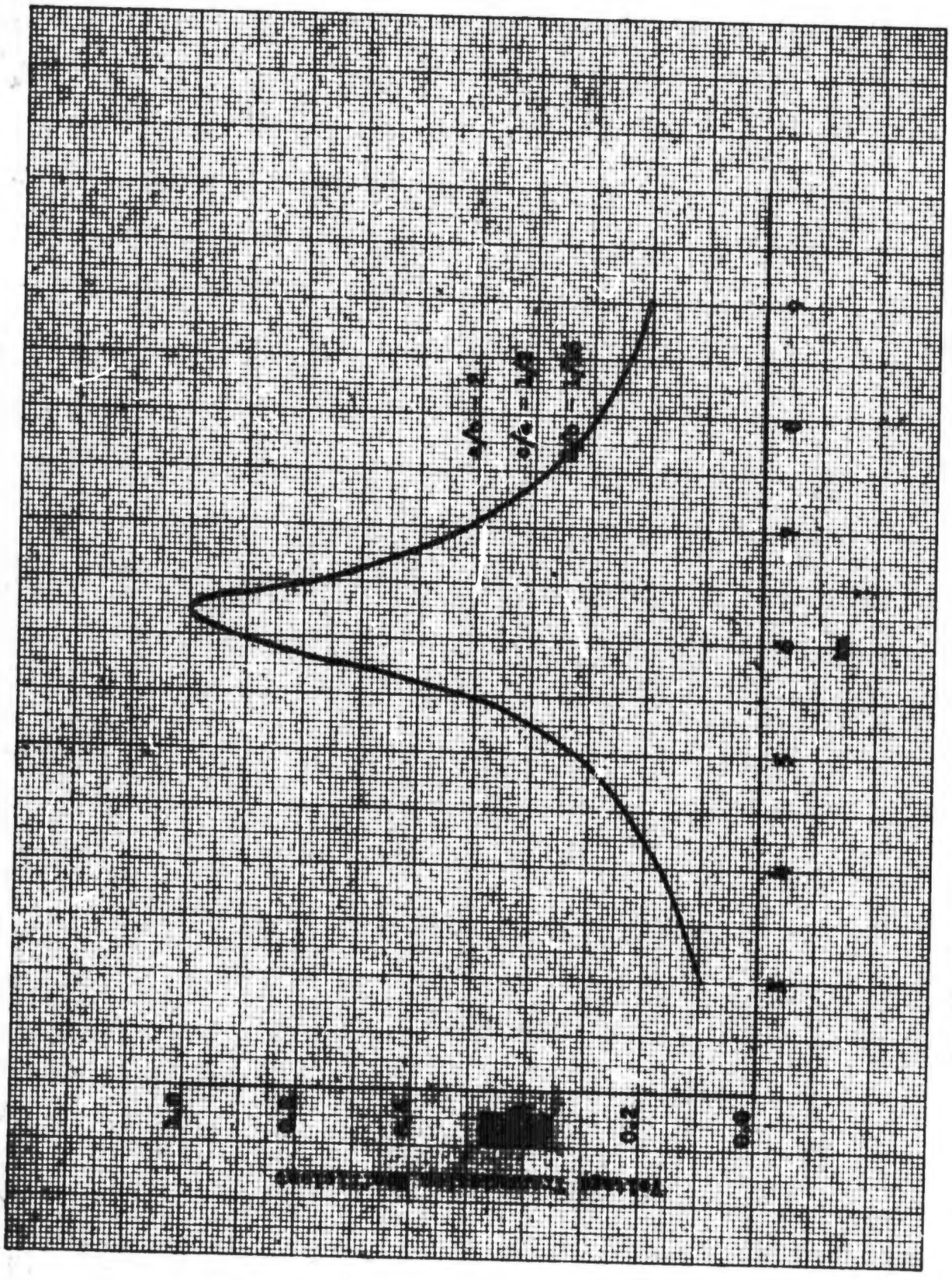

Fig. 43: Voltage Transmission Coefficient vs. ka for Normal Incidence

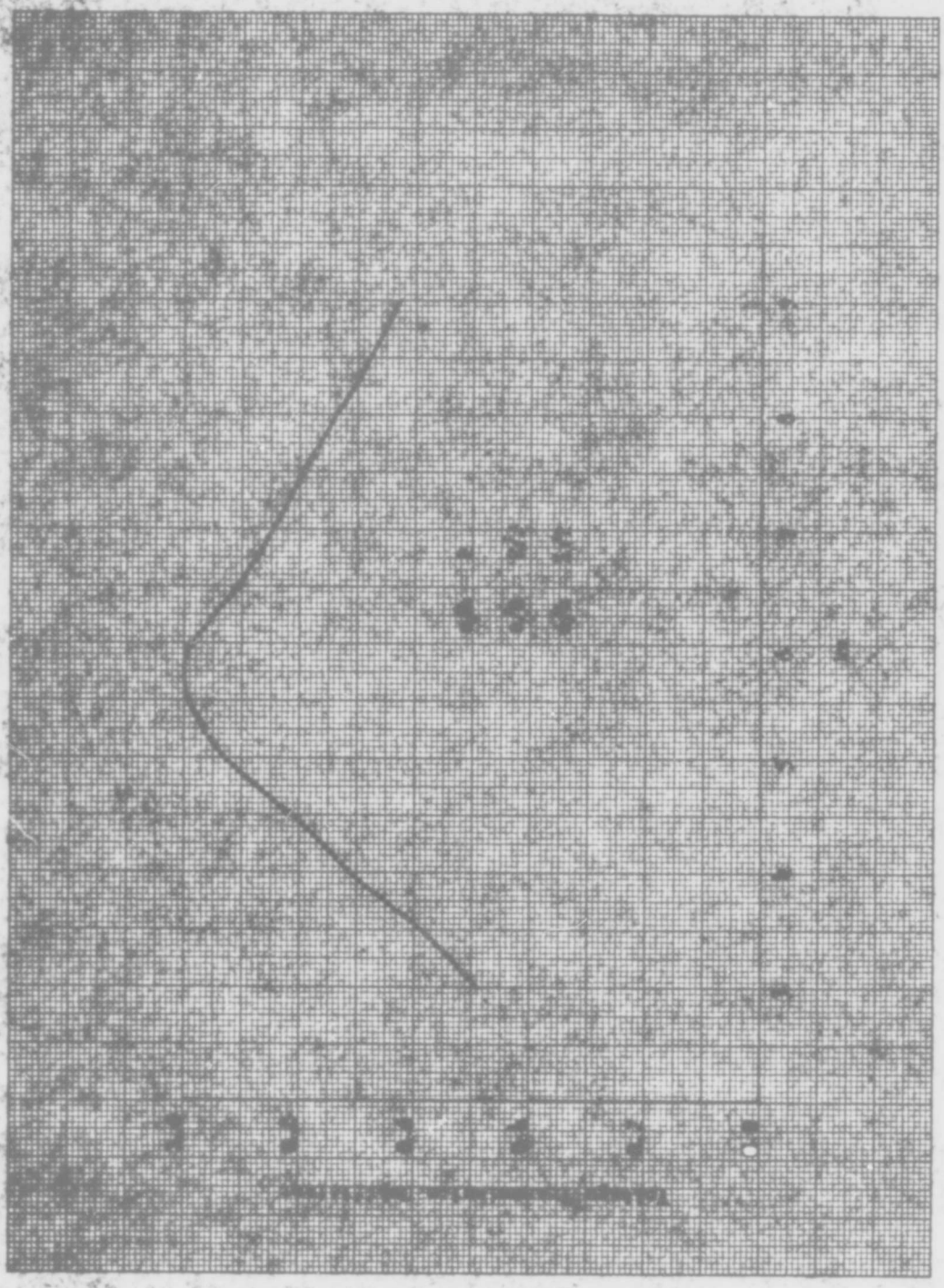

Fig. 39: Voltage Transmission Coefficient vs. ka for Normal Incidence

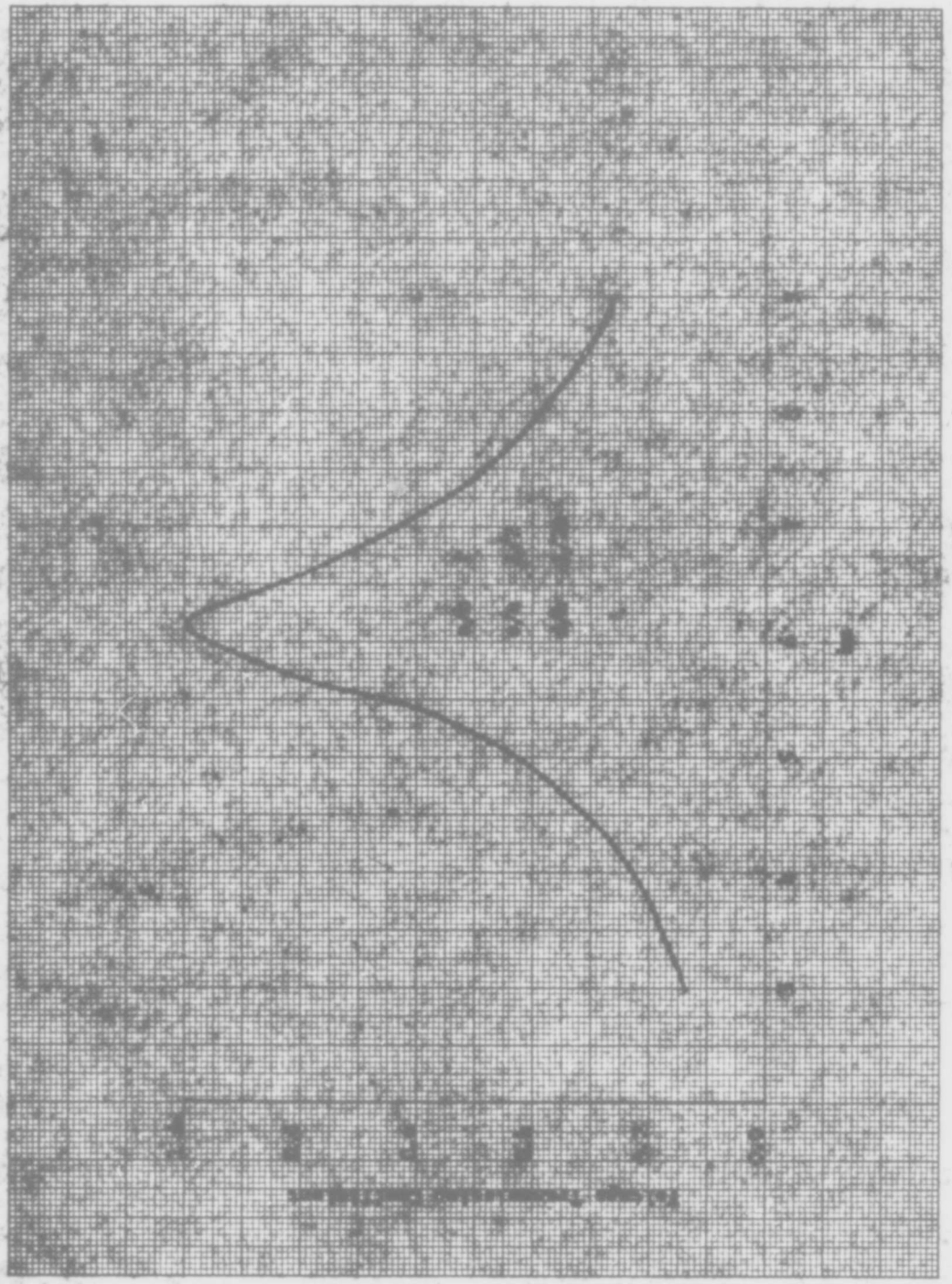

Fig. 45: Voltage Transmission Coefficient vs. ka for Normal Incidence

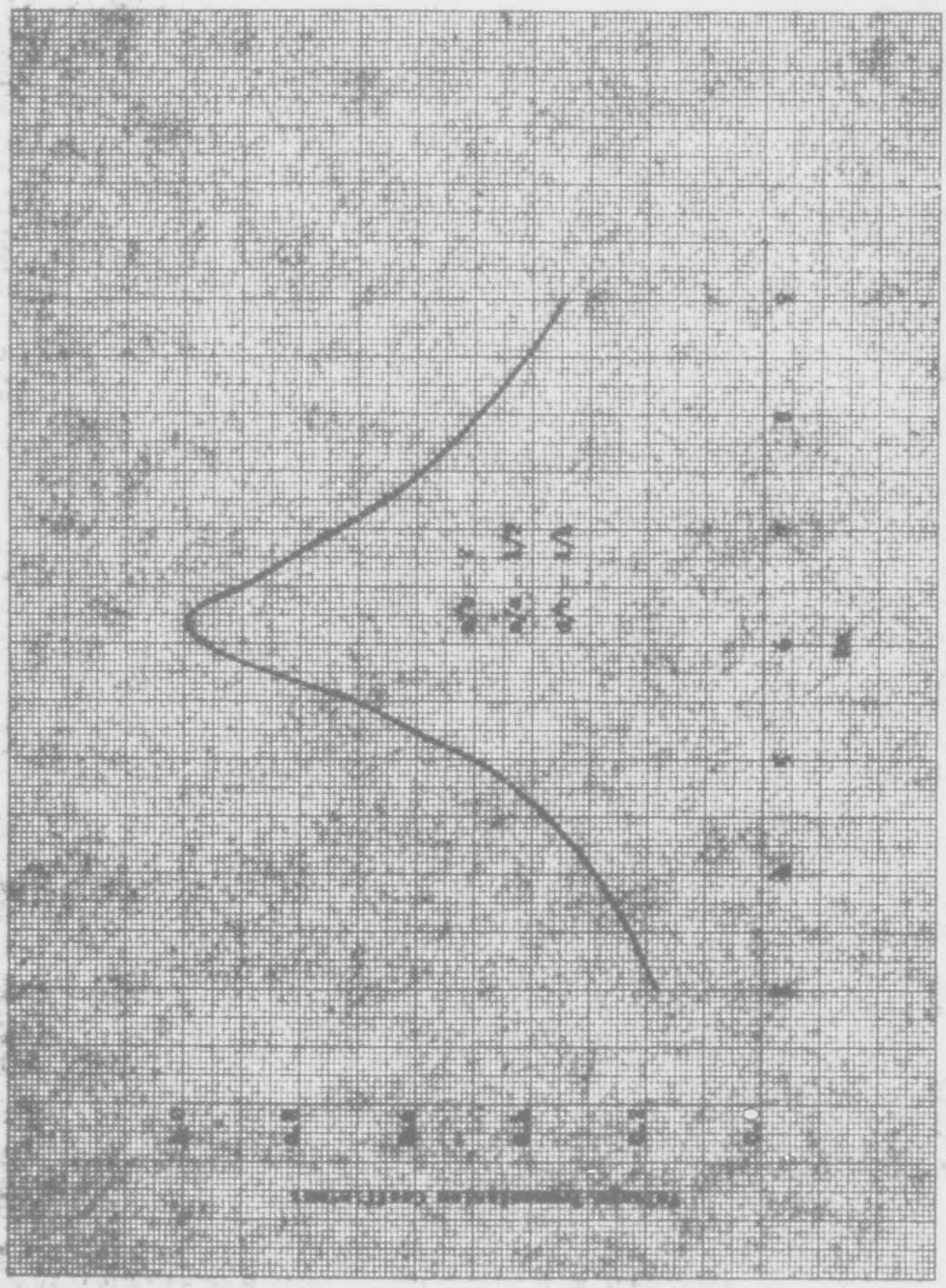

Fig. 46: Voltage Transmission Coefficient vs. ka for Normal Incidence

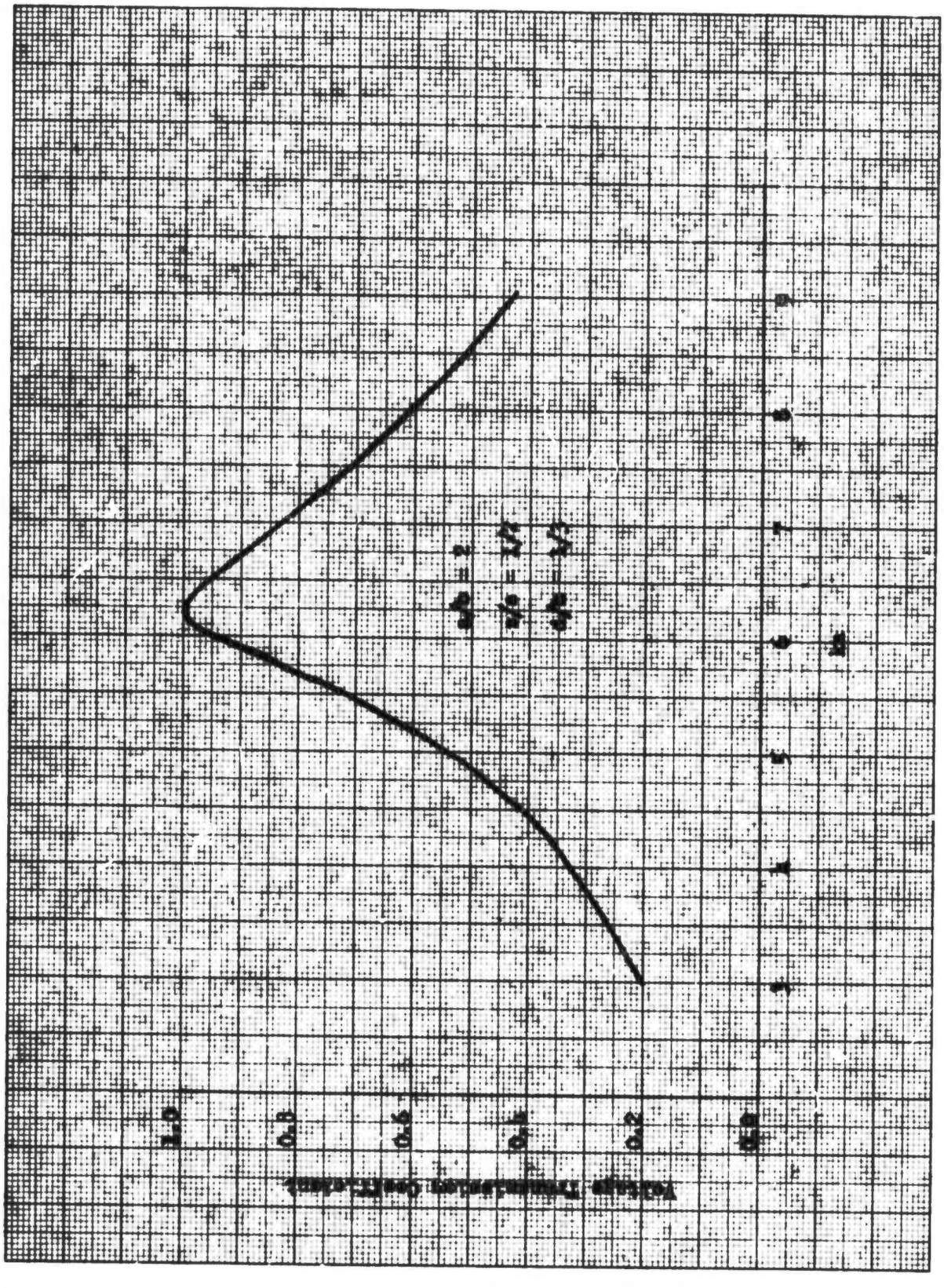

Fig. 47: Voltage Transmission Coefficient vs. k_0 for Normal Incidence

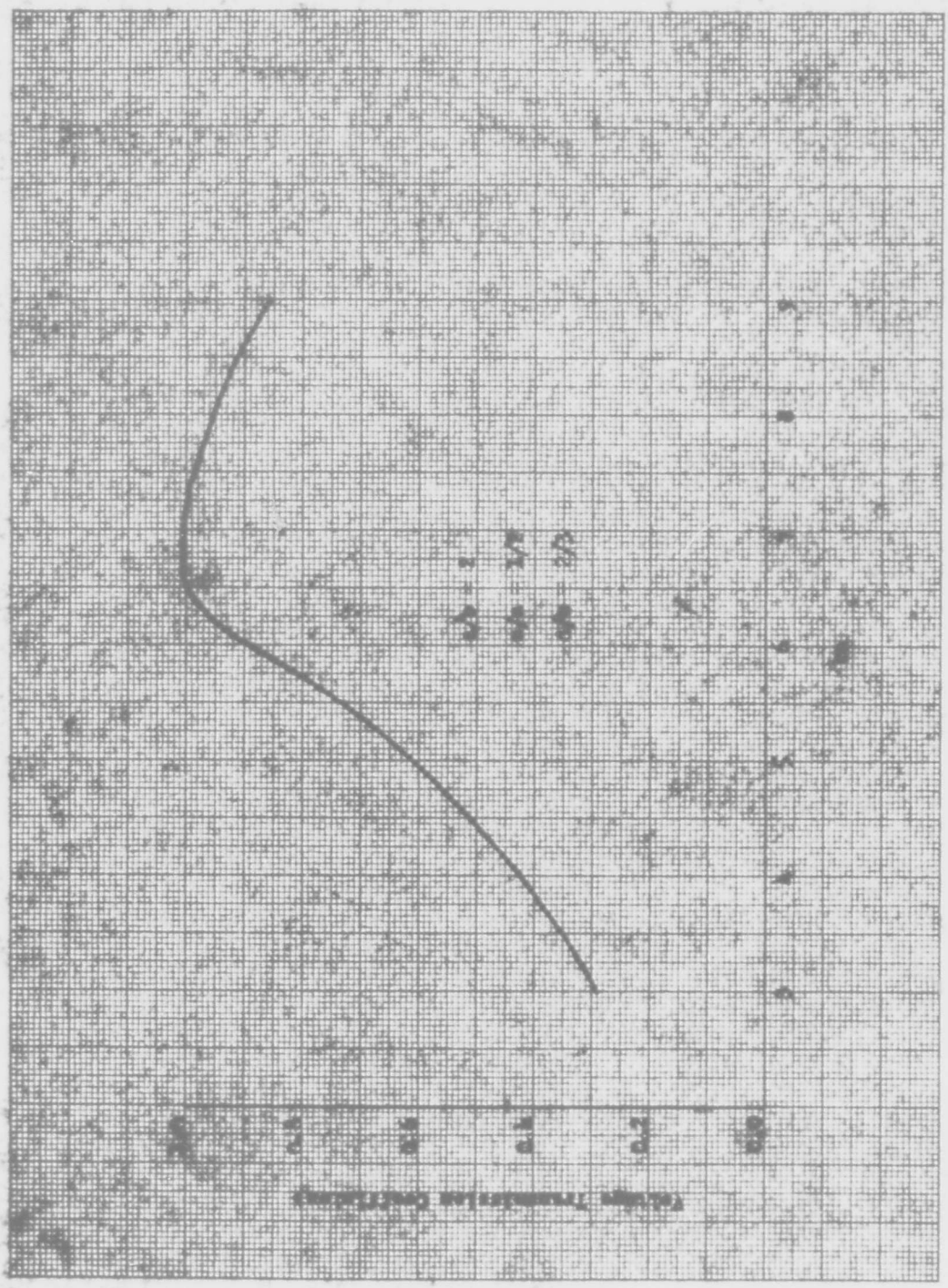

Fig. 48: Voltage Transmission Coefficient vs. ka for Normal Incidence

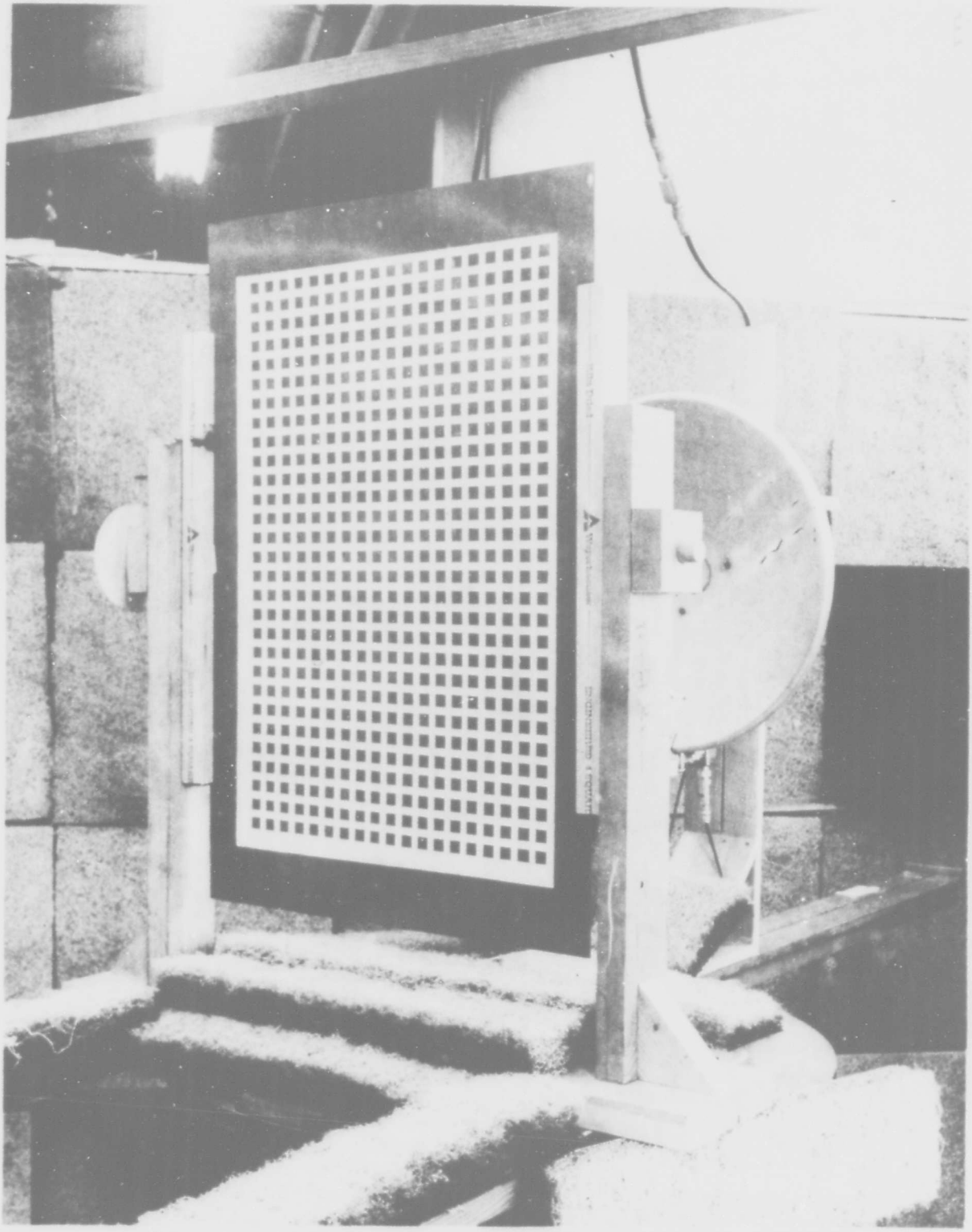

Figure 49 EXPERIMENTAL MEASUREMENT FOR NORMAL INCIDENCE

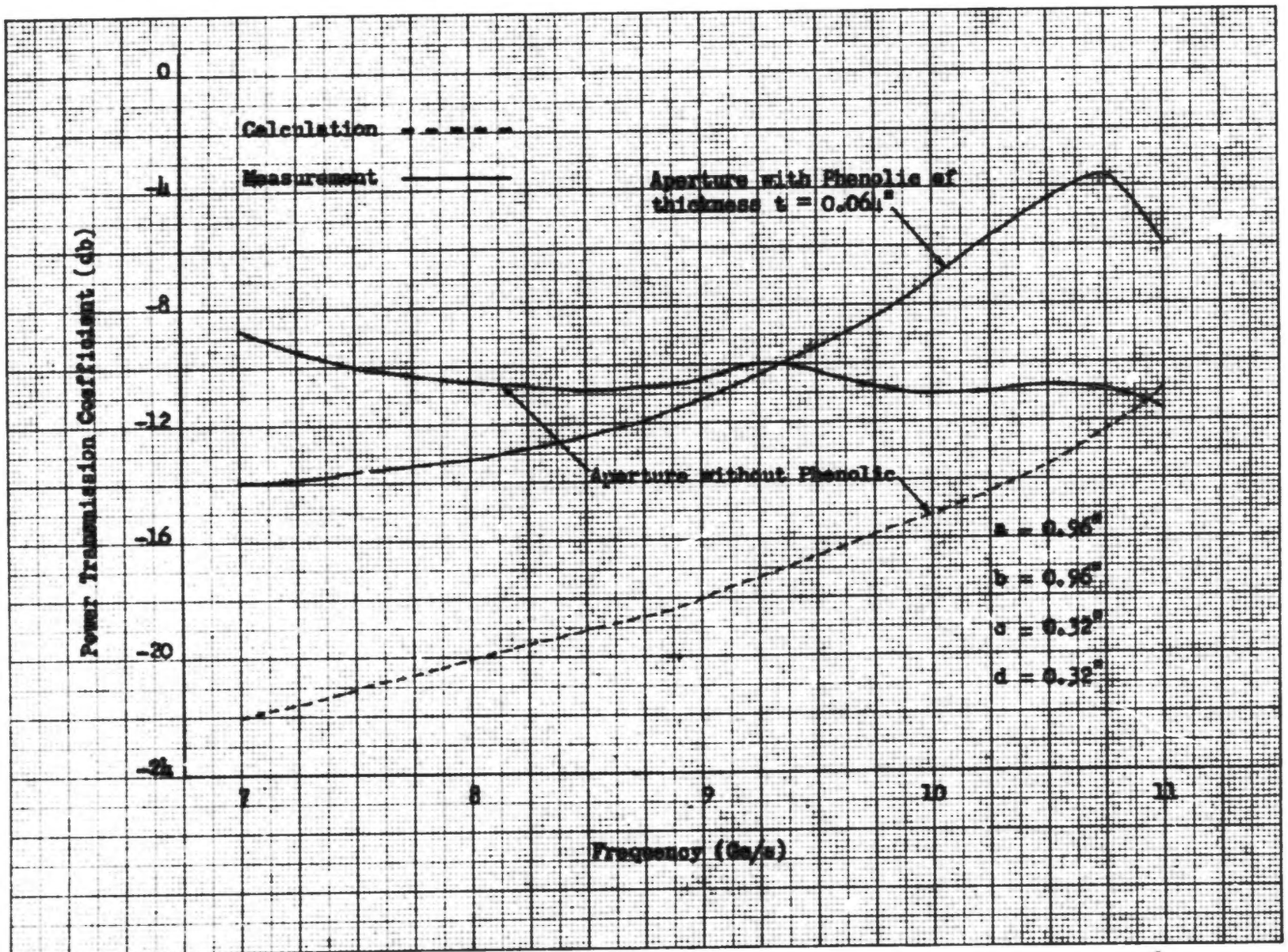

Fig. 50: Power Transmission Coefficient vs. Frequency for Normal Incidence

agreement of variation between calculations and measurements (Figs. 51-54), except that the calculations exaggerated the variation more. As mentioned before, the disagreement in the magnitude of transmission between calculations and measurements was mainly caused by the limitation of the sensitivity of the equipment.

It is also interesting to notice the occurrence of a dielectric effect on the frequency of peak transmission. It is seen that the frequency of peak transmission is very sensitive to the dielectric in apertures. The thicker the dielectric in the aperture, the lower is the frequency of the peak transmission (Figs. 51-54). This is true also for higher dielectric constants. Details of this dielectric effect on the transmission should be investigated but falls out of the scope of this report.

Further calculations were made and compared to the calculations and measurements which were reported by other researcher[1] (Figs. 55-57). Good agreement was obtained between the measurements and new calculations. Errors in the old calculations were probably made by misuse of Bessel functions.

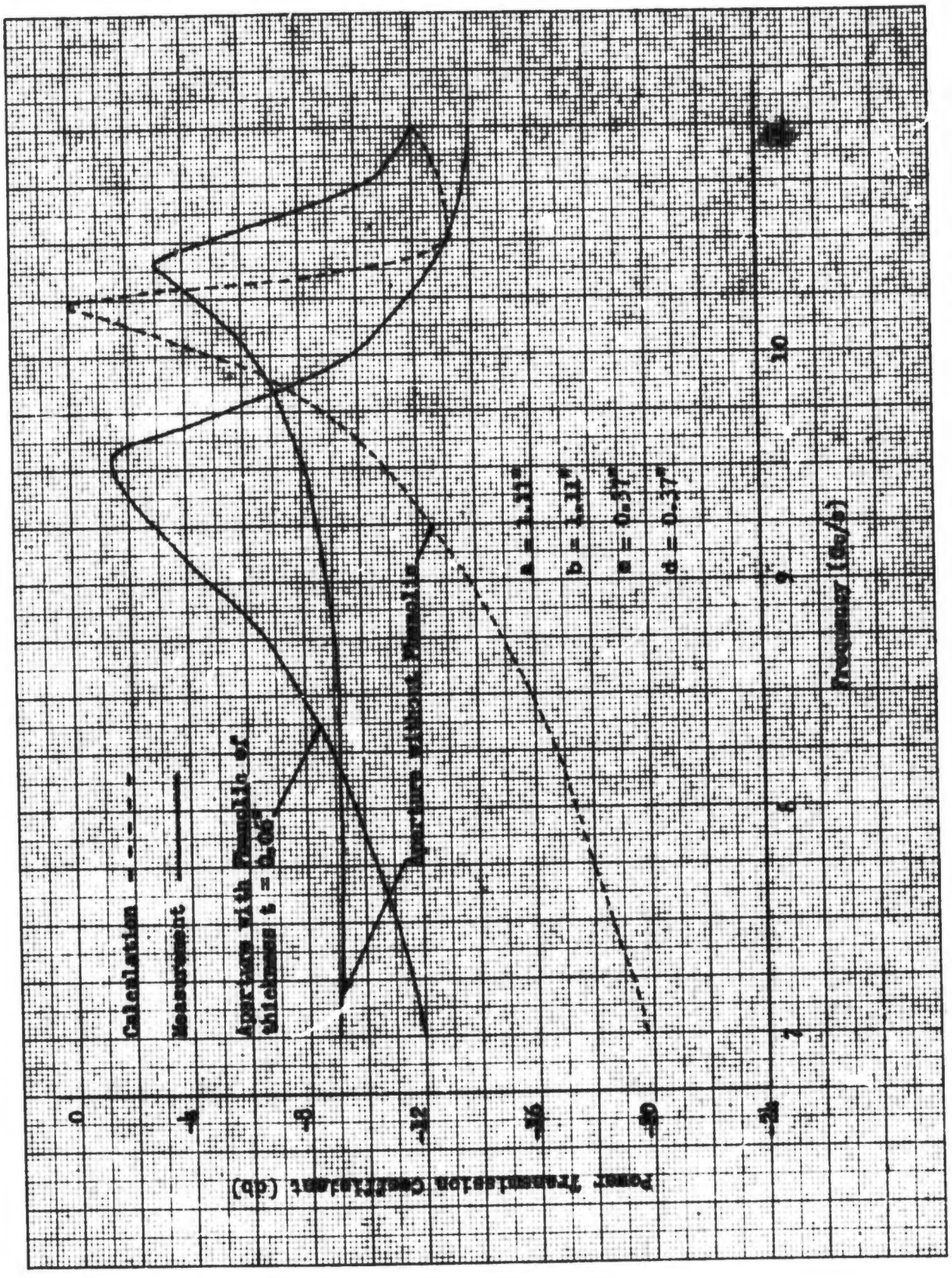

Fig. 51: Power Transmission Coefficient vs. Frequency for Normal Incidence

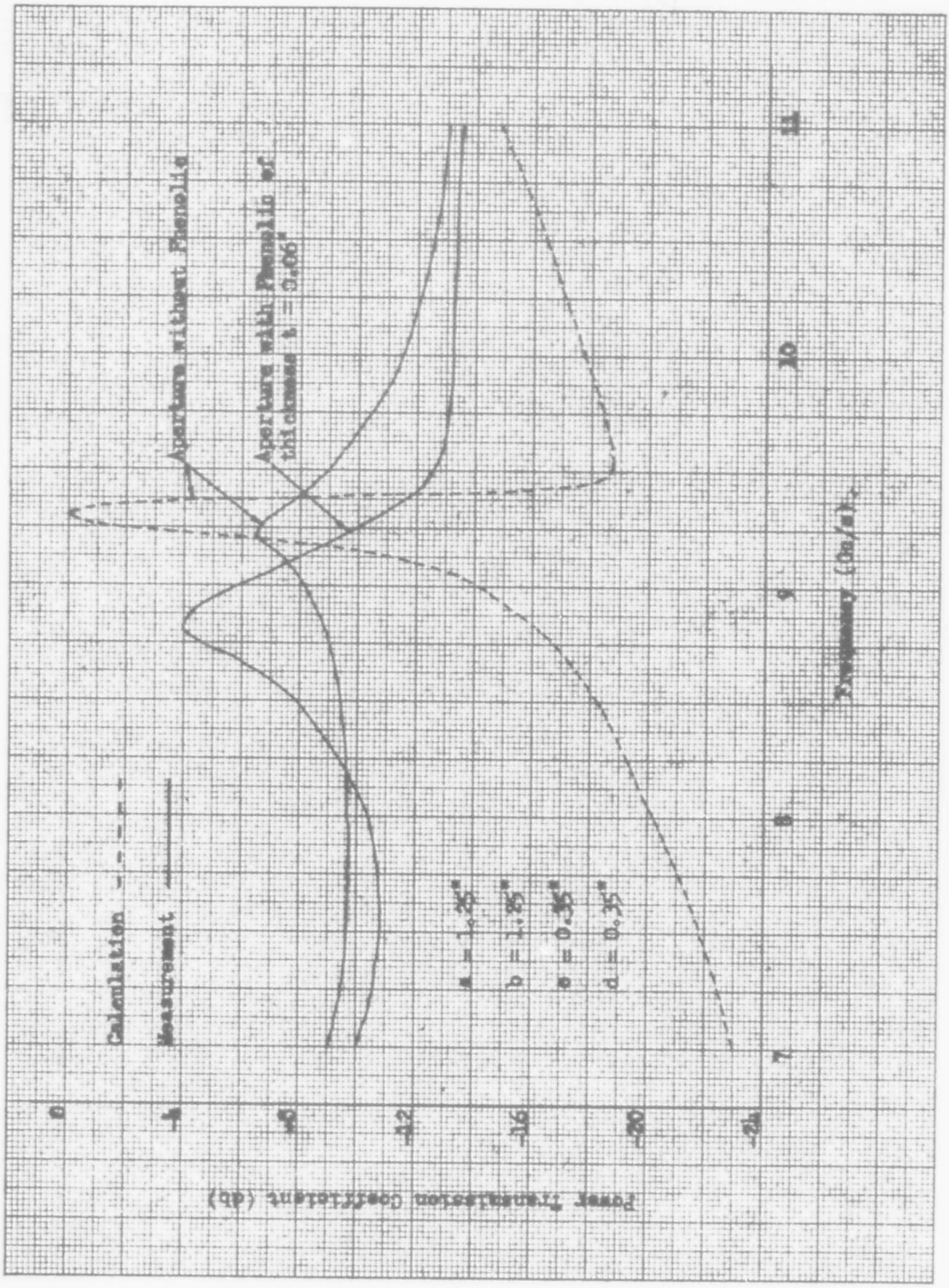

Fig. 52: Power Transmission Coefficient vs. Frequency for Normal Incidence

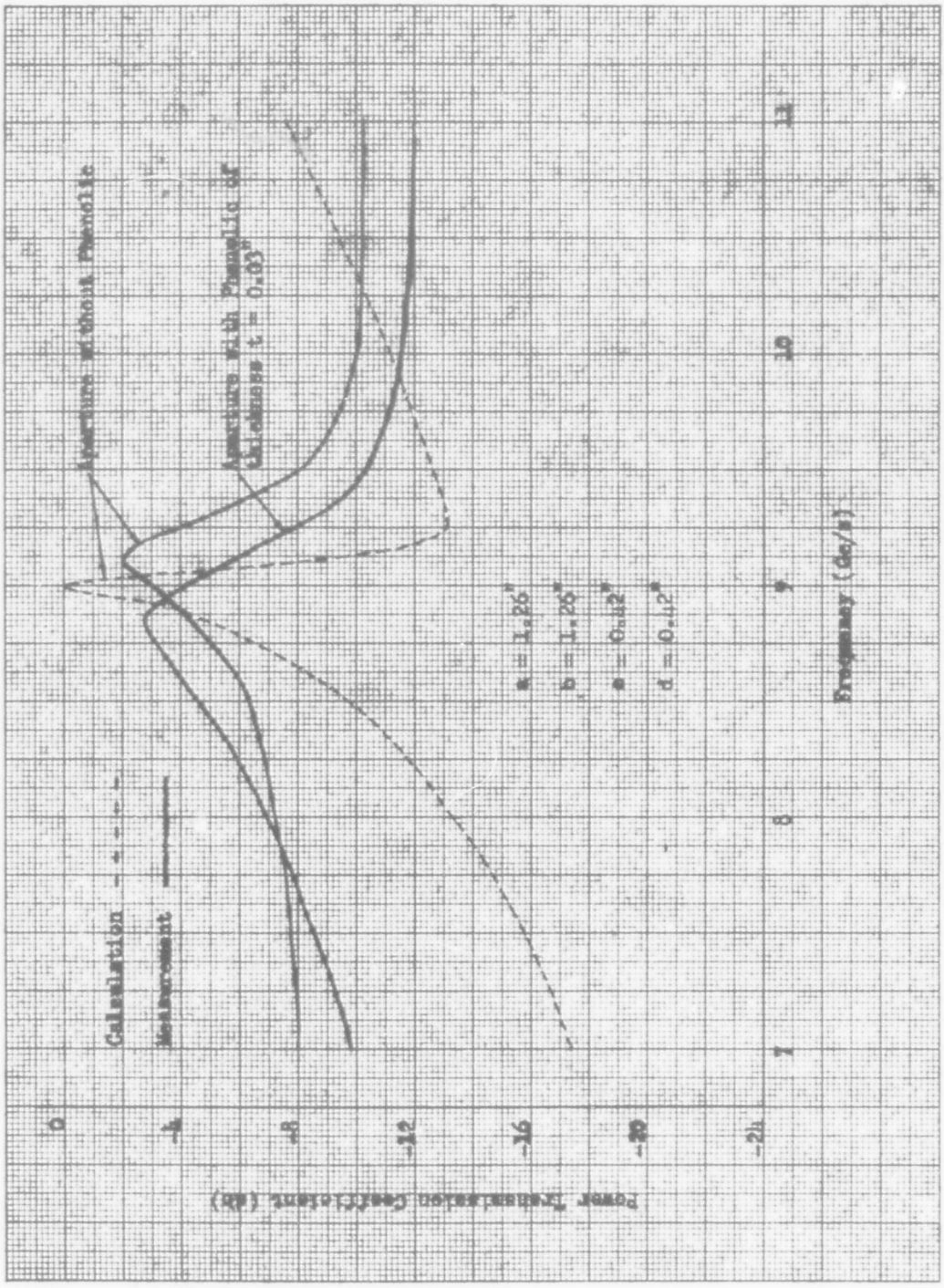

Fig. 53: Power Transmission Coefficient vs. Frequency for Normal Incidence

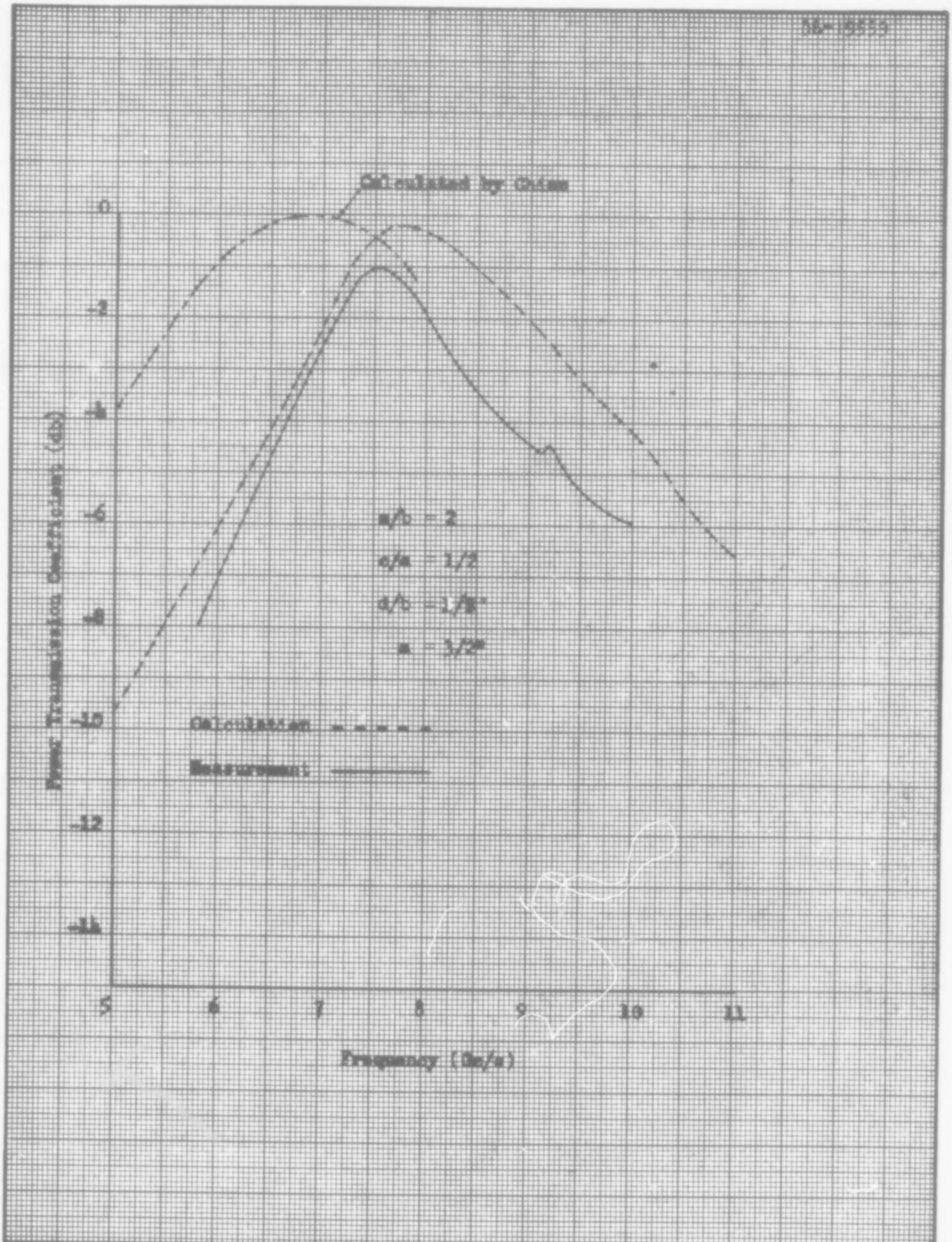

CALC			REVISED	DATE	Fig. 54: Power Transmission Coefficient vs. Frequency for Normal Incidence	
CHECK						
APR						
APR					THE BOEING COMPANY	PAGE 79

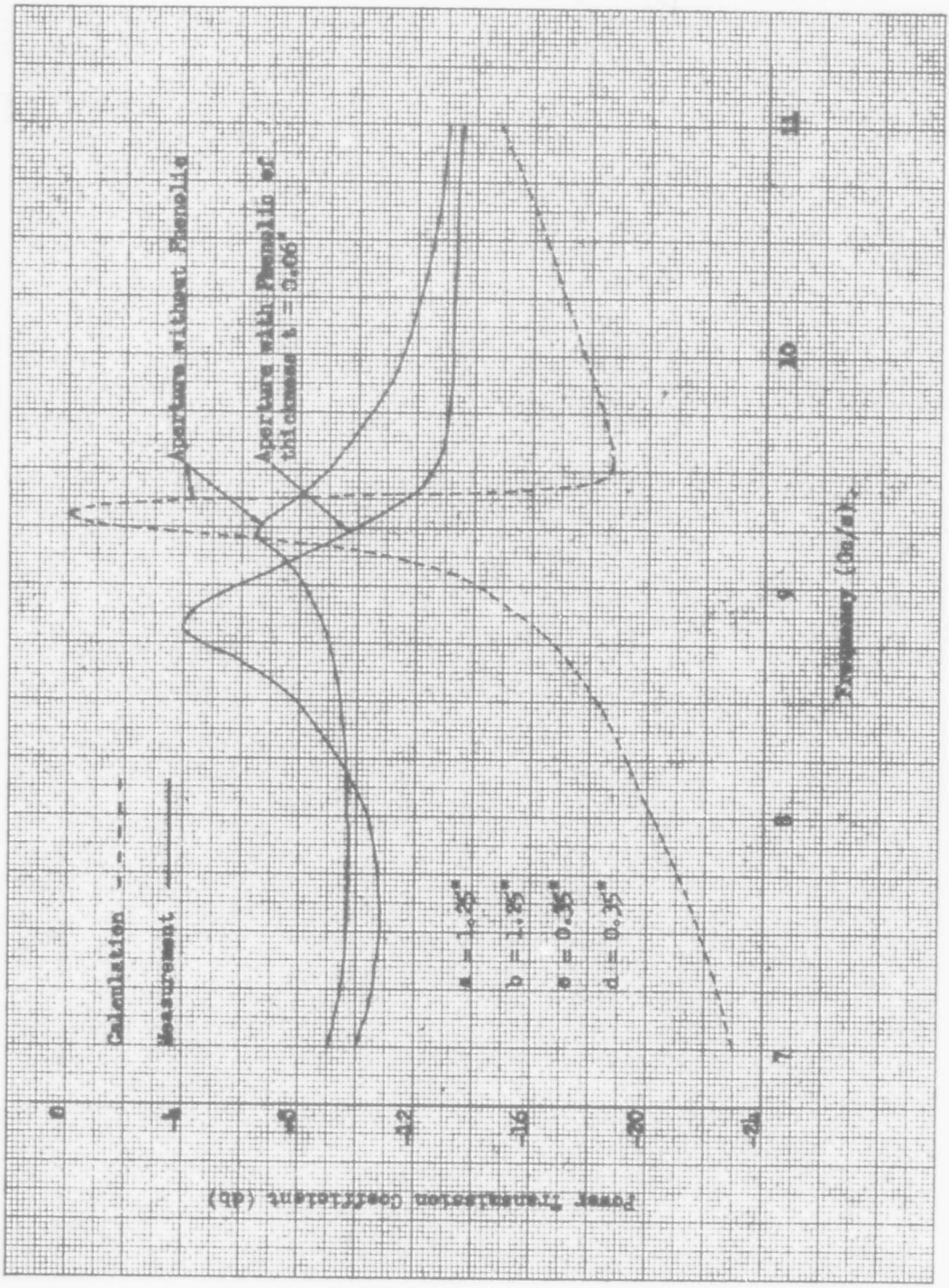

Fig. 52: Power Transmission Coefficient vs. Frequency for Normal Incidence

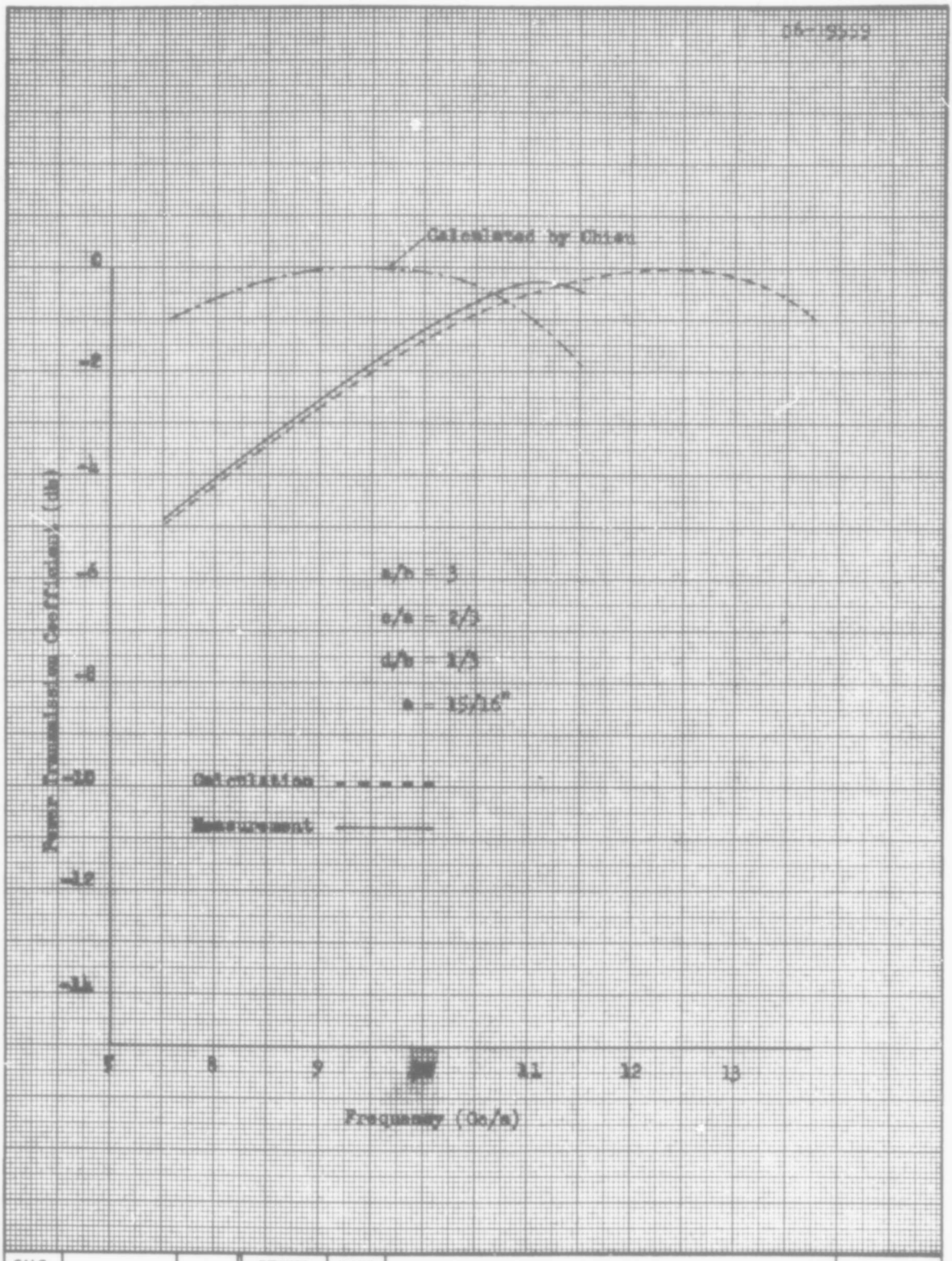

CALC			REVISED	DATE	Fig. 55: Power Transmission Coefficient vs. Frequency for Normal Incidence	
CHECK						
APR						
APR					THE BOEING COMPANY	PAGE 80

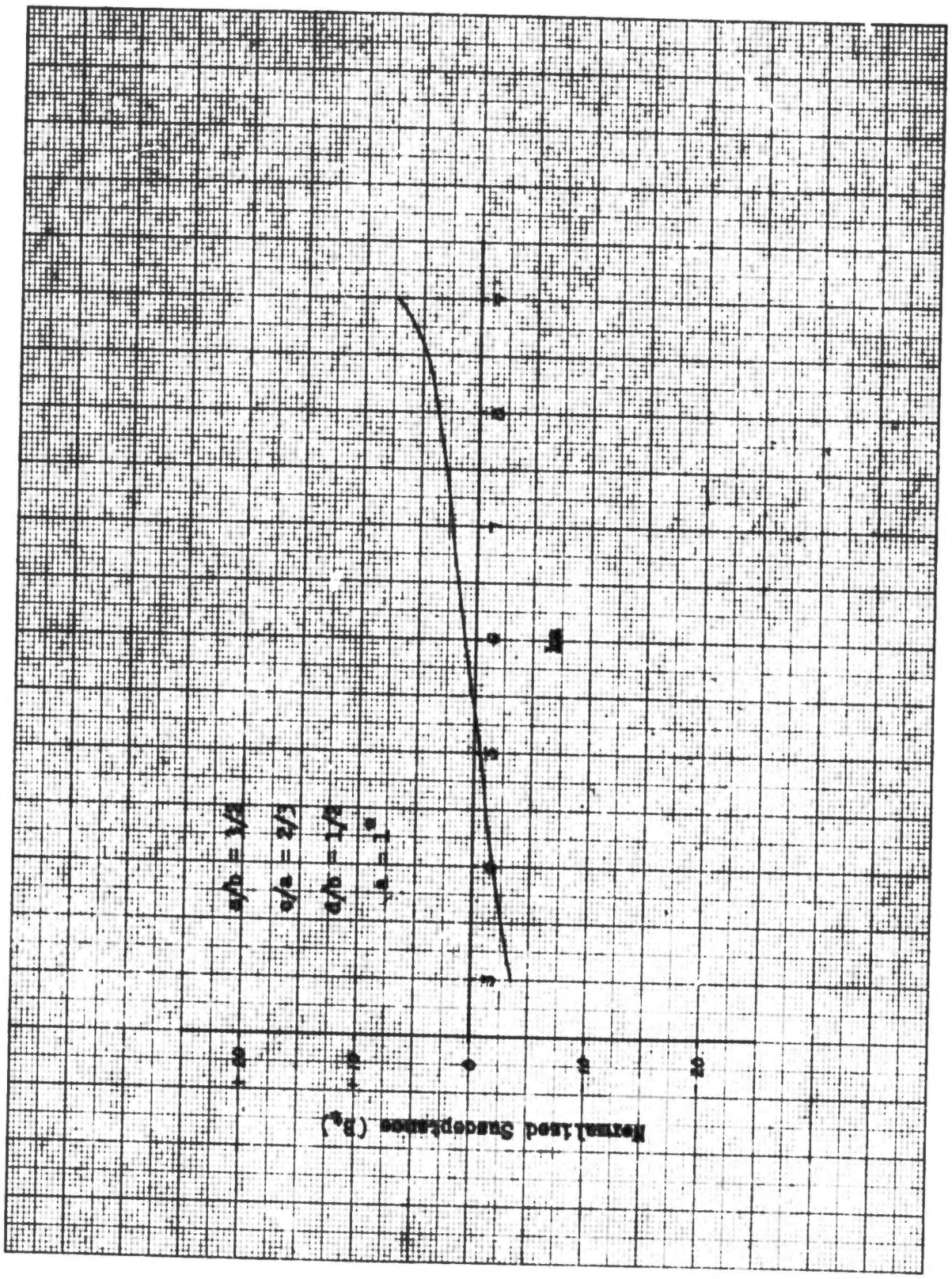

Fig. 57: Equivalent Susceptance vs. ka for Normal Incidence

D. Equivalent Susceptance

A study of the transparency of a fenestrated conducting screen can be simulated as a transmission line model problem as has been mentioned before. If the screen is lossless, it can be treated purely as an equivalent susceptance B_t as shown in Fig. 2. To get full power transmission through the screen at the incident frequency, the susceptance has to be zero at that particular frequency. In other words, the electric energy stored in the screen is completely cancelled by the magnetic energy.

It is interesting to see how the susceptance will vary with the aperture spacings and sizes at different frequencies. For this purpose, the susceptance for normal incidence was calculated and shown in four different sets of curves. In the first set (Figs. 58-63), the aperture spacing a, which is perpendicular to the electric field, is varying, while the other parameters, b, c and d are constant. It is seen that as the value of a increases (much greater than b), the susceptance will become zero at higher value of a/λ. This may suggest that the transition from evanescent to propagation mode takes place for the higher order modes.

In the second set of curves (Figs. 64-69), the aperture spacing b which is parallel to the electric field is varying, while the other parameters a, c and d are constant. It shows that, as the ratio of a/b is around one, the susceptance changes rapidly with k_n a and becomes zero at few places close to one another along k_n a-axis (figs. 67-68). This implies the Wood anomalies, i.e., the transition from maximum to minimum transmission, takes place within a slight change of frequencies.

In the third set of curves (Figs. 70-75), the aperture side, c, is varying while the others are constant. The susceptance becomes smaller as the value of c increases, and the frequency at which the susceptance is zero will be lowered.

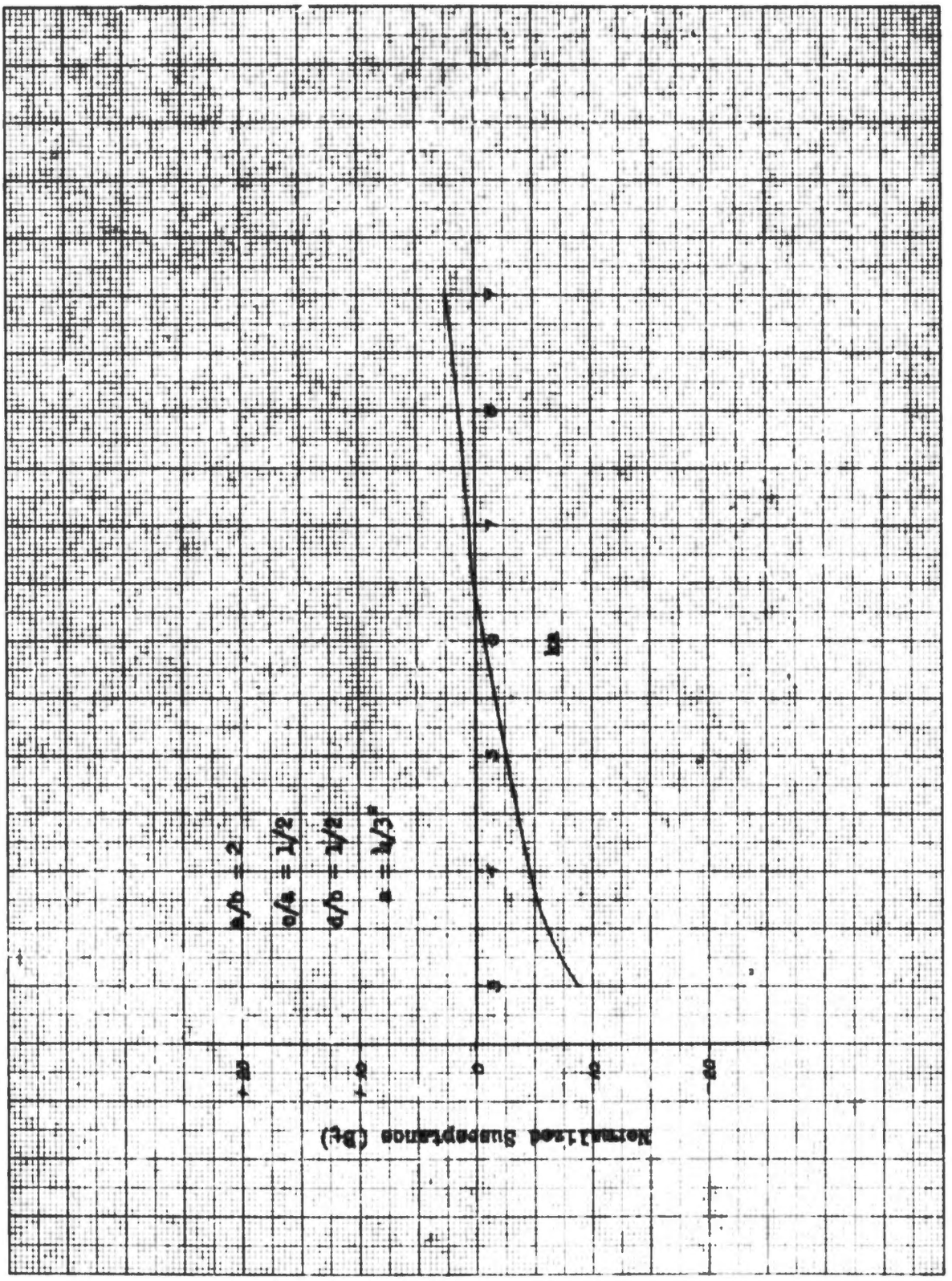

Fig. 58: Equivalent Susceptance vs. ka for Normal Incidence

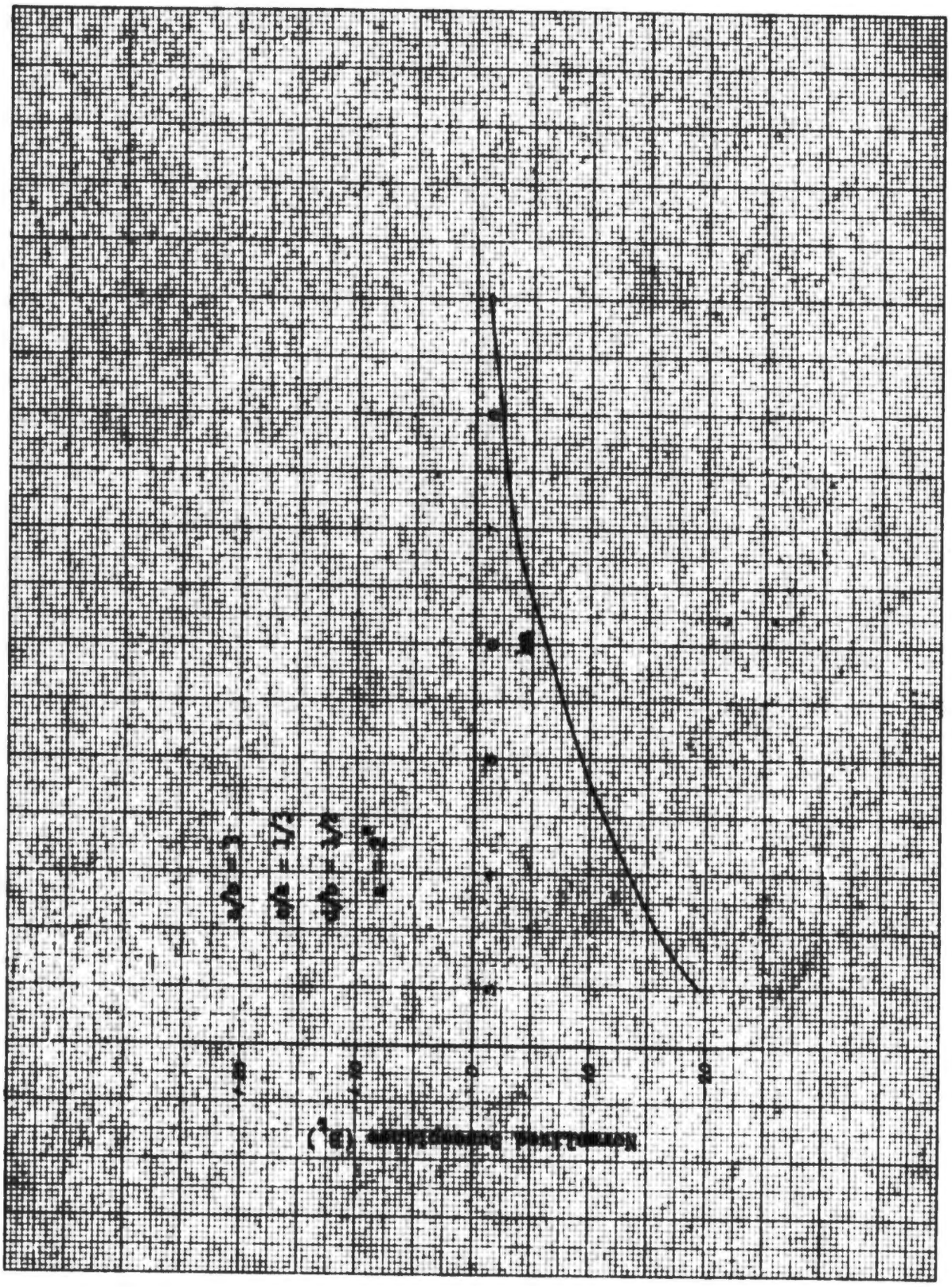

Fig. 59: Equivalent Susceptance vs. ka for Normal Incidence

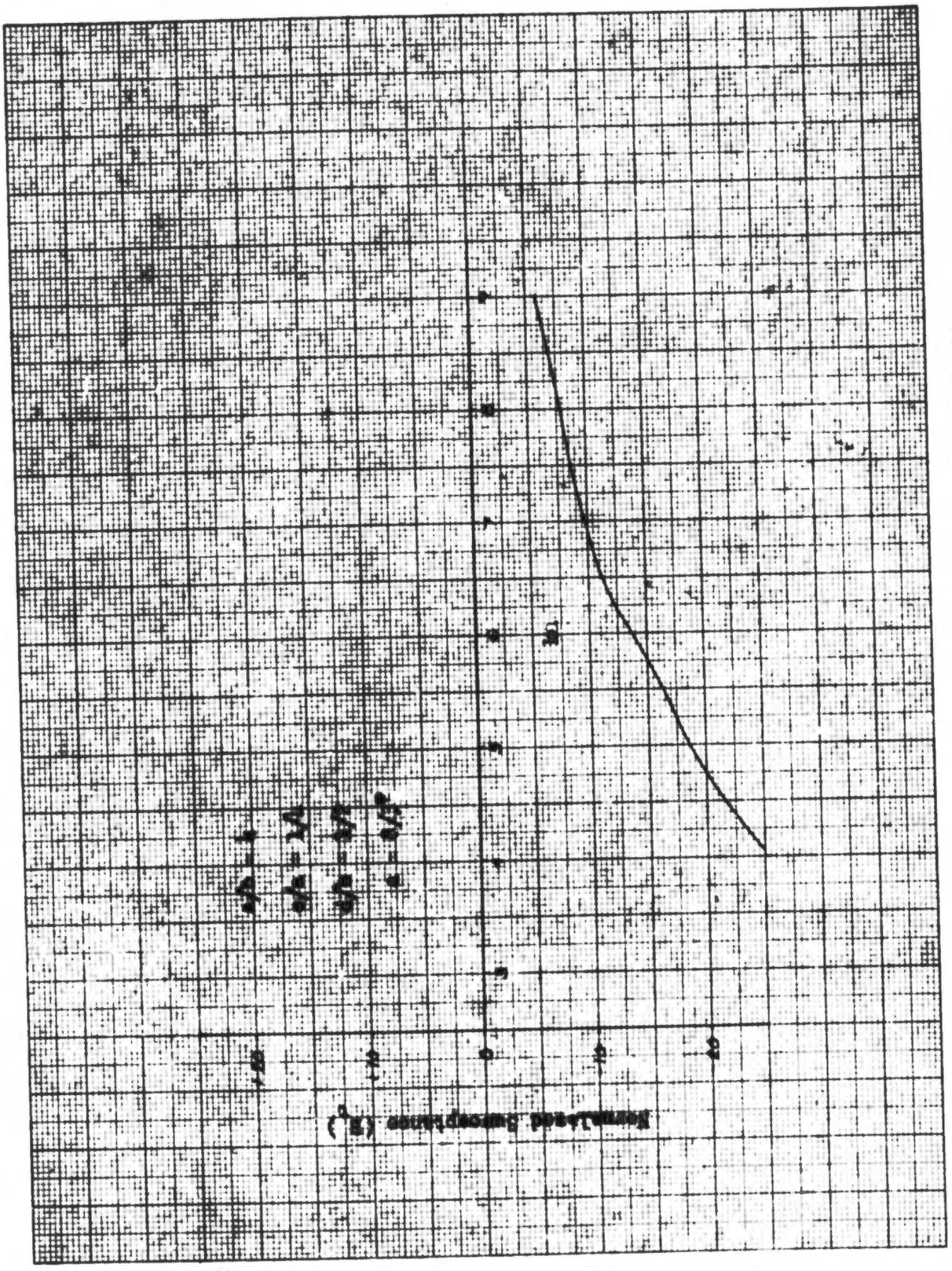

Fig. 60: Equivalent Susceptance vs. ka for Normal Incidence

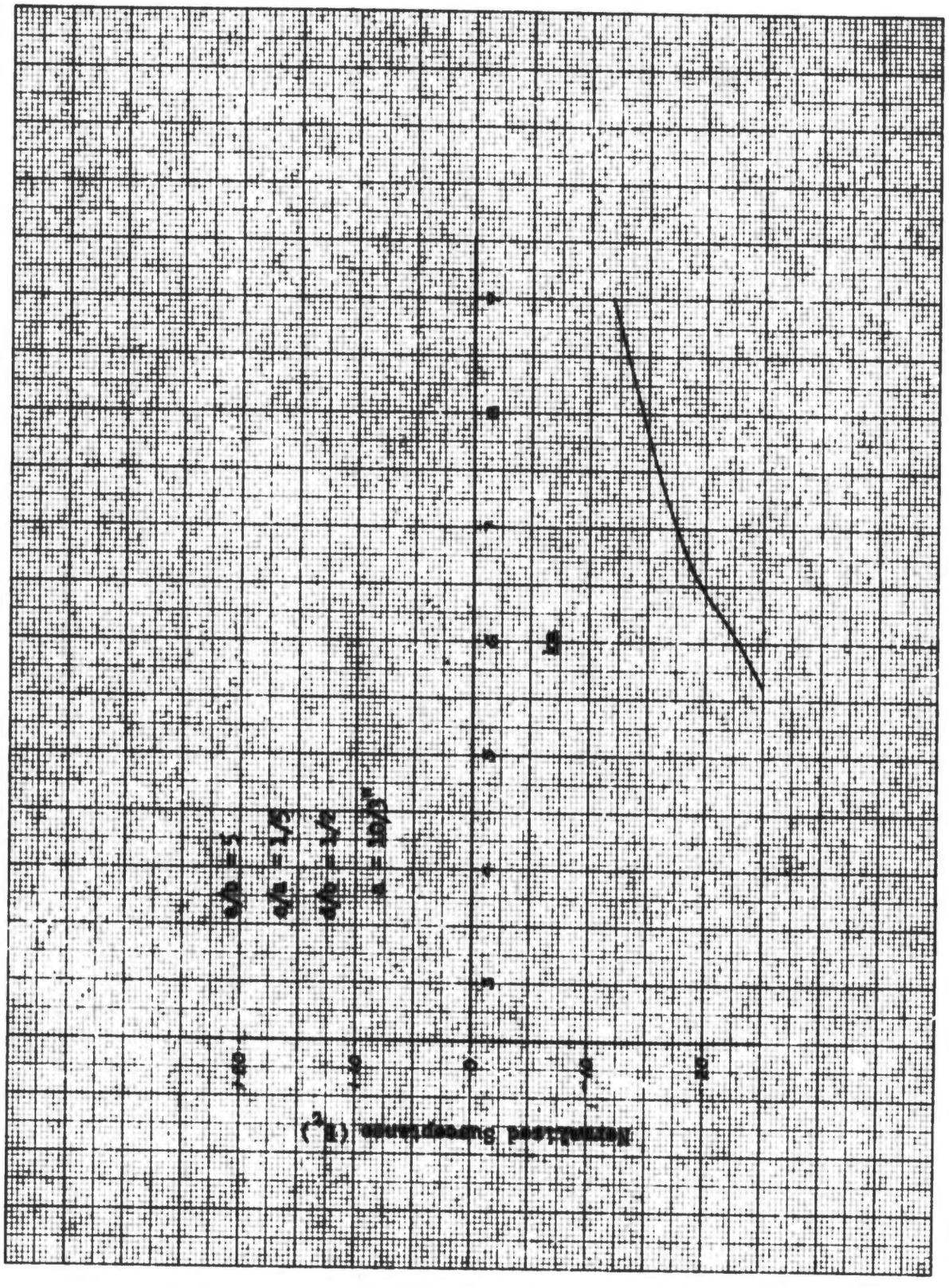

Fig. 61: Equivalent Susceptance vs. ka for Normal Incidence

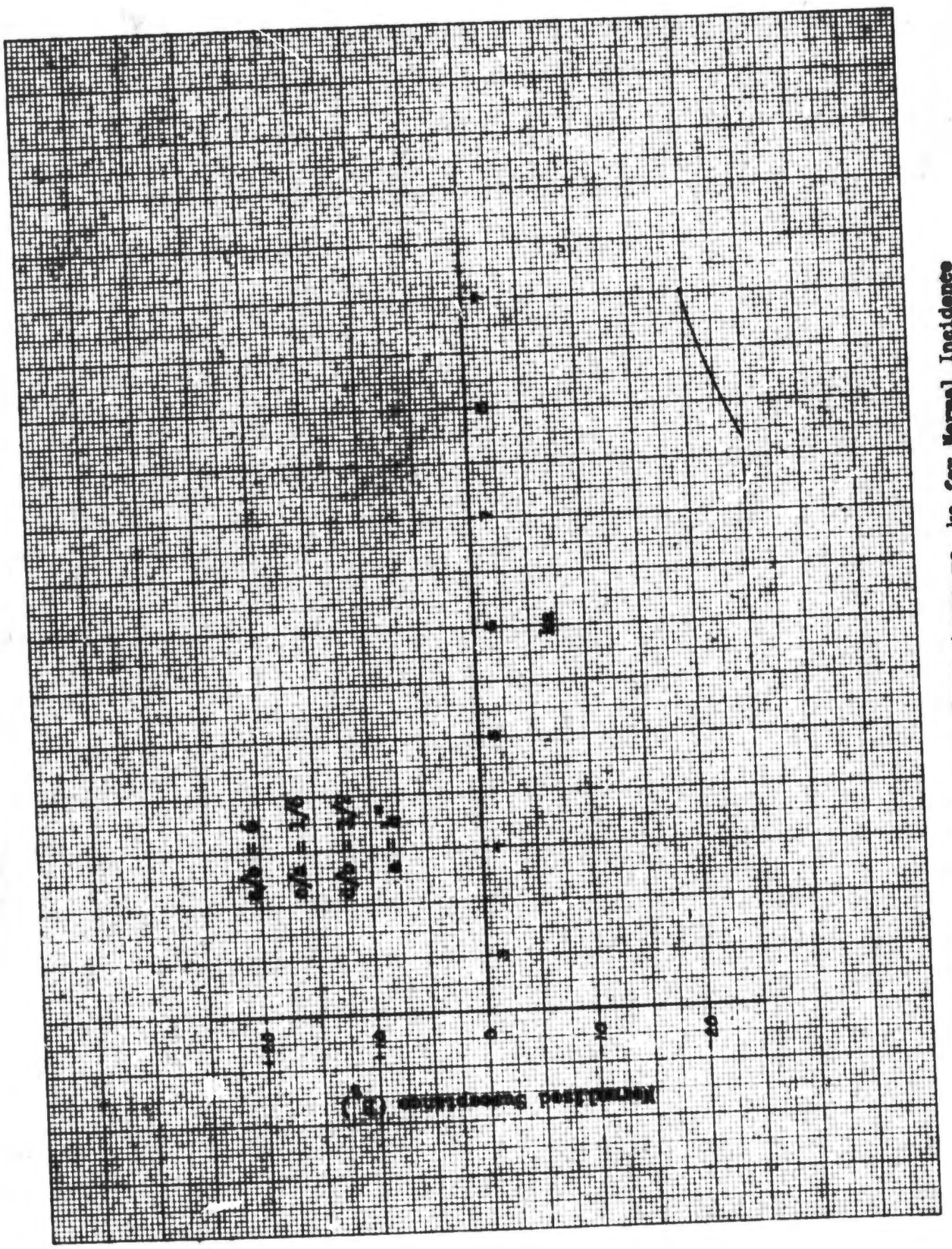

Fig. 62: Equivalent Susceptance vs. ka for Normal Incidence

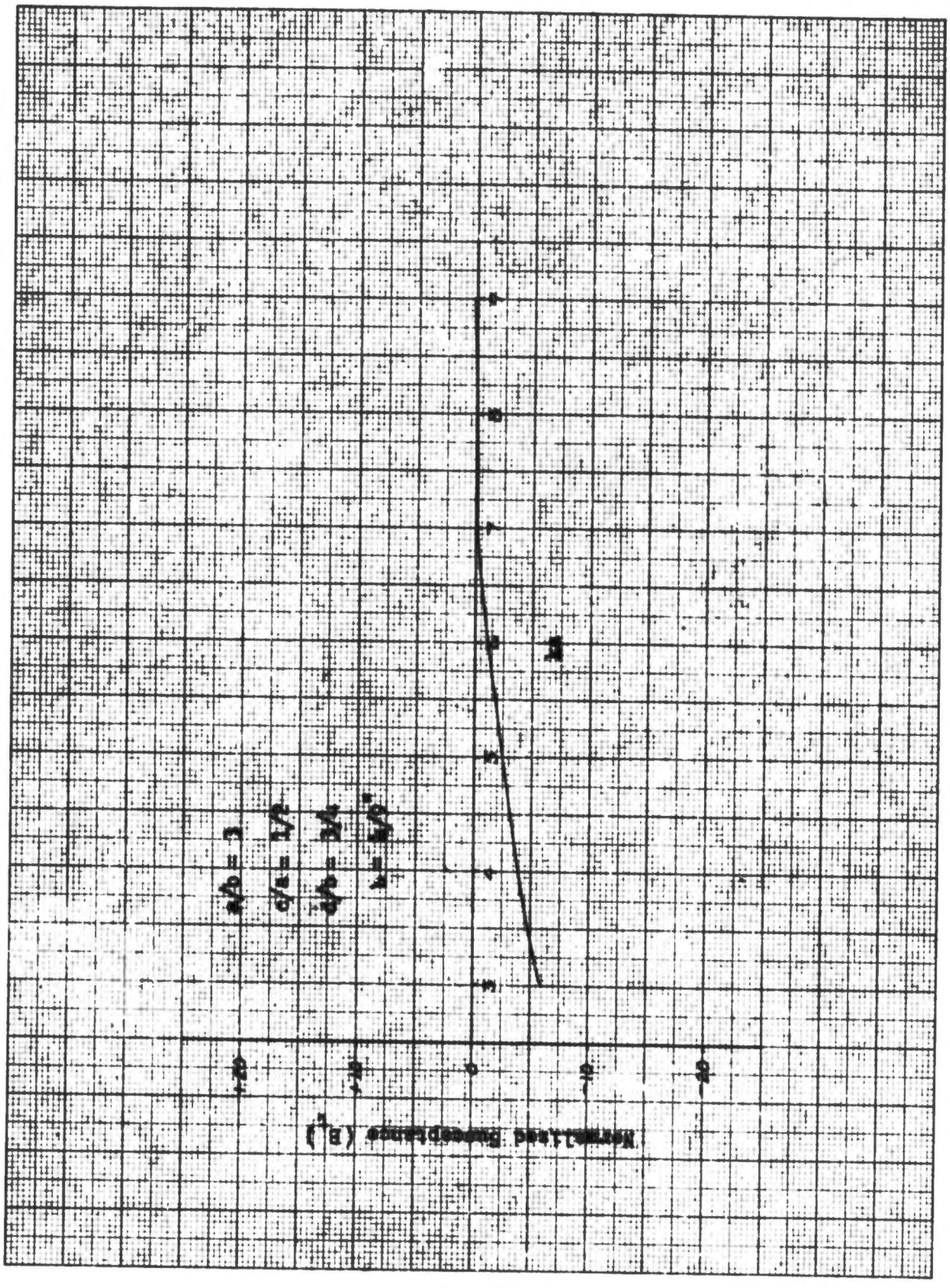

Fig. 63: Equivalent Susceptance vs. ka for Normal Incidence

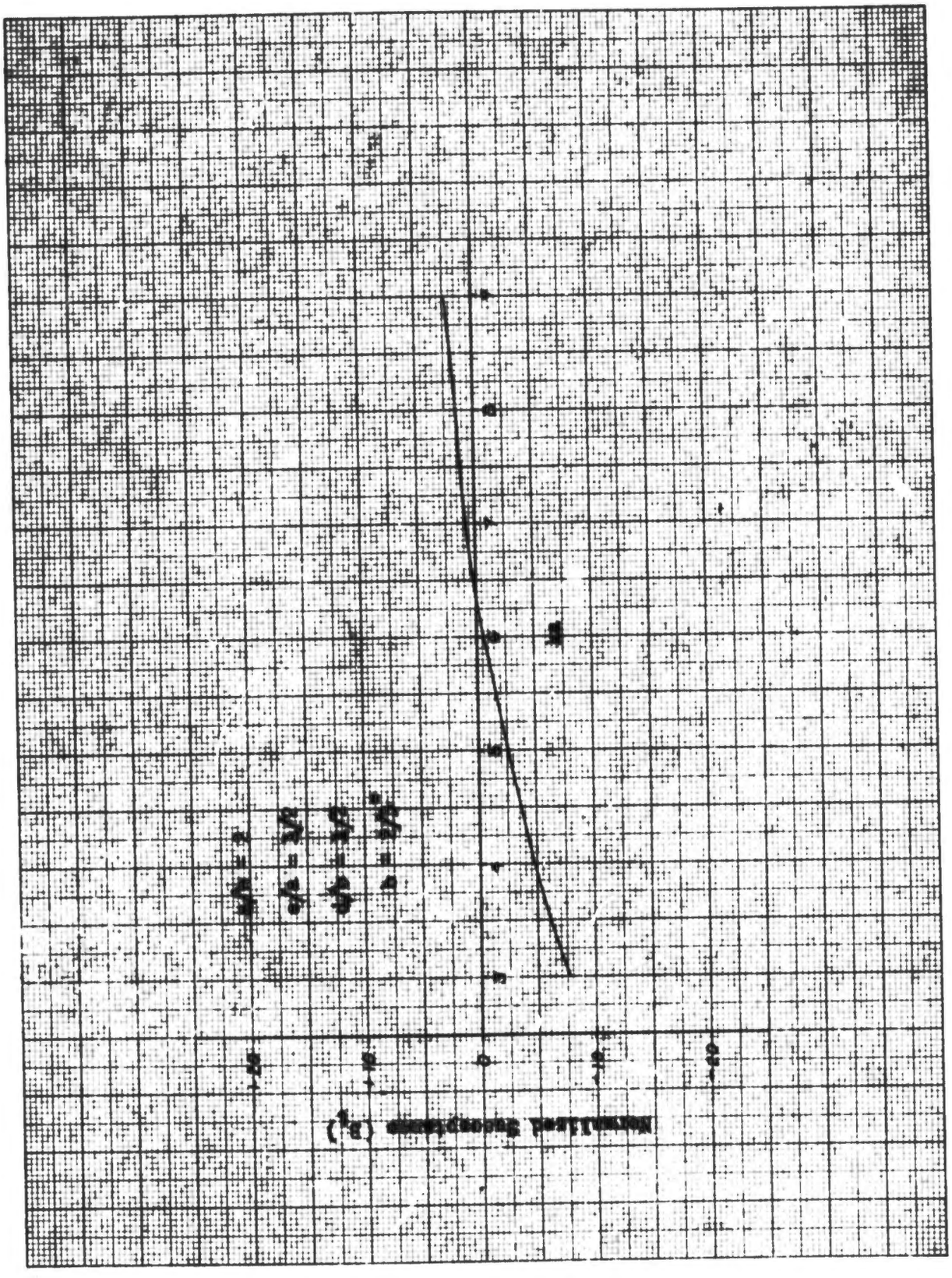

Fig. 64: Equivalent Susceptance vs. ka for Normal Incidence

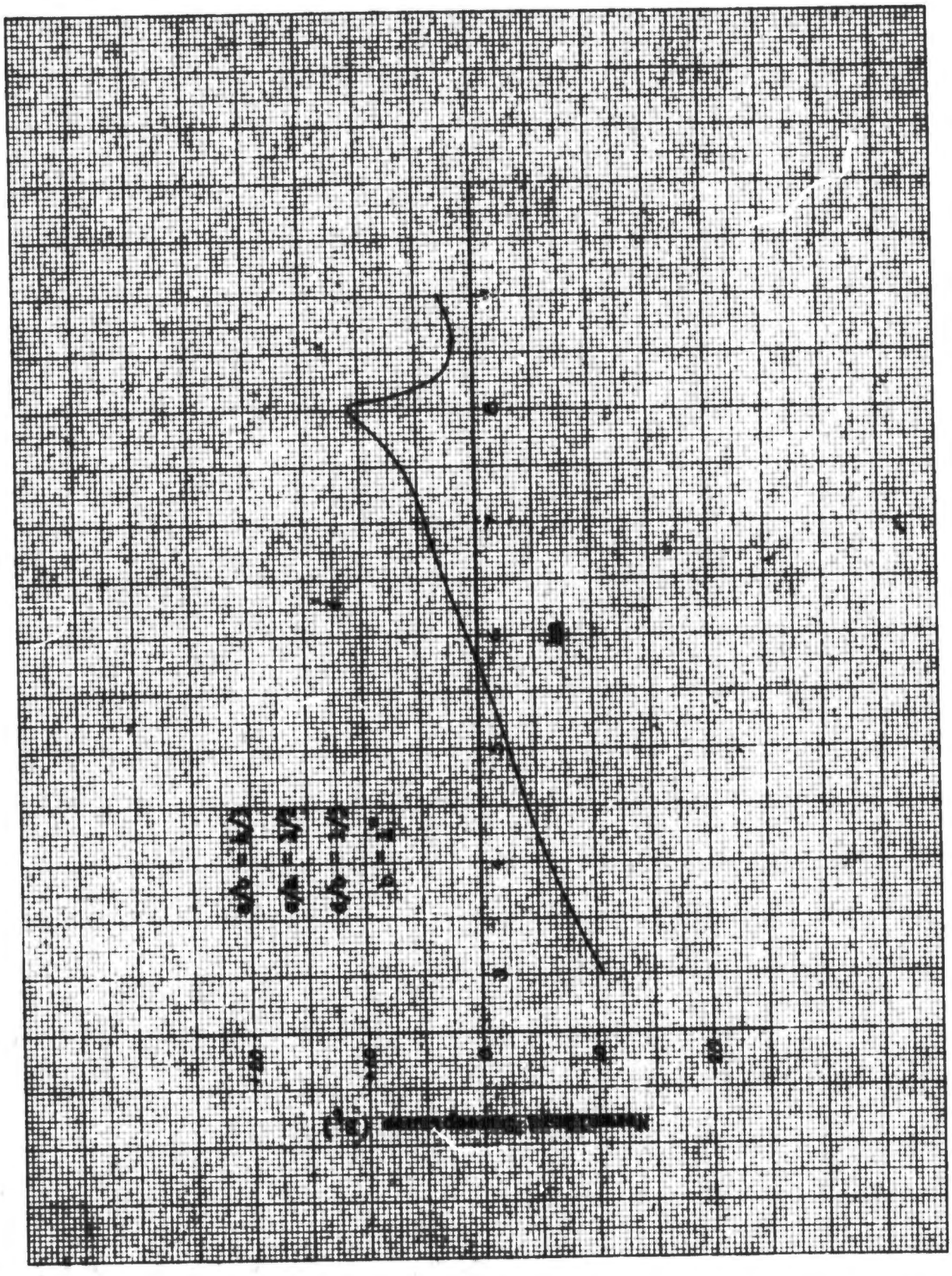

Fig. 65: Equivalent Susceptance vs. ka for Normal Incidence

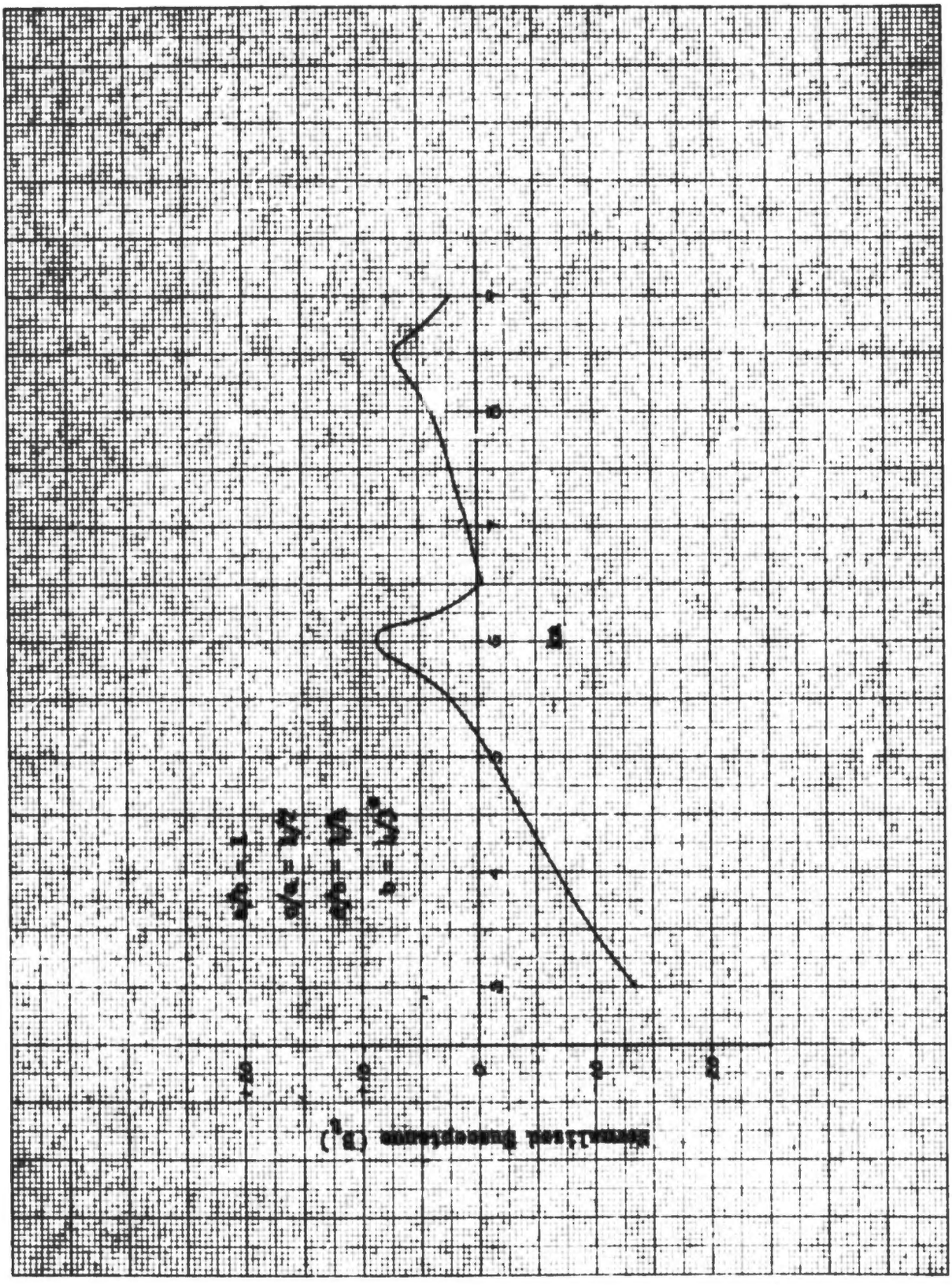

Fig. 66: Equivalent Susceptance vs. ka for Normal Incidence

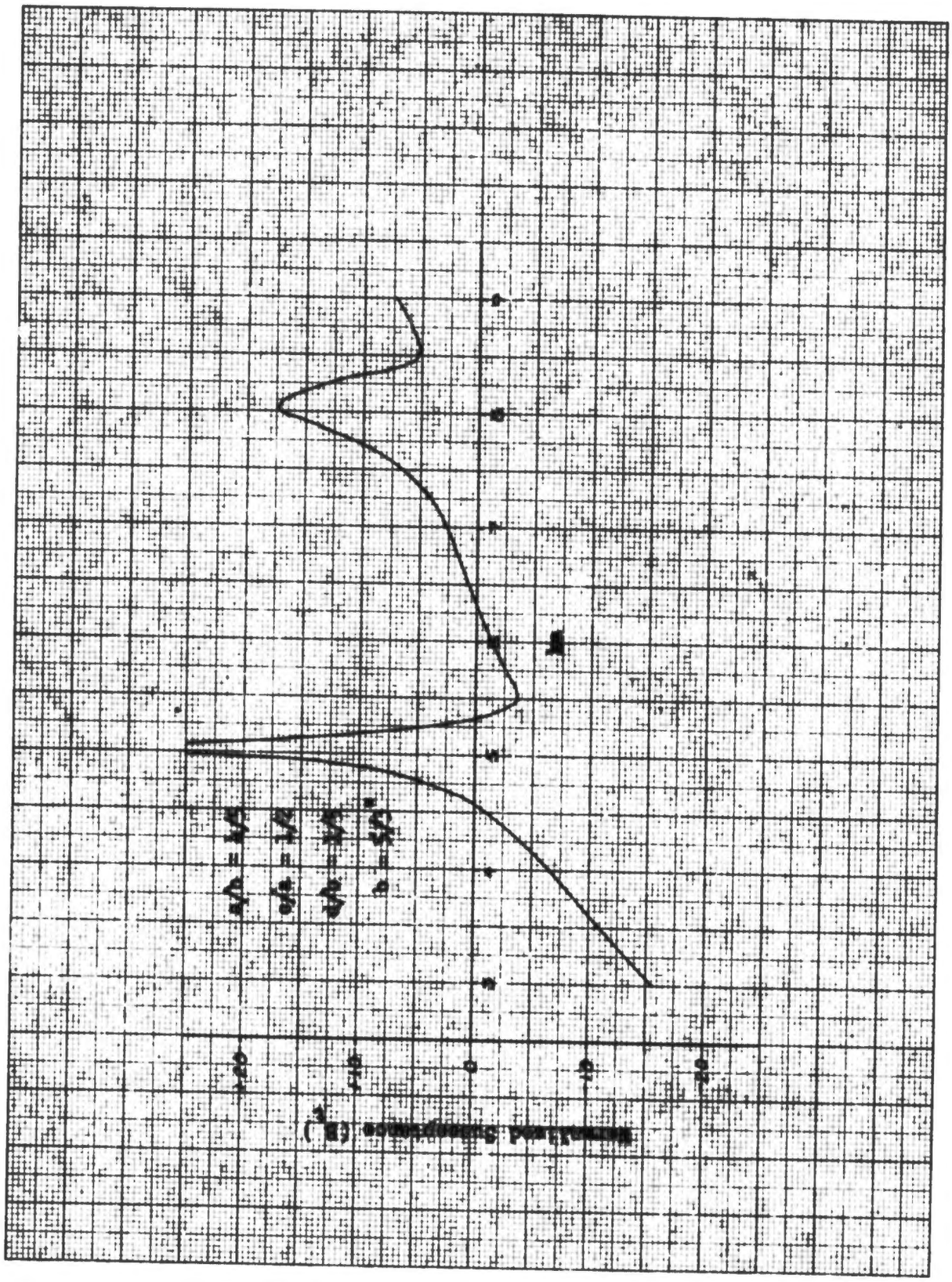

Fig. 67: Equivalent Susceptance vs. ka for Normal Incidence

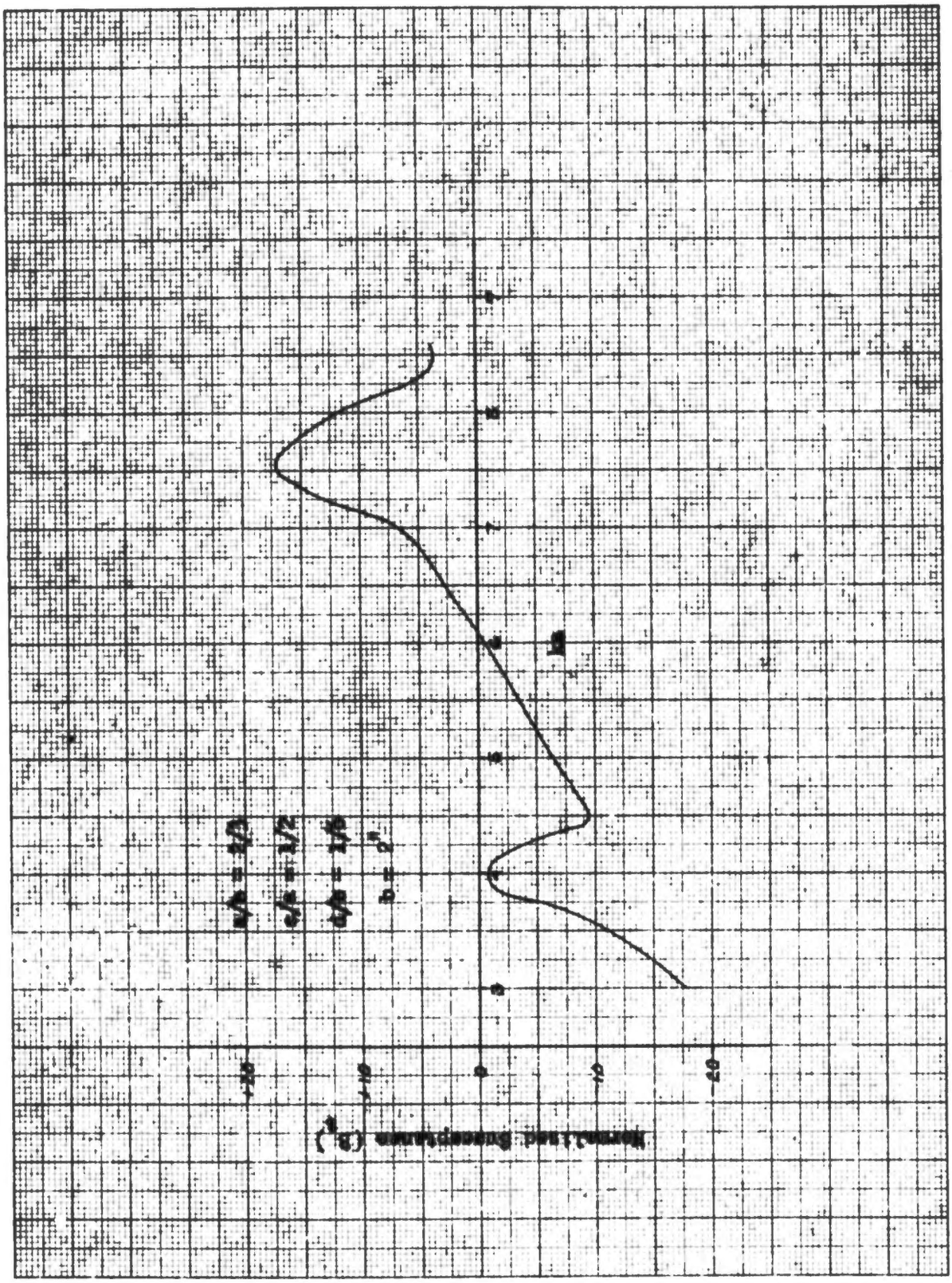

Fig. 68: Equivalent Susceptance vs. ka for Normal Incidence

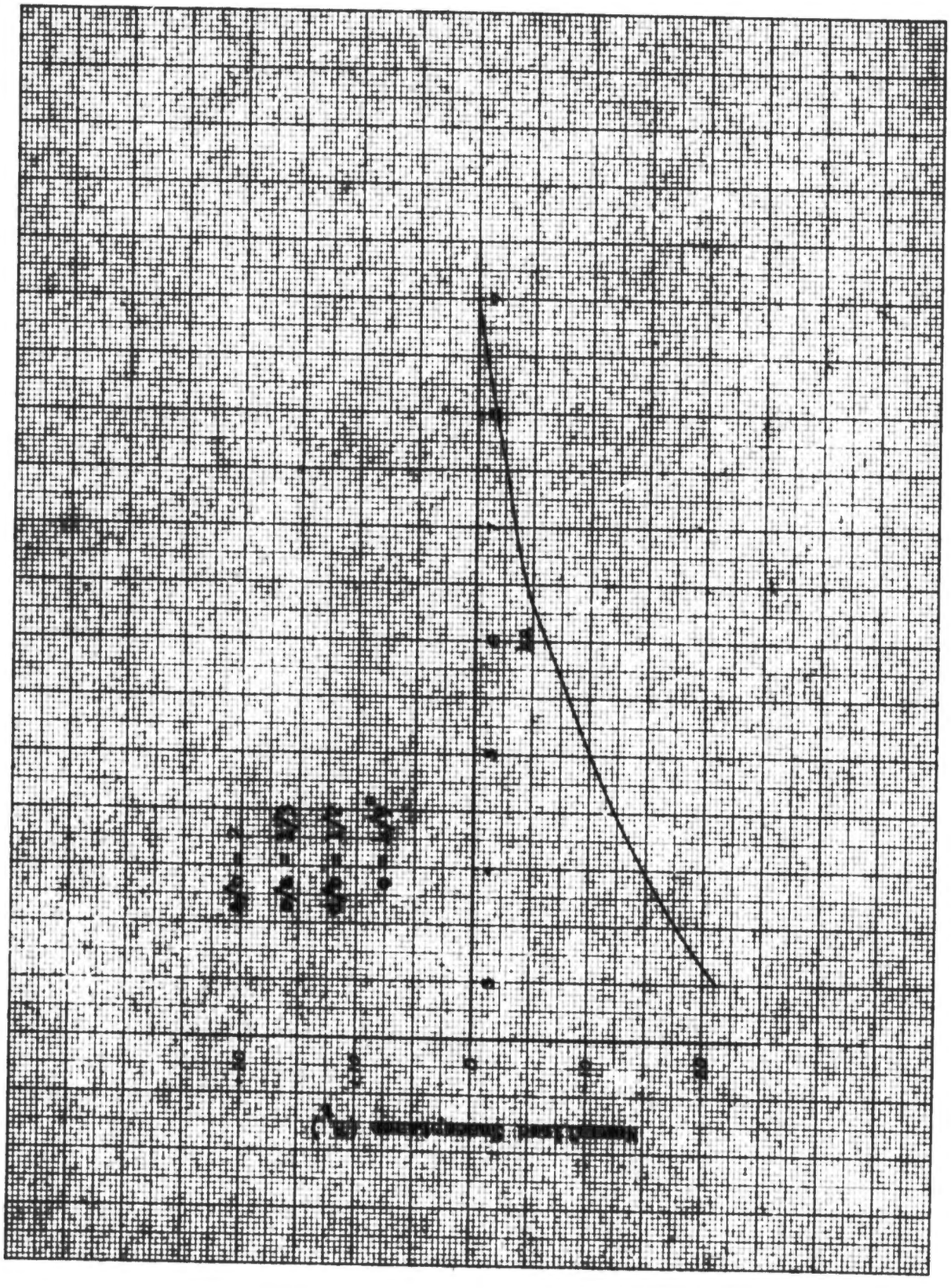

Fig. 69: Equivalent Susceptance vs. ka for Normal Incidence

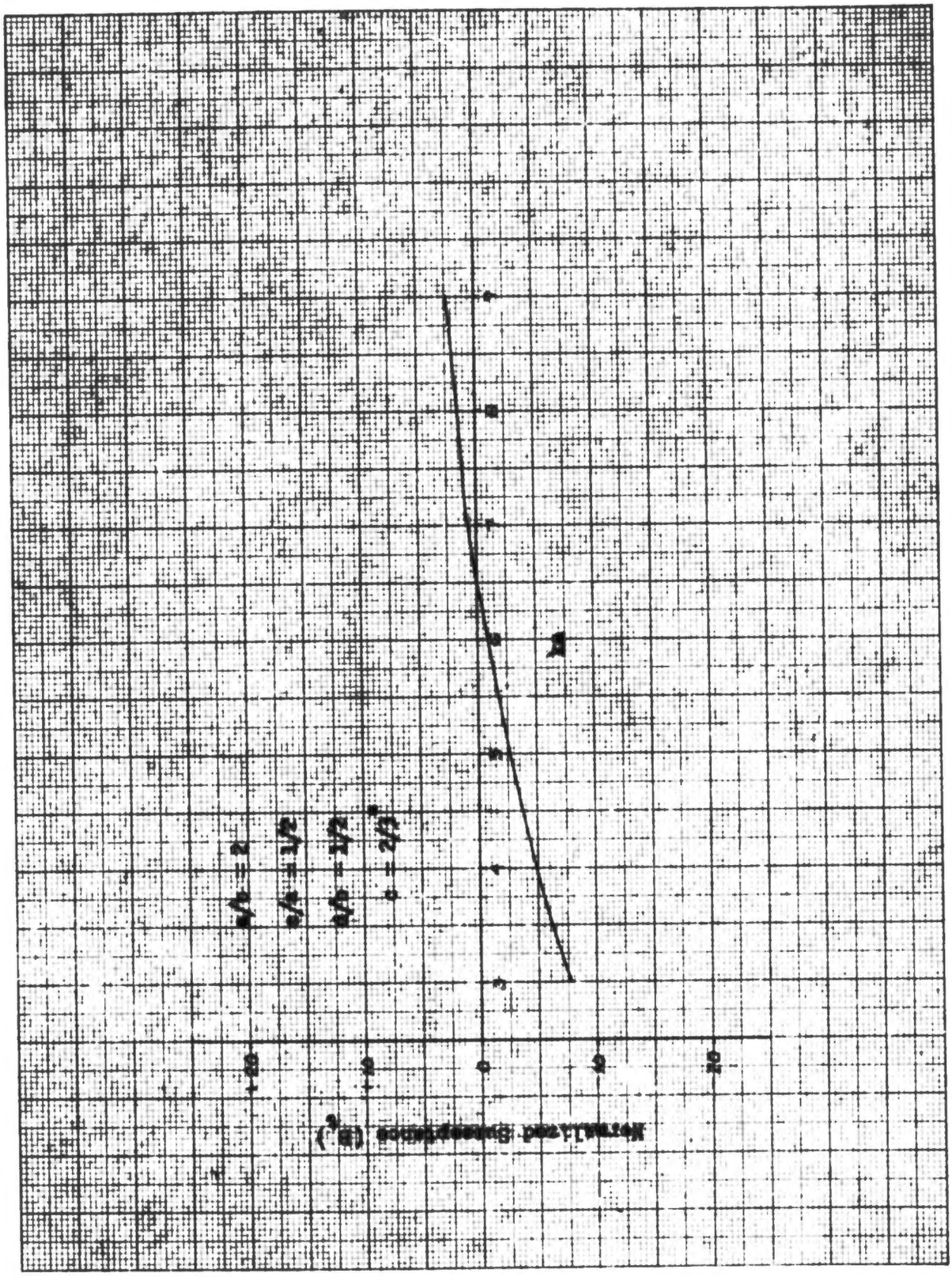

Fig. 70: Equivalent Susceptance vs. ka for Normal Incidence

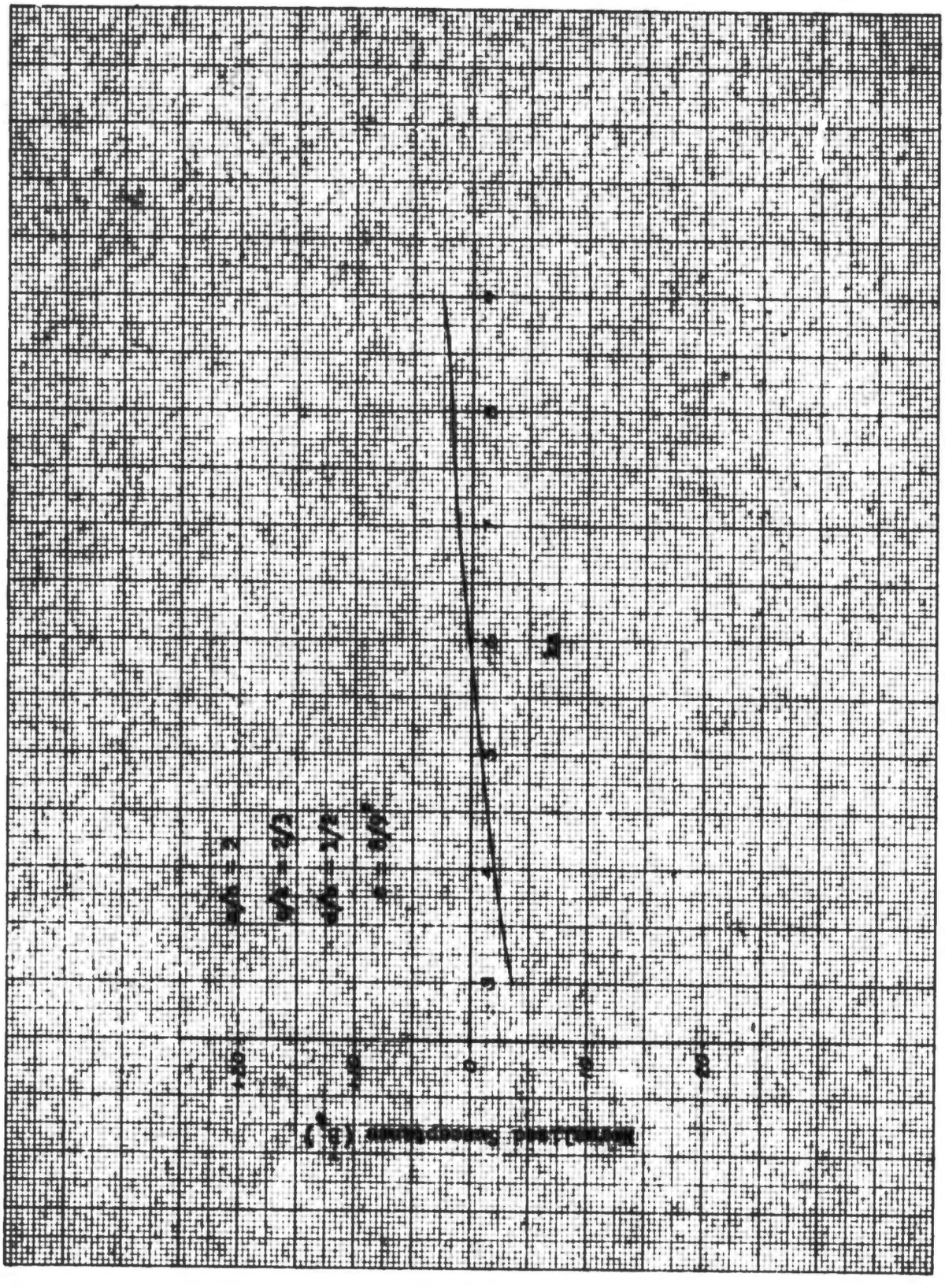

Fig. 71: Equivalent Susceptance vs. ka for Normal Incidence

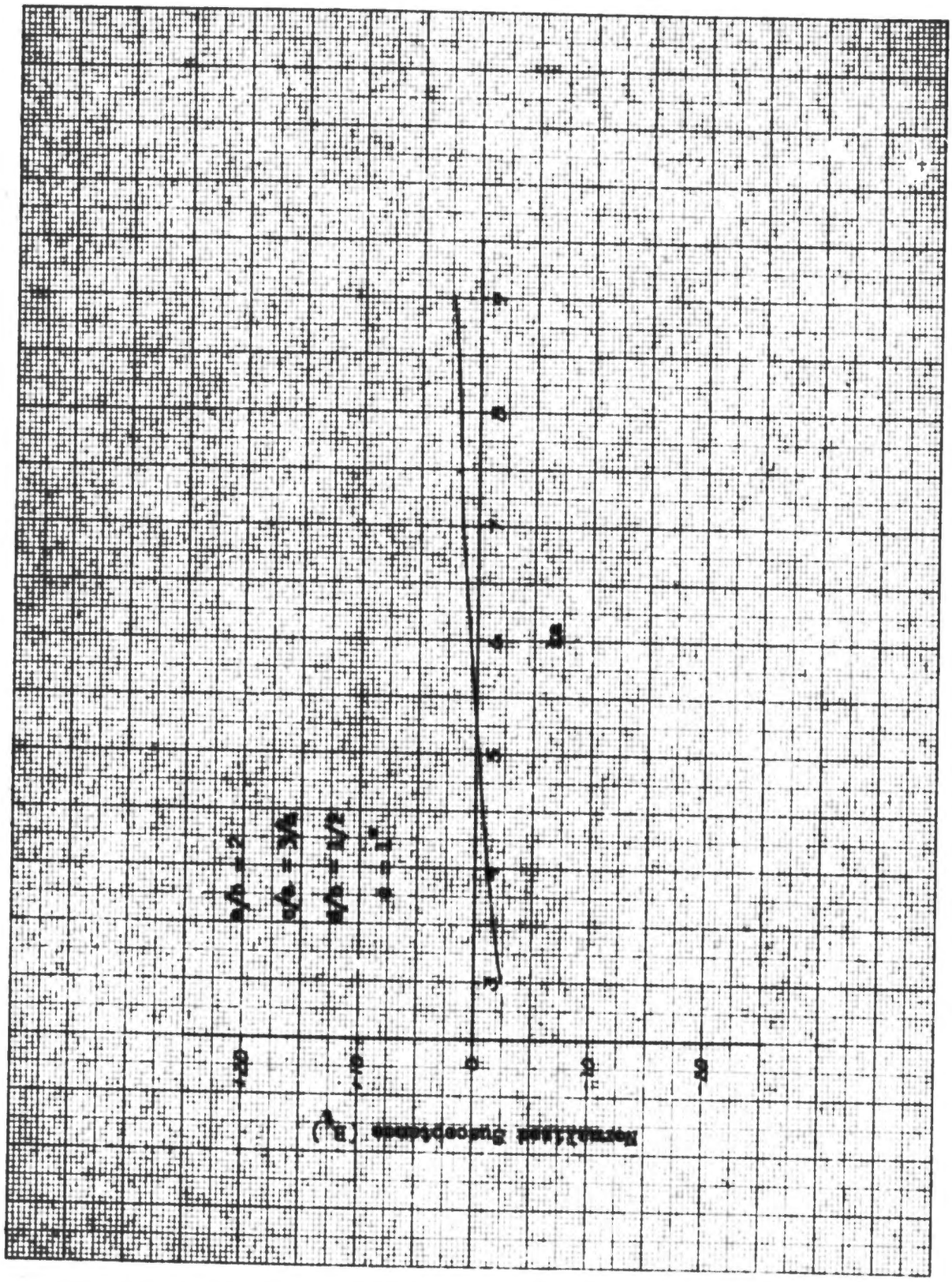

Fig. 72: Equivalent Susceptance vs. ka for Normal Incidence

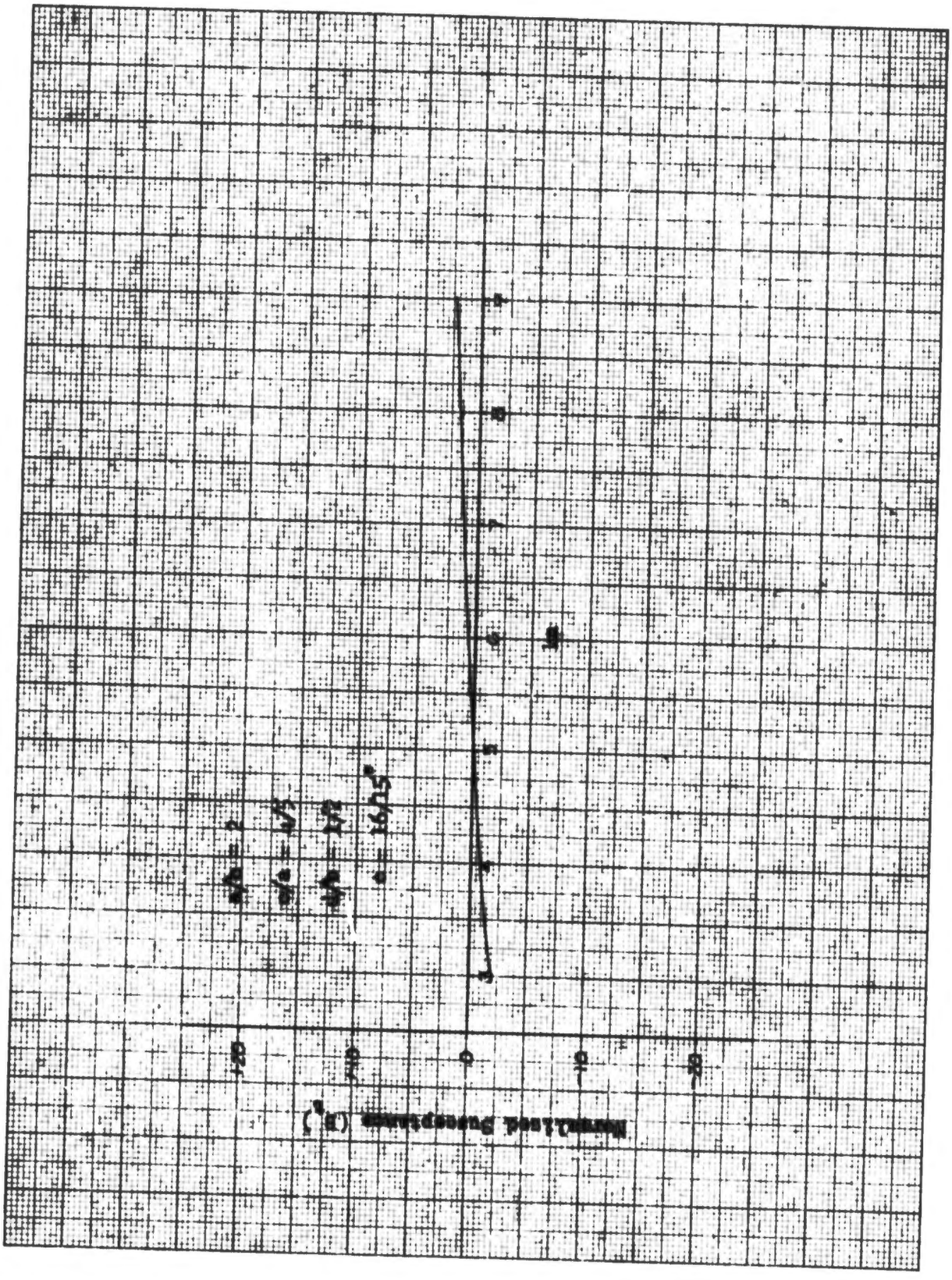

Fig. 73: Equivalent Susceptance vs. ka for Normal Incidence

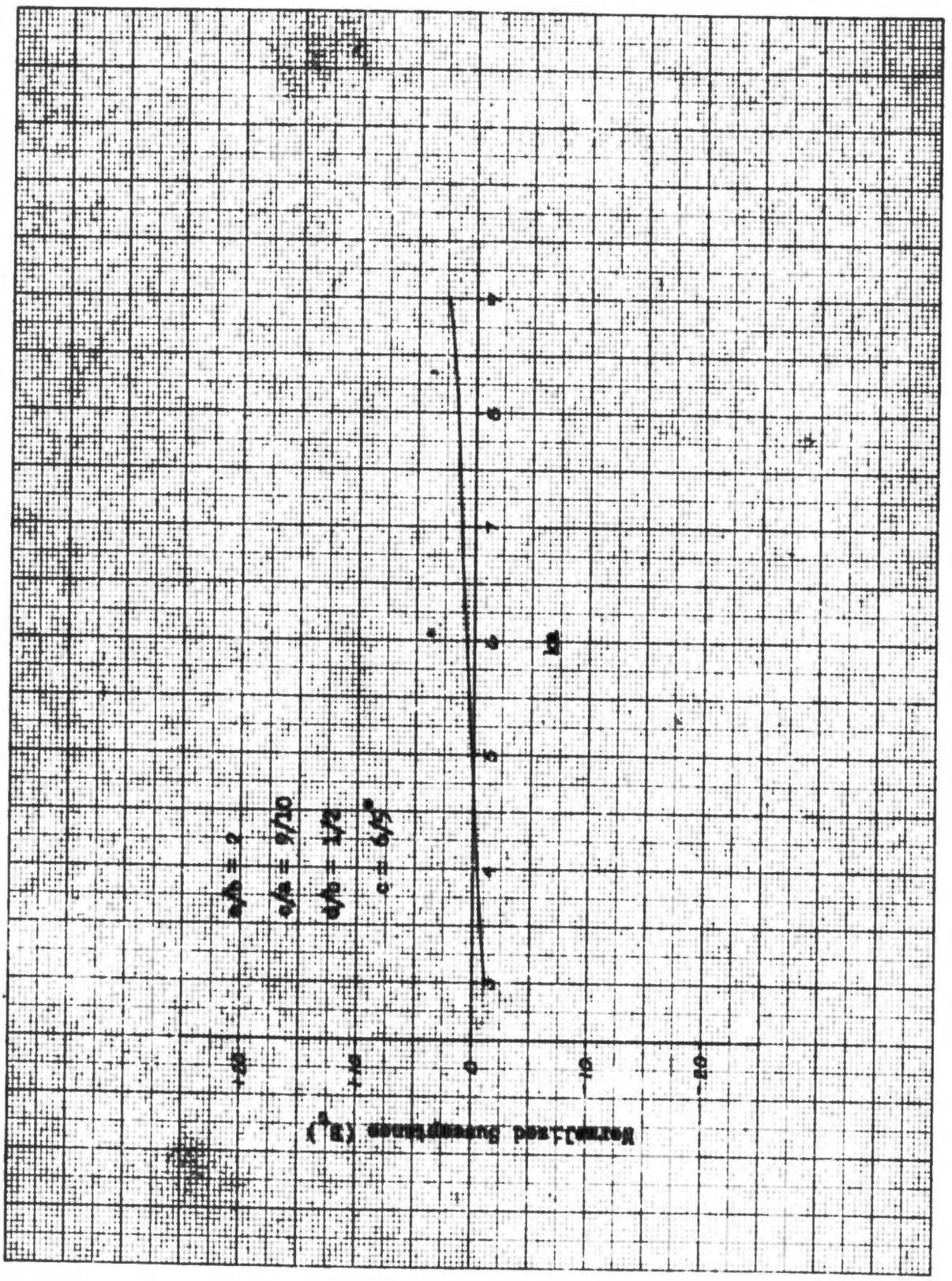

Fig. 74: Equivalent Susceptance vs. ka for Normal Incidence

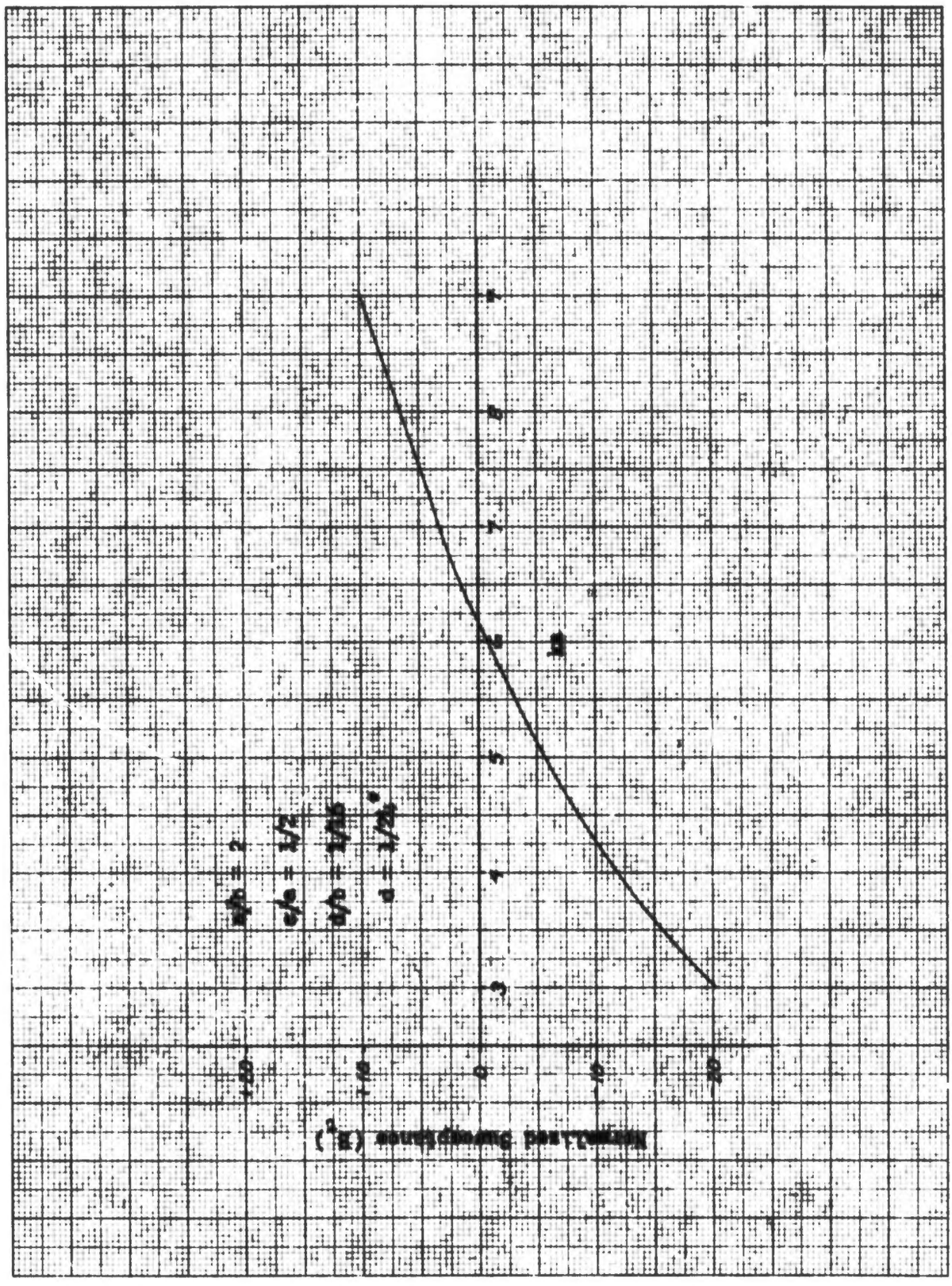

Fig. 75: Equivalent Susceptance vs. ka for Normal Incidence

And in the fourth set of curves (Figs. 76-80), the aperture width, d, is the only variable. As the value of d increases, the susceptance will decrease and the frequency at which susceptance is zero will not be changed.

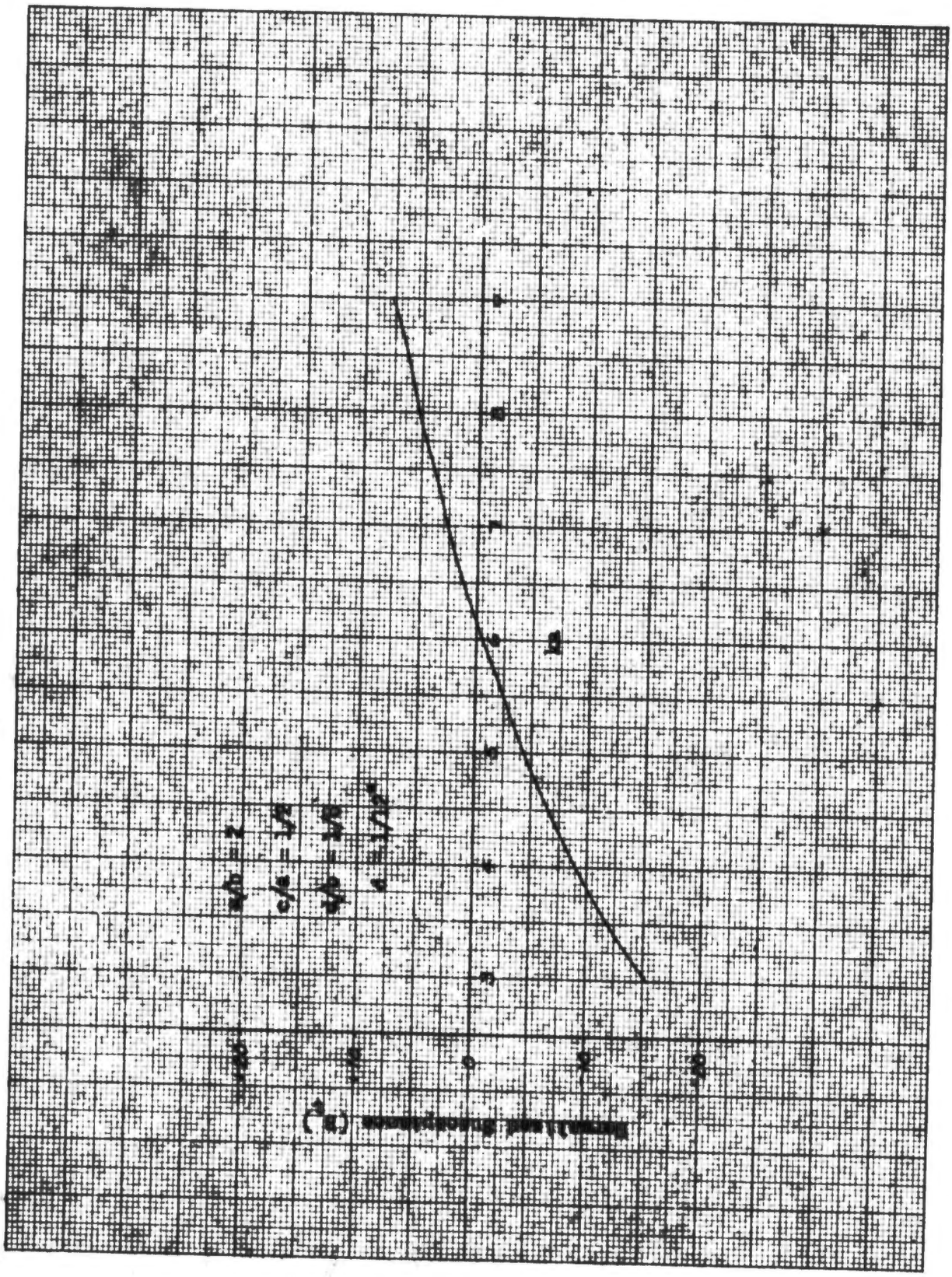

Fig. 76: Equivalent Susceptance vs. ka for Normal Incidence

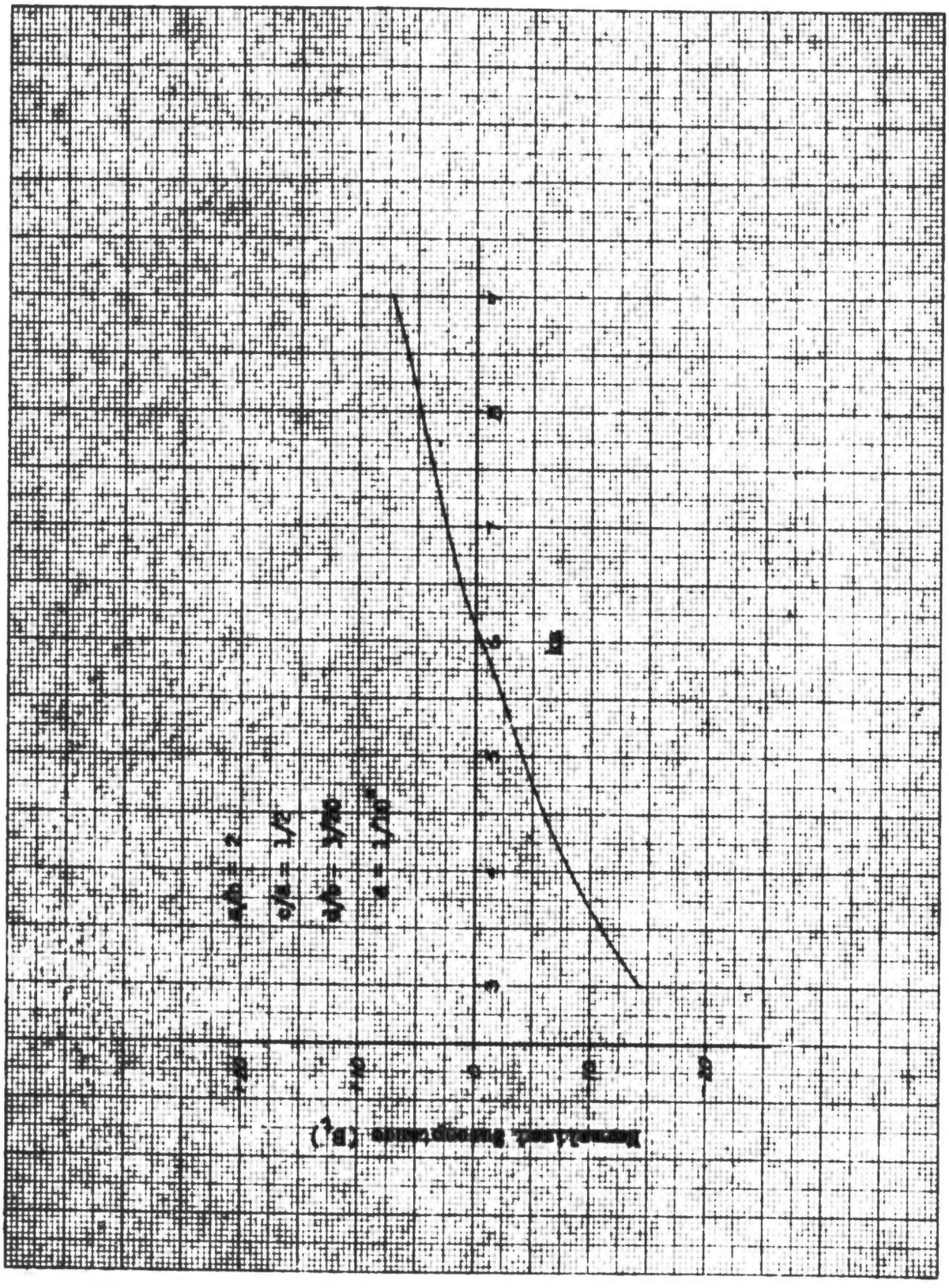

Fig. 77: Equivalent Susceptance vs. ka for Normal Incidence

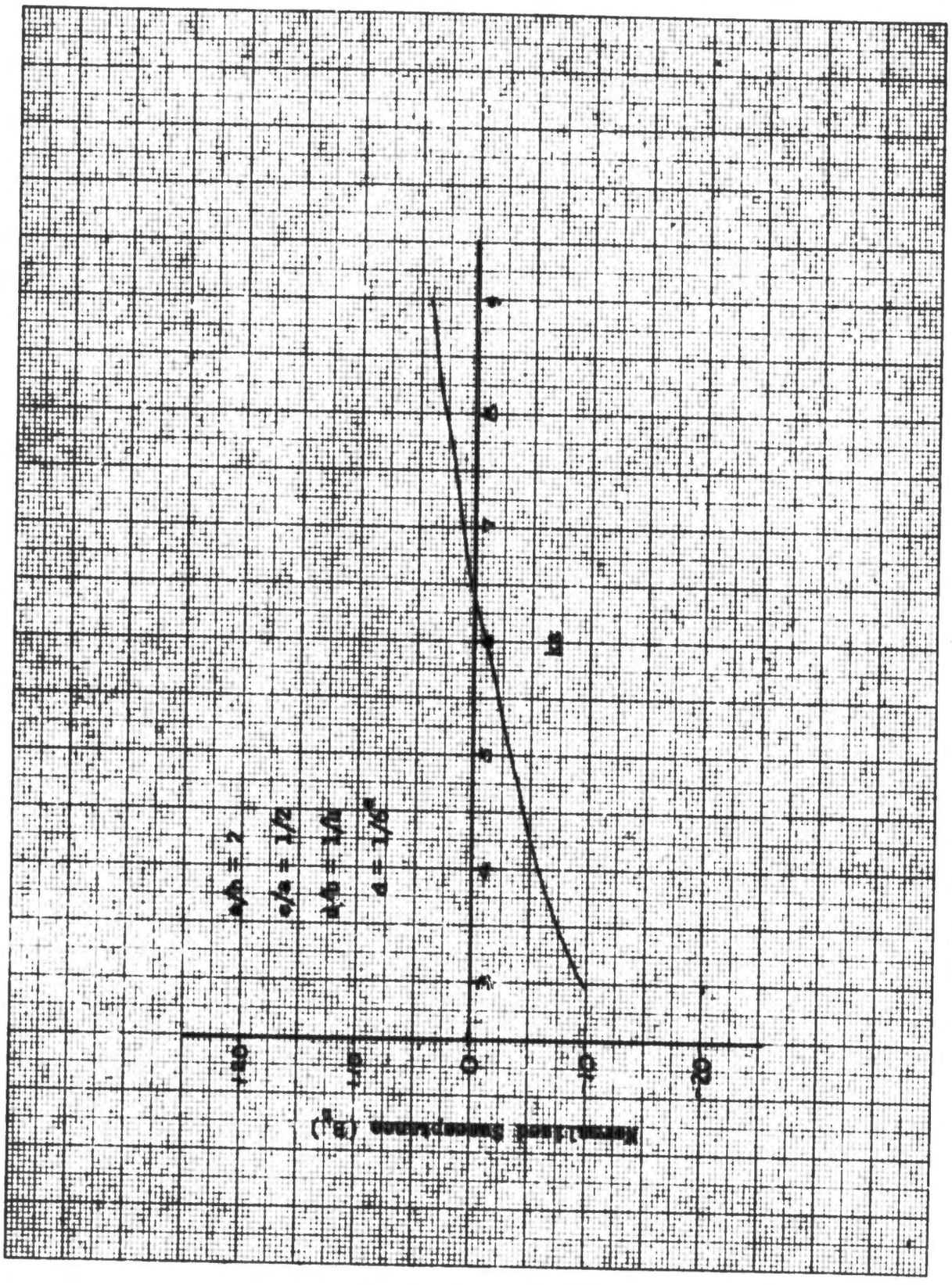

Fig. 78: Equivalent Susceptance vs. ka for Normal Incidence

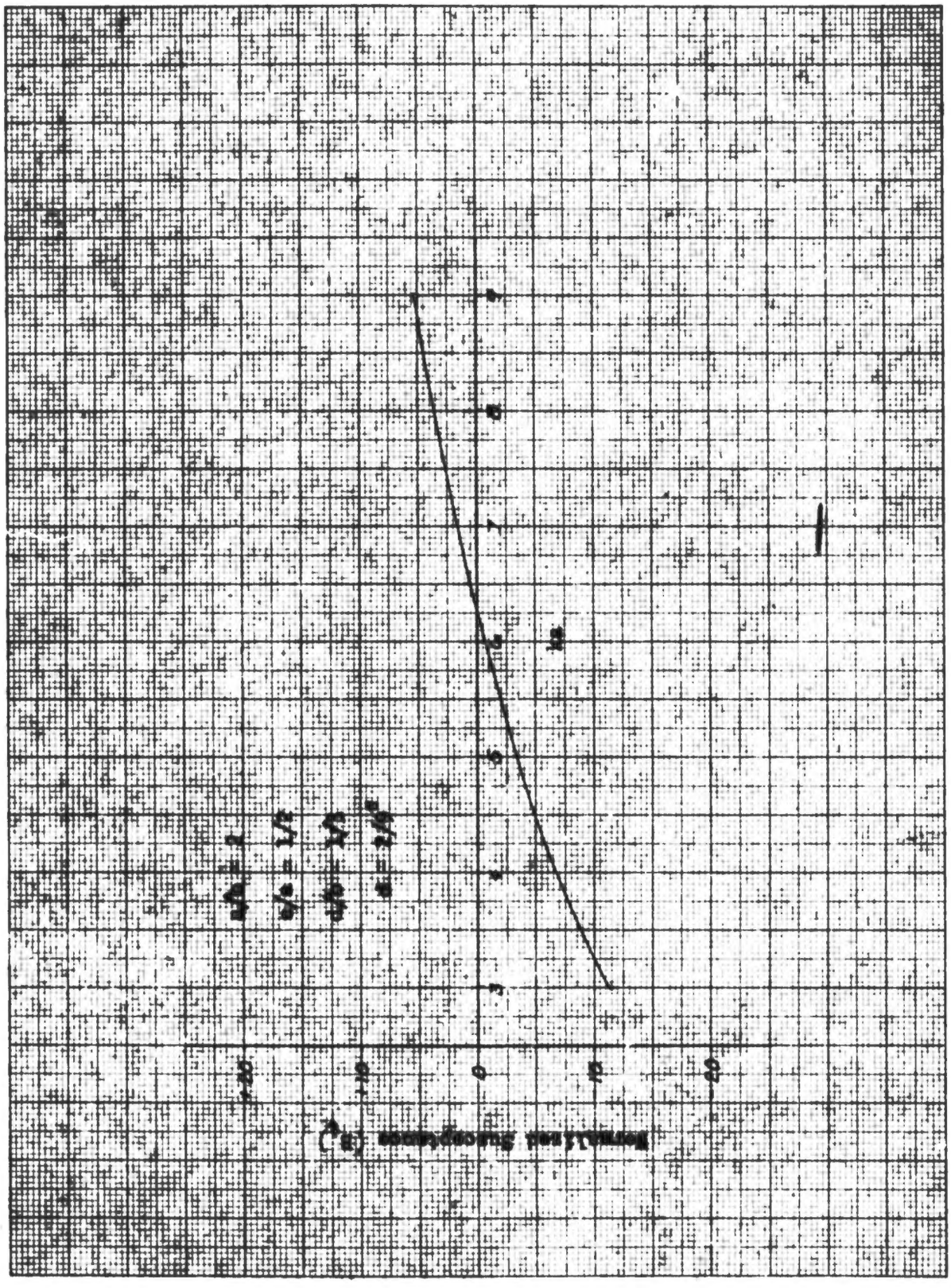

Fig. 79: Equivalent Susceptance vs. ka for Normal Incidence

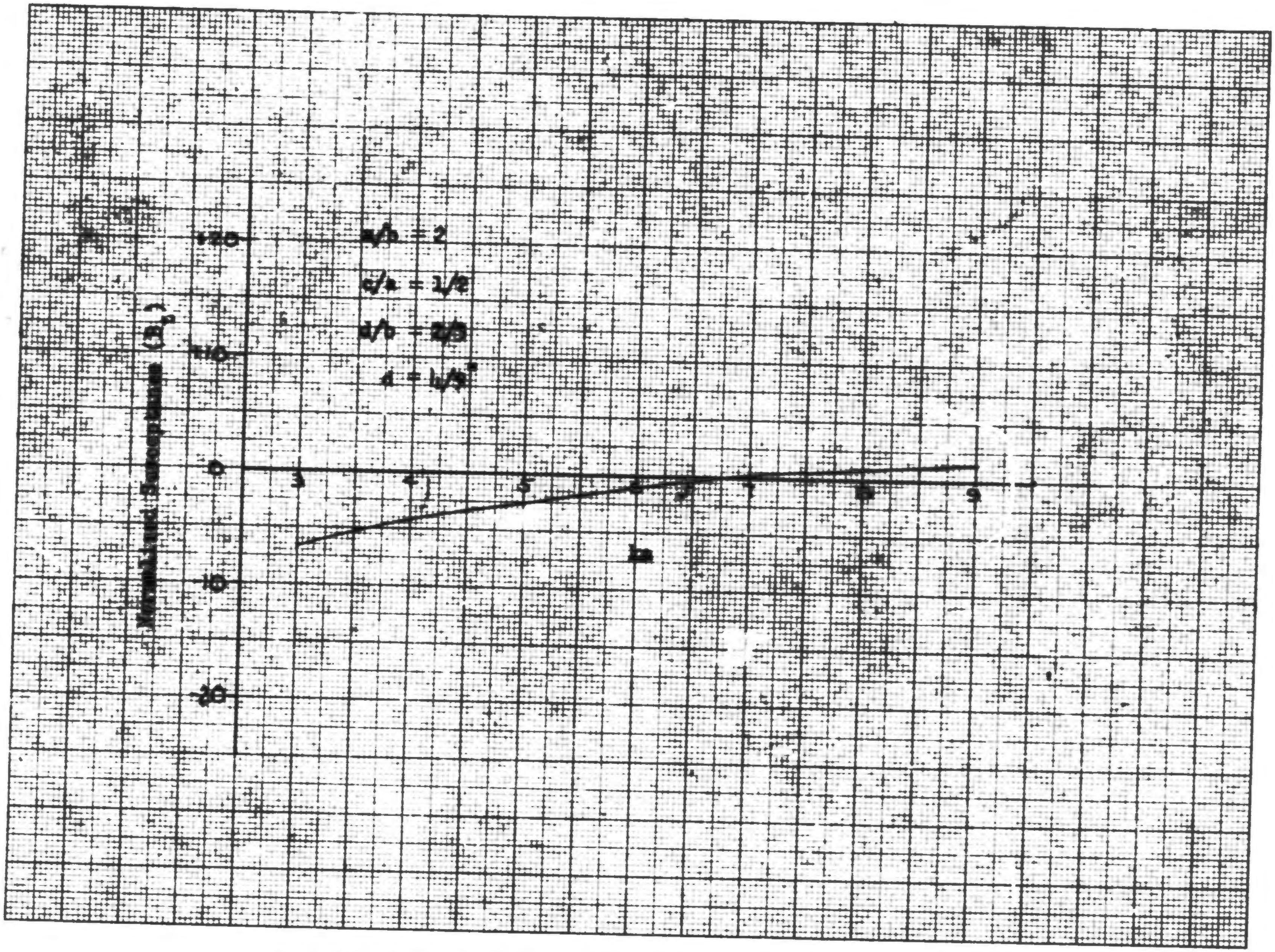

Fig. 80: Equivalent Susceptance vs. ka for Normal Incidence

VI. CONCLUSIONS

The transmission coefficient of a fenestrated conducting screen with rectangular or square apertures is analyzed by variational method for all incident angles of plane E-M waves. Theoretical calculations are made and are verified by experimental measurements.

Numerical results are given for a number of cases from which the influence of the aperture spacings and sizes on the transmission coefficient, and the resonant frequency at which the peak transmission occurs, is seen. The transmission coefficient generally increases as a function of decreasing the aperture spacings and increasing the aperture sizes, while the resonant frequency generally increases also as a function of decreasing the aperture spacings but decreasing the aperture sizes.

The susceptance of normal incidence is also given. Generally speaking, with increasing aperture spacings (greater than incident wavelength), the susceptance increases, while with increasing aperture sizes, the susceptance decreases.

The effect of the aperture spacings and sizes on the bandwidth of the transmission is also seen from the numerical results. The larger the aperture spacings, the larger is the bandwidth. However, at the ratio of the aperture spacings, a/b, close to unity, the bandwidth will be very narrow and the Wood anomaly occurs. That is, slight change of the wavelength will cause a rapid change in the transmission. As to the aperture size, the larger the size the larger is the bandwidth.